CRACK GROWTH DURING BRITTLE FRACTURE IN COMPRESSION

by

BARTLETT W. PAULDING, JR.

Geol. Eng., Colorado School of Mines
(1959)

SUBMITTED IN PARTIAL FULFILLMENT OF THE
REQUIREMENTS FOR THE DEGREE OF
DOCTOR OF PHILOSOPHY
at the
MASSACHUSETTS INSTITUTE OF TECHNOLOGY
June 1965

Signature of Author .....
Department of Geology and Geophysics,
February 9, 1965

Certified by .....
Thesis Supervisor

Accepted by .....
Chairman,
Departmental Committee on Graduate Students

ABSTRACT

Title: Crack Growth During Brittle Fracture in Compression.

Author: Bartlett W. Paulding, Jr.

Submitted to the Department of Geology and Geophysics February 9, 1965 in partial fulfillment of the requirements for the degree of Doctor of Philosophy at the Massachusetts Institute of Technology.

Photoelastic analysis of several two-crack arrays predicts that compressive fracture is initiated at cracks oriented in a particular en échelon manner. Observation of partially-fractured samples of Westerly granite, obtained during uniaxial and confined compression tests by stopping the fracture process, indicate that fracture is initiated by en échelon arrays of biotite grains and pre-existing, trans-granular, cracks. Crack growth is predominantly parallel with the direction of maximum compression and the partial fractures incorporate both grain boundaries and trans-granular cracks. The porosity due to crack growth was determined by compressibility tests. Crack growth was found to be time dependent. Certain characteristics of the volumetric strain vs maximum stress difference curves for several rocks indicate that crack growth is initiated at a stress difference of about half the compressive strength. Therefore, neither the Griffith theory nor the McClintock-Walsh modification can be expected to predict the strength of common rocks. However, good agreement exists between the McClintock-Walsh modification and the stress difference at the onset of crack growth. Because of the volume increase due to crack growth about 15 per cent of the work required to fracture a specimen in compression goes into work against the pressure medium.

Thesis Supervisor: William F. Brace

Title: Associate Professor of Geology

TABLE OF CONTENTS

INTRODUCTION

Even though the mechanical properties of rock have been extensively studied, we are still severely limited in predicting the behavior of rocks under crustal conditions or in interpreting the conditions present during the development of geologic features such as folds, joints, and faults. Since one cannot hope to extrapolate experimental data to geologic dimensions and time intervals, the solution of these problems requires a general theory of the mechanical behavior of rocks.

Of the many phenomena which are important during deformation, brittle fracture is best understood at present because of the limited number of microscopic processes which occur.

Up to now the study of the mechanics of brittle fracture of rocks has been primarily oriented toward determining the applicability of the Griffith theory (Griffith, 1921, 1924). Griffith postulated that materials contain flaws or cracks and that large tensile stresses exist on the surface of certain critically oriented cracks when the material is stressed. Griffith proposed that fracture occured when the most severely stressed crack propagated.

McClintock and Walsh (1962) modified Griffith's anaylsis by considering the fact that the cracks in rocks close under pressure. Once a crack has closed, frictional stresses exist along the crack surfaces. These frictional stresses tend to resist additional deformation of the crack and, as a result, the maximum stress concentration near the ends of the cracks is less than for a similar crack whose walls are not in contact. Therefore, their analysis predicts higher strengths than Griffith's.

The McClintock-Walsh modification gives the confined compressive strength in terms of the uniaxial compressive strength, the coefficient of friction of the crack surfaces, and the stress normal to a crack which is required to close it. They find good agreement with the experimental results of several investigators when the coefficient of friction is taken to be unity and the cracks are considered to close at stresses which are negligible when compared with the strength.

Brace (1960) showed that for a coefficient of friction of about unity, the McClintock-Walsh modification is nearly identical with the empirical Coulomb failure law observed for rocks during compression.

By considering the straight segments of grain boundaries as Griffith cracks, Brace (1961) found that the uniaxial compressive strength and maximum grain size for

two crystalline limestones agreed according to Griffith's analysis of the dependence of fracture strength on crack length. In addition, Brace (1964) found that the tensile strength of certain rocks could be predicted to within a factor of two by substituting measured values of Young's modulus, surface energy and crack length (i.e., maximum grain size) into Griffith's equation

$$T_o = \left(\frac{2E\gamma}{\pi c}\right)^{\frac{1}{2}} .$$

Further evidence that a mechanism such as suggested by Griffith is operative was obtained by Brace (1964) from examination of partially fractured specimens. He found that grain boundaries became loosened as the stress was increased prior to failure and the rock appeared to be a crack-filled material as envisaged by Griffith. Furthermore, Brace found that the fracture often grew from an en échelon array of cracks.

Brace and Bombolakis (1963) studied the growth of cracks in a uniaxial compressive stress field. Their general method consisted of introducing critically-oriented cracks into homogeneous materials and stressing the sample until the crack propagated. They found that the point of maximum tensile stress on the surface of the most critical crack did not occur at the very end of the crack, as in tension (Wells and Post, 1958), but in the sector between

the long axis of the crack and the direction of maximum compression. Initial growth was normal to the crack surface at the point of maximum tension. The crack then continued to propagate along a curved path which approached the direction of uniaxial compression. Crack growth stopped after the crack had attained a length of two to three times the original length. This evidence, of a critically-stressed crack growing into a stable position, was the first indication that the process of fracture in compression might not be as suggested by Griffith.

A second fundamental question of the applicability of the Griffith theory arose from a photoelastic study by Bombolakis (1963). He found that the magnitude of the maximum tensile stress on the surface of an elliptical slit was strongly dependent on the relative position of neighboring slits. Griffith's theory is based on Inglis' (1913) solution of the stress conditions around an isolated, elliptical, opening. Since Brace and Bombolakis showed that cracks must be quite close in order to coalesce, the stress conditions derived by Inglis might not be applicable to the actual case.

Even though evidence was beginning to accumulate which seriously questioned if the Griffith theory should predict the compressive strength of rocks, his idea that brittle fracture is due to the growth of cracks had gained support.

This investigation was undertaken to obtain a better understanding of the mechanics of crack growth during brittle fracture. This involved several experimental techniques: photoelastic analysis, uniaxial compression tests, compressibility tests and confined compression tests.

The purpose of the photoelastic analysis was to determine the stress conditions of a crack when in the proximity of another crack. Several two-crack arrays were studied to investigate the relationship between the geometry of an array and (1) the magnitude of the maximum tensile stress on the surface of each crack, and (2) the principal stress directions.

Uniaxial compression tests on Westerly granite were next undertaken to see if the growth of cracks corresponded to the results of the photoelastic analysis. Westerly granite was chosen as a typical, siliceous, crystalline rock which was known to be brittle (Brace, 1964). In addition, experimental technique could be checked by comparing Young's modulus and compressive strength with earlier results (Brace, 1964).

It was decided to obtain partially-fractured specimens in order to study the development of cracks leading to a macroscopic fracture. Since it was felt that a large amount of crack growth occured during the final stress

increments, the samples had to be loaded to just below the fracture strength and yet be recovered, intact. This required that the press-rock system remain stable even though the load carrying ability of the sample decreased.

Walsh (1965a) showed that the porosity due to narrow cracks could be measured by means of a compressibility test. Compressibility tests were conducted to find the porosity due to crack growth which occured during the uniaxial compression tests. In addition, the compressibility tests proved useful in determining the predominant direction of crack propagation.

Measurement of the axial and lateral strains allowed computation of the volumetric strain. The onset of crack growth was determined by noting certain characteristics of the plots of volumetric strain vs maximum stress difference. Certain characteristics of crack growth during the uniaxial compression tests suggested that the investigation should be extended to include confined compression tests.

The influence of confining pressure on the maximum stress difference required to initiate crack growth was compared with the McClintock-Walsh modification of the Griffith theory. The stress difference at the onset of crack growth was substituted for their stress difference at fracture.

The pronounced volume increase which occurred during the uniaxial compression tests suggested that if crack

growth in confined compression tests causes a significant increase in volume then some of the work required to fracture a specimen may go into work against the confining pressure. In order to determine the importance of the work against the pressure medium, the total work and pdV work were compared.

The text is divided into five chapters: PHOTOELASTIC TESTS, UNIAXIAL COMPRESSION TESTS, COMPRESSIBILITY TESTS, CONFINED COMPRESSION TESTS, and CONCLUSIONS, in that order. The first four chapters are divided into Introduction, Experimental Procedure, Experimental Results, and Discussion of Experimental Results. The implications of the results of this study toward the brittle fracture of rocks and suggestions for further investigation are presented in the last chapter.

PHOTOELASTIC TESTS

Introduction

For homogeneous materials such as glass it has been found (Griffith, 1921) that, in tension, the stress required to initiate crack growth is, in fact, the strength of the material. This is because a critically orientated crack grows normal to the direction of applied tension (Wells and Post, 1958), becomes increasingly more critical and immediately leads to fracture.

In contrast, Brace and Bombolakis (1963) showed that a crack does not propagate much further than its original length when subjected to uniaxial compression. Their results suggest that fracture in compression requires the activation of more than one crack and for a fracture to develop from the coalesence of cracks, the cracks must initially be within a distance of approximately one crack length of each other.

Griffith based his theory on a solution of the stress state around an isolated, elliptical, opening (Inglis, 1913). Bombolakis (1963) showed that the magnitude of the maximum tensile stress on the boundary of an elliptical opening was strongly influenced by the relative position of neighboring

ellipses. Since cracks must be quite close in order to coalesce, the stress conditions derived by Inglis for an isolated crack might not be applicable to the actual case.

It was decided to systematically study the stress concentration factor of cracks in several different arrays to determine the relationship between the magnitude of the maximum tensile stress and the geometry of the array. Several parameters are necessary for describing the geometry of an array and it was hoped that some consistent behavior would become apparent whereby one or more parameters necessary for a critical array would be known.

Experimental Procedure

Photoelasticity was chosen in preference to analytic methods of solution because of the mathematical difficulties associated with a multiply-connected body. A brief discussion of the photoelastic phenomena is presented for a better understanding of the experimental method and results. A detailed description may be found in Frocht (1941).

In general, a photoelastic model consists of a plate of isotropic plastic which has been cut to the shape of the prototype. The model is then loaded and observed in a polariscope. The isotropic plastic becomes temporarily doubly-refracting when stressed and the amount of bire-

fringence is proportional to the magnitude of the shear stress. Under certain light conditions, the points of equal shear stress appear dark. Lines composed of these points are called interference fringes. As the model is loaded several interference fringes may emanate from a point of high stress. The fringes are consecutively numbered as they emerge and this number is called the order, n, of the interference fringe. The magnitude of the principal stress difference is given by

$$\sigma_3 - \sigma_1 = F.C. \frac{n}{t} \qquad \text{(Equation 1)}$$

where F.C. = fringe constant of the material and
t = thickness of the model.

The absolute value of the tangential stress at a boundary may be determined from Equation 1, since the normal stress is zero.

The photoelastic plastic also appears dark if the transmission planes of the polarizer and analyzer of the polariscope are parallel, respectively, with the principal stress directions. The lines composed of these dark points are called isoclinics. The complete isoclinic pattern is obtained by simultaneously rotating the analyzer and polarizer by small increments, e.g., 10 degrees, and mapping the isoclinics at each position.

It is convenient to choose a material of low fringe constant when mapping interference fringes in order to avoid the necessity of high loads. On the other hand, it is convenient to choose a material of high fringe constant when mapping isoclinics to minimize or eliminate the presence of interference fringes which tend to obscure the isoclinics. In this investigation identical models were cut from Columbia resin (No. 39) and plexiglass, to study, respectively, interference fringes and isoclinics.

Cracks were represented by slots which consisted of parallel sides and semicircular ends. Slots were chosen in preference to ellipses to facilitate preparation. Bombolakis (1963) showed that the stress around a slot is nearly the same as the stress around an elliptical hole in the region of the tensile stress concentration.

Two-slot arrays were used to study the influence of the relative position of cracks on the magnitude of the maximum tensile stress of a crack. The parameters necessary for describing a two-slot array are shown in Figure 1. The length and width of the slots are a, and b, respectively. The distance between the centers of curvature of the nearest ends of the two slots is d. Ψ is the inclination from vertical of the long axis of the slot and ϕ is the inclination from vertical of the line joining the centers of curvature of the nearest ends of the two slots. Negative values of ϕ are measured clockwise.

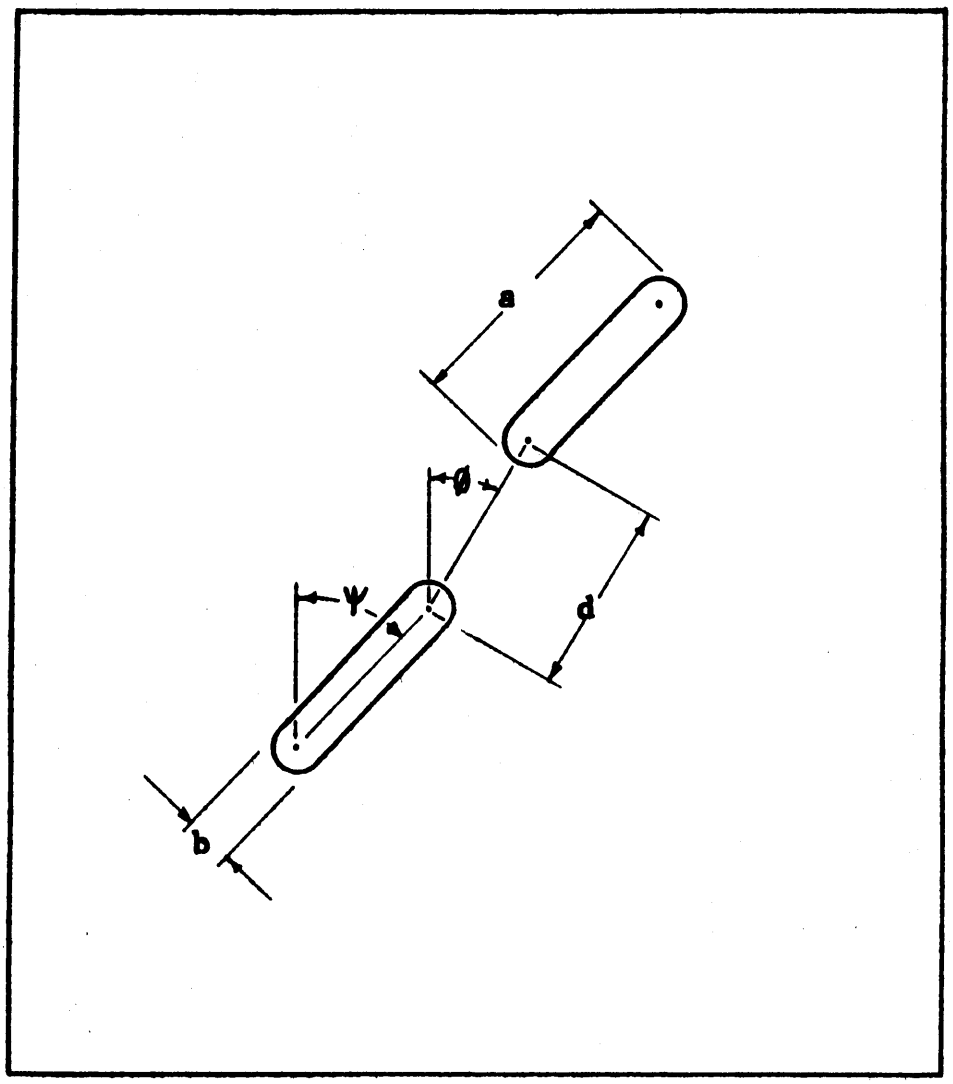

Parameters Used in Describing the Geometry
of a Two-Slot Array

Figure 1

The plate was placed in a loading frame designed to apply a uniform compressive stress along the horizontal edges of the model. For a description of the loading frame, see Bombolakis (1963, Appendix B, p. 8). Each plate was calibrated by recording the loads at which a fringe emerged from the two points on the horizontal diameter of a circular hole. The magnitude of the compressive stress at such points is three times the applied compressional stress, (Timoschenko and Goodier, 1951). A straight line was obtained by plotting load vs fringe order. The slope of this line is denoted by $(\frac{P}{n})_{circle}$. A slot was then cut which included the calibration circle and the plate was again loaded. The load was recorded as the fringes emerged from the points of maximum tension. The approximate location of the maximum tensile stress on the boundary of an inclined slot in a plate subjected to uniaxial compression is shown in Figure 2. The tensile stress concentration factor of the slot, K, was found according to

$$K = \frac{(3)(\frac{P}{n})_{circle}}{(\frac{P}{n})_{slot}} \quad , \qquad \text{(Equation 2)}$$

where $(\frac{P}{n})_{slot}$ = slope of load vs fringe order for the slot.

An additional slot was then cut to form the two-slot array and the K of the array was determined. Several arrays

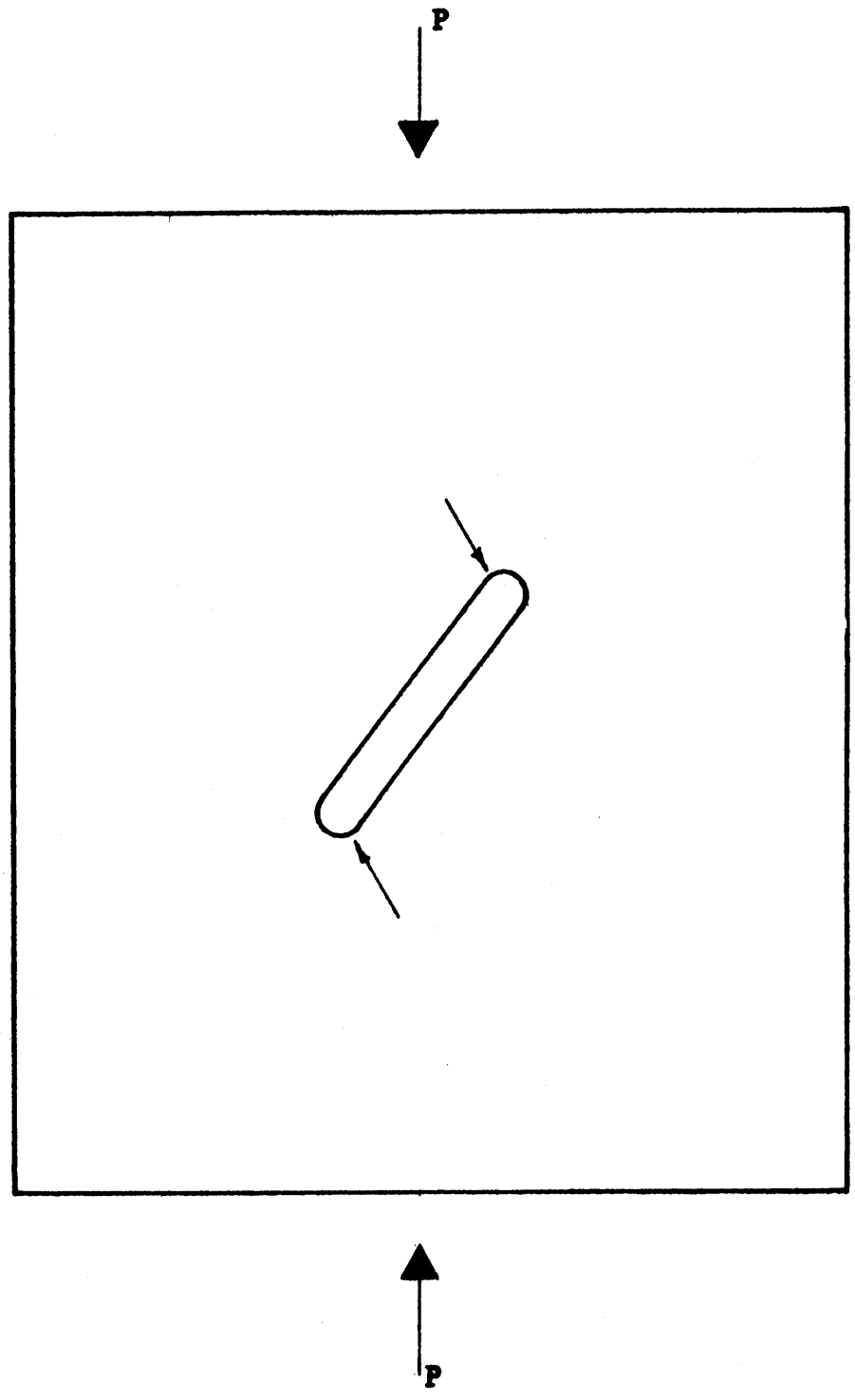

Points of Maximum Tensile Stress on an Inclined Slot in a Plate Subjected to Uniaxial Compression

Figure 2

were studied from one plate by alternately enlarging the slots and plotting load vs fringe order.

The isoclinic pattern was found by tracing the isoclinics at each ten-degree interval. The stress trajectories were found by placing a piece of tracing paper over the isoclinic pattern and drawing the stress directions as dictated by the isoclinics.

Experimental Results

The value of K for the isolated slots was determined photoelastically for comparison with K when the slots are in an array. The results are presented in Table 1. The uncertainty of $\pm$13 per cent was determined by comparing the ratio of the stress concentration factors at the points on the horizontal and vertical diameters of the circular hole.

The value of K was determined for about 50 different two-slot arrays. In these tests a varied from $\frac{1}{2}$ to $\frac{9}{8}$ inches, b from $\frac{1}{8}$ to $\frac{3}{16}$ inches and ϕ from 10 to -50 degrees. ψ and d were held constant at 35 degrees and $\frac{15}{32}$ of an inch, respectively. The dimensions were chosen to give the maximum possible number of arrays and yet restrict the overall size of the array. The value of 35 degrees was chosen as representative of the most critical orientation for the range of $\frac{a}{b}$ studied (Appendix I).

TABLE 1

Stress Concentration Factor of Isolated Slots

$\frac{a}{b}$	K
4	1.26 ± 0.16
5	1.60 ± 0.21
6	1.95 ± 0.25
7	2.13 ± 0.28

The results of the photoelastic tests of the two-slot arrays are presented in Table 2. The values of $\underline{a}$, $\underline{b}$, and $\frac{a}{b}$, are presented in the first three columns. The values of K for the arrays of different $\underline{\phi}$ are presented in the first half of each succeeding column. Normalized K, K_N, is found by dividing the K of the array by the K of the isolated slot. K_N was tabulated to provide a convenient comparison of the effect of neighboring slots on the K of a slot for different values of $\underline{\phi}$.

The variation of K with $\underline{\phi}$ for different values of $\frac{a}{b}$ is shown in Figure 3. In each case $\underline{b}$ was $\frac{1}{8}$ of an inch. The maximum value of K consistently occurred at about $\underline{\phi}$ = -20 degrees.

The smallest distance between two slots was (d - b). In order to determine if the relationship between K_N and (d - b) followed the same rule as the decrease in stress with distance from a crack (Irwin, 1958), the values of K_N were plotted against $(\frac{a}{d - b})^{0.5}$. This is shown for $\underline{\phi}$ equal to -20 and -30 degrees in Figure 4. The behavior of K_N $\underline{vs}$ $(\frac{a}{a - b})^{0.5}$ was approximately linear for all values of $\underline{\phi}$ and the slopes of the straight lines drawn through the points are presented in Table 3.

One set of the stress trajectories for an isolated slot of $\frac{a}{b}$ = 6 and $\underline{\Psi}$ = 35 degrees is shown in Figure 5. The stress trajectories for a two-slot array with $\frac{a}{b}$ = 6, $\underline{\phi}$ = -20 degrees and $\underline{\Psi}$ = 35 degrees are shown in Figure 6.

TABLE 2

Stress Concentration Factor of Two-Slot Arrays

a	b	$\frac{a}{b}$	ø = 10		ø = 0		ø = -10		ø = -20		ø = -30		ø = -40		ø = -50	
			K	K_N	K	K_N	K	K_N	K	K_N	K	K_N	K	K_N	K	K_N
$\frac{1}{2}$	$\frac{1}{8}$	4	1.11	0.88	1.13	0.89	1.39	1.10	1.82	1.44	1.73	1.37	1.67	1.32	1.53	1.21
$\frac{5}{8}$	$\frac{1}{8}$	5	1.37	0.68	1.55	0.97	1.88	1.17	2.06	1.39	1.94	1.21	1.75	1.09	1.53	0.96
$\frac{3}{4}$	$\frac{1}{8}$	6	1.57	0.80	1.93	0.99	2.14	1.10	2.53	1.30	2.32	1.19	1.77	0.91	1.58	0.81
$\frac{7}{8}$	$\frac{1}{8}$	7	1.90	0.89	1.84	0.86	2.35	1.10	2.84	1.33	2.87	1.35	2.02	0.95	1.82	0.85
$\frac{15}{16}$	$\frac{5}{32}$	6	2.28	1.17	2.57	1.32	2.68	1.37	3.09	1.57	2.82	1.45	2.38	1.22	2.06	1.06
$\frac{35}{32}$	$\frac{5}{32}$	7	2.70	1.27	3.20	1.50	2.97	1.40	3.06	1.44	2.53	1.19	2.63	1.23	---	---
$\frac{9}{8}$	$\frac{3}{16}$	6	1.32	1.32	3.00	1.54	3.00	1.54	3.52	1.81	3.28	1.68	2.79	1.43	2.28	1.17

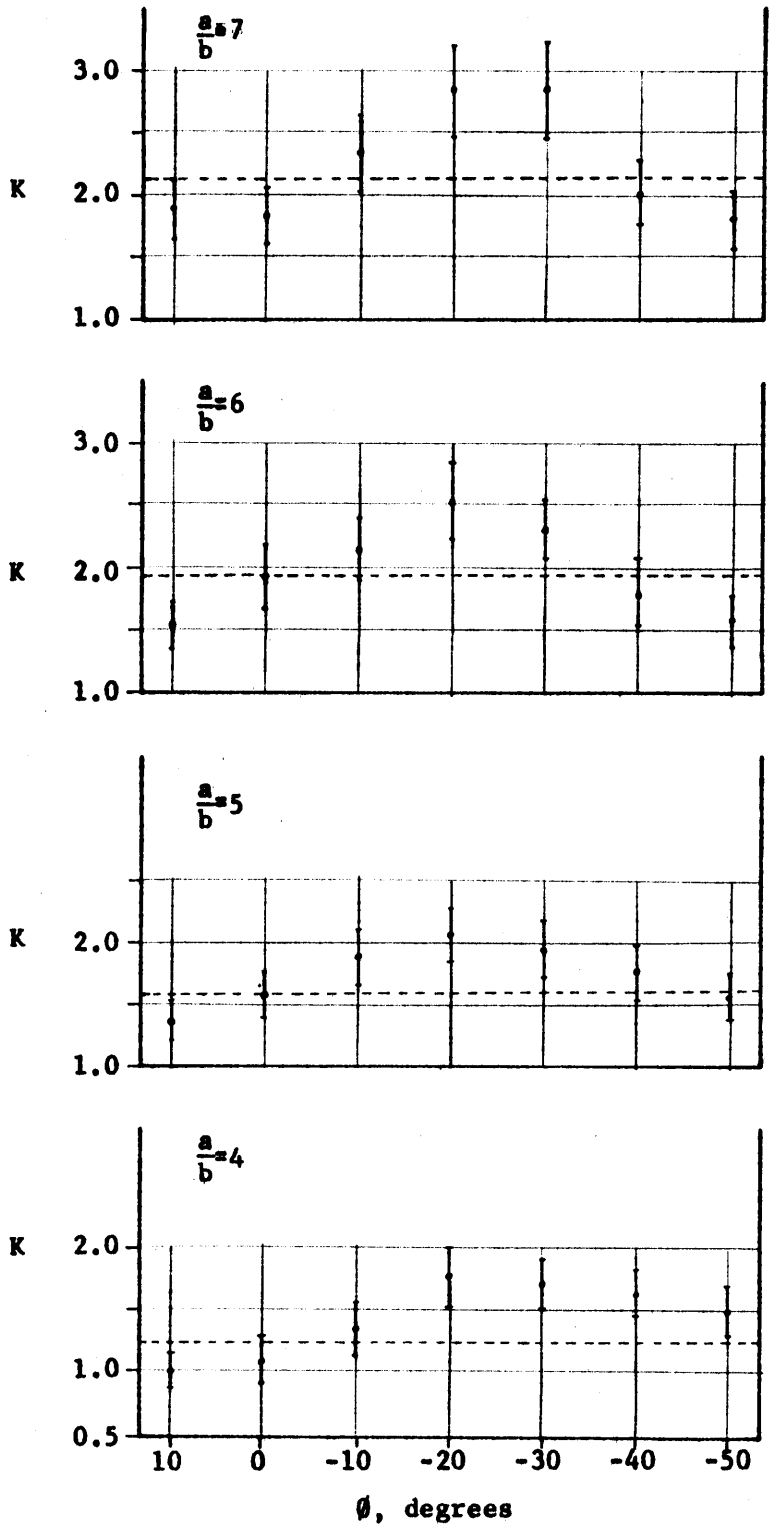

Stress Concentration Factor, K, vs Ø

Dashed Line is K for Isolated Slot
Vertical Bars Indicate Maximum Error

Figure 3

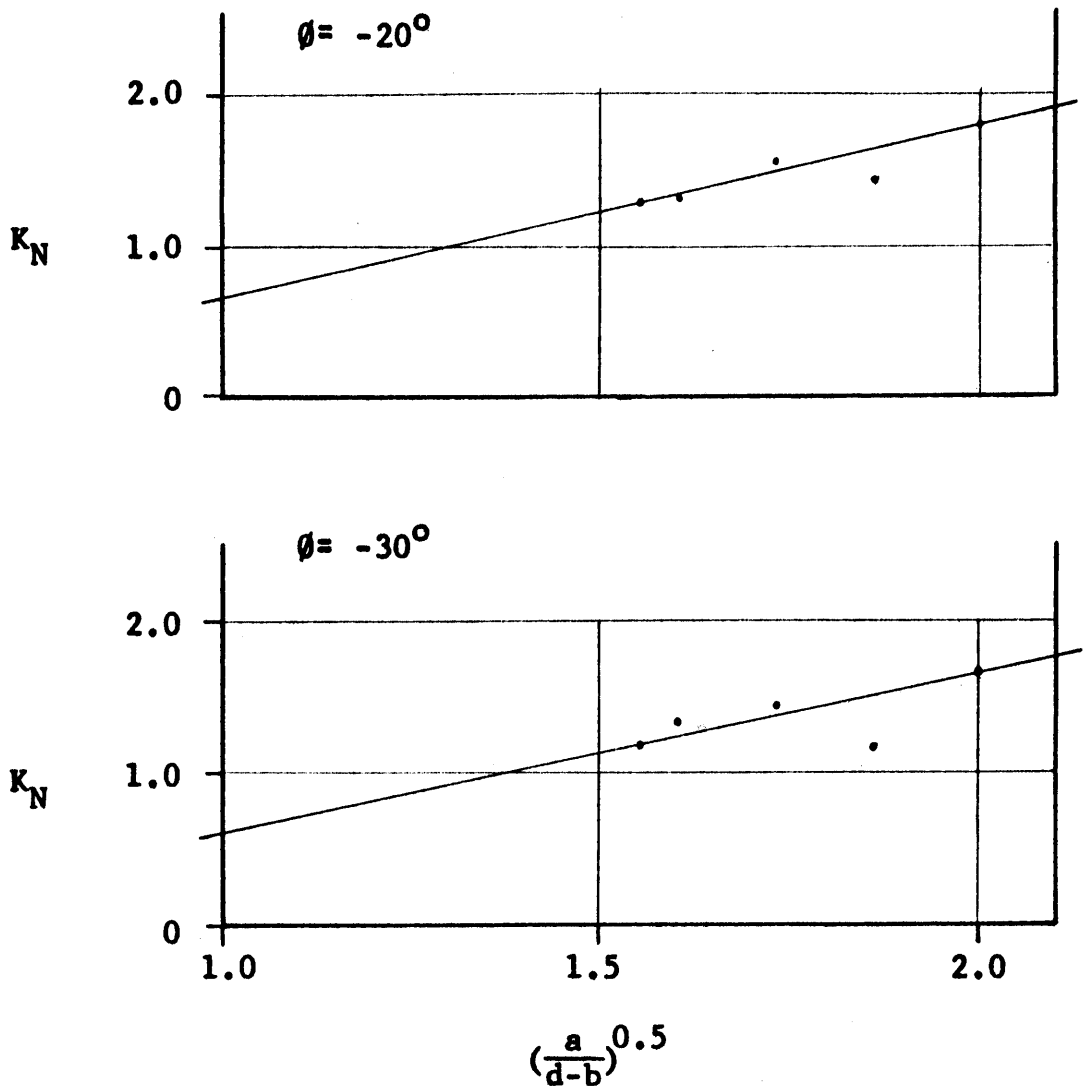

Normalized K vs $(\frac{a}{d-b})^{0.5}$

Figure 4

TABLE 3

Slope of K_N vs $\left(\frac{a}{d - b}\right)^{\frac{1}{2}}$

ϕ	Slope
10^o	0.55
0^o	0.68
-10^o	0.50
-20^o	0.57
-30^o	0.52
-40^o	0.55
-50^o	0.44

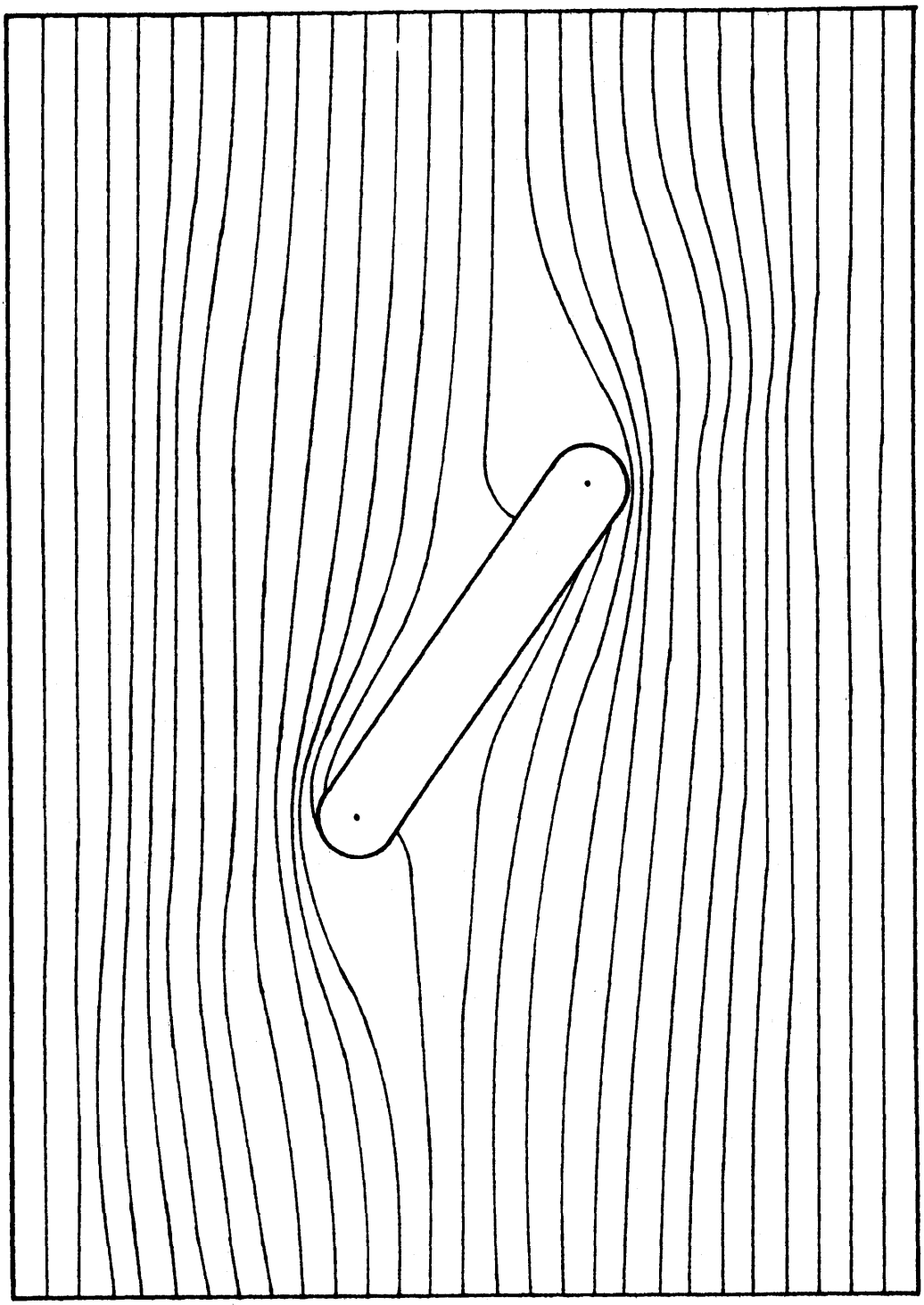

Stress Trajectories

$\frac{a}{b}=6, \ \Psi=35^{o}$

Figure 5

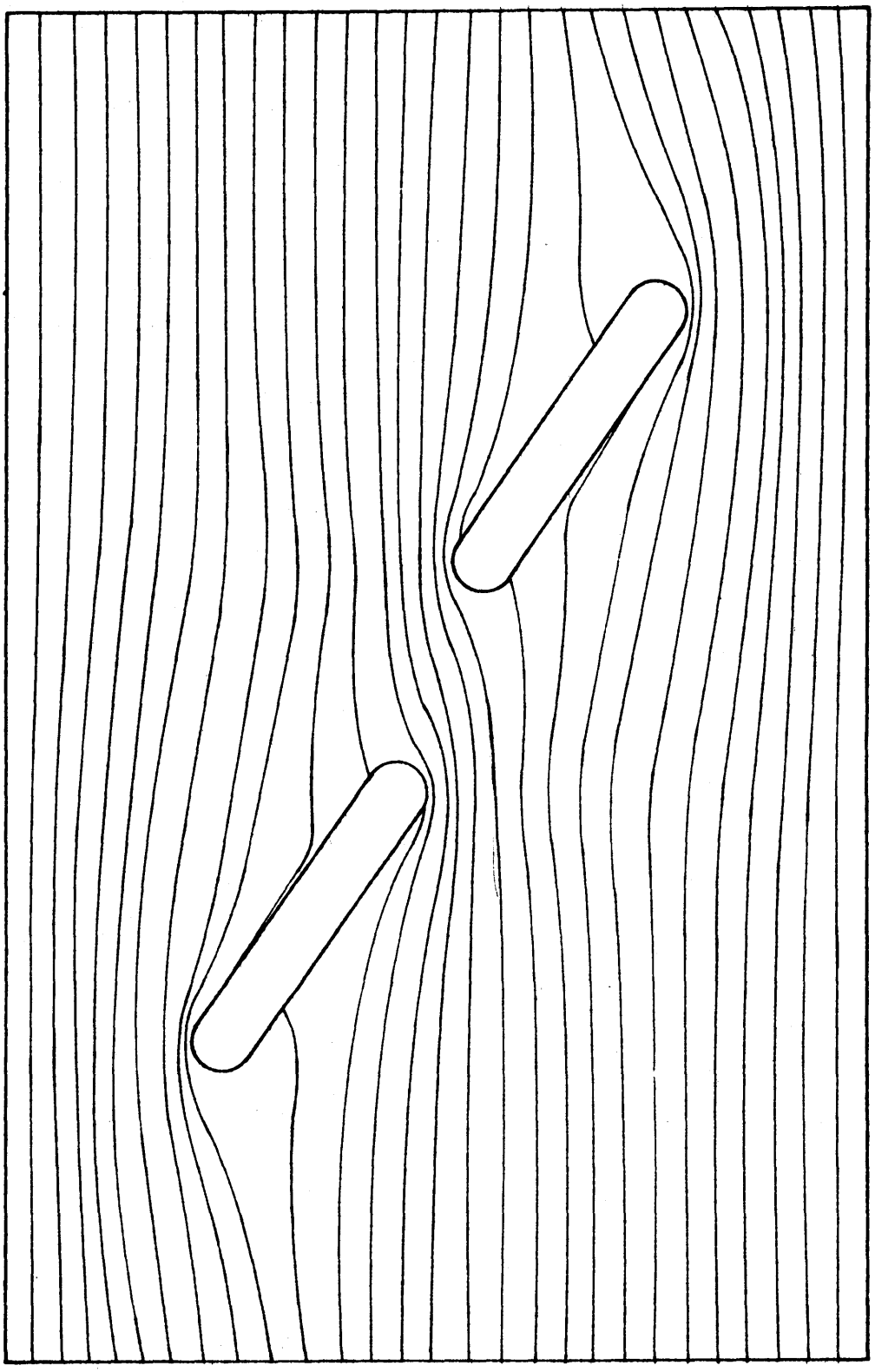

Stress Trajectories

$\frac{a}{b}=6$, $\phi=-20^{\circ}$, $\Psi=35^{\circ}$

Figure 6

Discussion of Experimental Results

The increase in relief, with increasing $\frac{a}{b}$, of the plots presented in Figure 3 and the consistent maximum at $\not{\alpha}$ = -20 degrees suggests that the most critical array of actual cracks of high $\frac{a}{b}$ may be an en échelon arrangement with $\not{\alpha}$ equal to about -20 degrees. Simple superposition of the stress states around a rectangular opening of $\frac{a}{b}$ = 5 and Ψ = 30 degrees (Savin, 1961) indicates that the most critical orientation is somewhere between $\not{\alpha}$ = -20 degrees and -30 degrees, but this is probably coincidental since the stress conditions around a two-slot array are not, in general, the sum of the individual stress states.

The decrease in K when $\not{\alpha}$ is positive agrees with the results of Bombolakis (1963). This behavior, i.e., a decrease in K when overlap occurs, suggests that a partial fracture, which is composed of a few connected cracks, tends to decrease K of cracks which it overlaps and therefore decreases their chance of propagating.

The plots of K_N vs $(\frac{a}{d - b})^{0.5}$ do not follow the relationship found by Irwin (1958) for the decrease in stress with distance from the end of a crack. This is not surprising since Irwin stated that the relationship was true only if the distance were small compared to the radius of curvature of the crack tip. However, the plots of K_N vs $(\frac{a}{d - b})^{0.5}$ are approximately linear, especially for

$\frac{a}{b}$ = 6 and 7, and the slope of the straight lines for the different $\not{\alpha}$ values are more or less consistent (Table 3). It is expected that the slope will decrease for decreasing $(\frac{a}{d - b})$ since the value of K_N must equal unity when the cracks are isolated.

For $\frac{b}{d}$ = 0.27, the value of K for the most critical arrays, i.e., $\not{\alpha}$ = -20 degrees, was about 35 per cent greater than for an isolated slot. This increase was apparently independent of the $\frac{a}{b}$ ratio. This suggests that actual cracks in such arrays would propagate when the applied stress is about 75 per cent of that required to cause growth of an isolated crack.

Comparison of the stress trajectories, shown in Figures 5 and 6, indicates that the directions of the principal stresses in the vicinity of a slot in an array were only slightly different than when the slot was isolated. This may be a reason why Bombolakis (1963) found that the direction of crack growth was not influenced by the proximity of other cracks.

UNIAXIAL COMPRESSION TESTS

Introduction

It was decided that partially-fractured samples should be obtained to study the growth of cracks leading to fracture. A considerable amount of crack growth occurs during the final stress increments and it is very important that the press-rock system remain stable so that intact specimens may be obtained. This stability was achieved by incorporating a stiffening element into a conventional hydraulic press. The stiffening element, which was a simply-supported beam, was placed in parallel with the rock specimen as shown in Figure 7. The beam was designed to carry most of the applied load and to limit the advance of the ram during fracture, (Appendix 2). There is a limit to how closely one may approach fracture. Any system of finite stiffness would become unstable when the slope of the decreasing portion of the load vs deflection curve for the sample is greater than the load vs deflection curve of the entire system, (Appendix 3).

The samples used in this study were simplified modifications of those used earlier, (Brace, 1964), and consisted of cylinders with a reduced central section (Appendix 4).

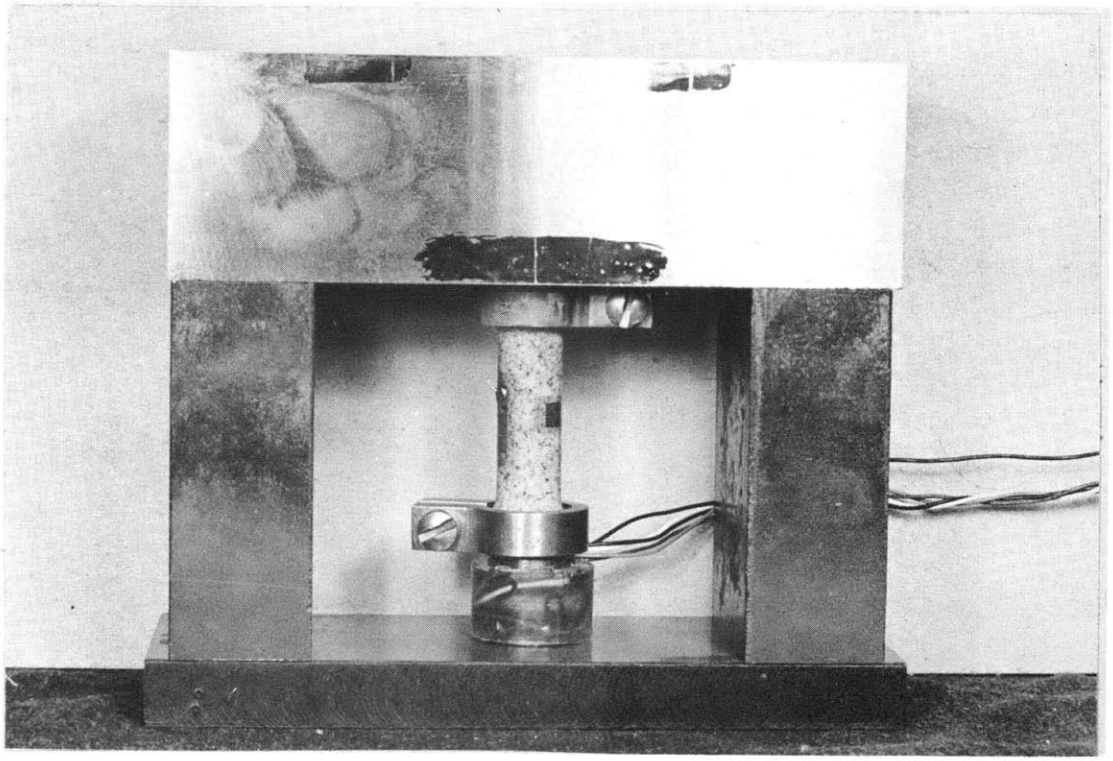

Sample in Parallel with Stiffening Element

Figure 7

Shaped samples were chosen in preference to the common straight cylinders to avoid the barrelling and fractures induced by the elastic mismatch at the ends of the specimen (Seldenrath and Gramberg, 1958, Salmassy, et al., 1955).

Experimental Procedure

Two strain gages were placed on each sample, one parallel with, the other normal to, the direction of applied compression. In the initial uniaxial compression tests, the heads of the sample failed along a vertical fracture which passed through the fillets. In the subsequent tests, steel rings, as shown in Figure 7, were positioned around the heads of the sample to prevent the premature failure. The sample was placed on a load cell and the stiffening element was positioned between the hydraulic ram and the specimen. The load cell consisted of a short cylinder of hardened steel to which four strain gages had been attached. It was calibrated to give the load on the sample in terms of the resistance changes of the strain gages, (Appendix 5). The stiffening element is only of value during the later stages of the fracture process. Therefore, in order to minimize the total force exerted by the ram, the sample was ground to a final length such that the steel beam did not come in contact with the steel supports until the rock had been stressed to about 75 per cent of its fracture strength.

The leads from the load cell and the two strain gages mounted on the specimen were connected to a three-channel recording system which gave a graphic trace of strain vs load, (Appendix 6). A convenient scale of the graphical tracing was obtained by calibration of the recorder prior to each test.

The stress was applied by manually pumping the hydraulic ram. Since it was felt that the growth of cracks might be time-dependent, the stress application during most tests was interrupted at various stress levels for periods of about five minutes.

The stress was decreased when excessive lateral strain and pronounced surface cracks indicated that fracture was impending. A plastic tube, slightly shorter than the steel supports, was positioned around the sample to protect the observer in the event of an explosive fracture.

Experimental Results

The experimental results of the uniaxial compression tests are grouped according to the manner in which the test was performed and the resulting deformational characteristics of the sample. The three groups, in order of presentation, consist of the results of (1), discontinuous tests, i.e. the stress was held nearly constant at various stress levels

for a few minutes; (2), cyclic tests, where each cycle went to a higher stress; and (3), tests which indicate the effect of strain rate.

Discontinuous Tests

In these tests the sample was continuously stressed to somewhat greater than one-half the fracture strength before the stress was held essentially constant for five-minute periods. The stress was then further increased by an arbitrary amount and again held nearly constant. This process was continued for some samples to just below the fracture strength. The load was then decreased discontinuously, the waiting periods occurring at the same stress levels as during the stress build-up.

A typical example of the stress-strain curves obtained from samples tested in this manner is shown in Figure 8. Both the lateral and axial strain are plotted as a function of stress.

The deformation which occurred during the five-minute waiting periods is represented by the rather large lateral strains at nearly constant stress and the relatively small axial strain. As the fracture strength was approached, the lateral strain increased rapidly with stress whereas the axial strain retained a relatively near-linear relationship

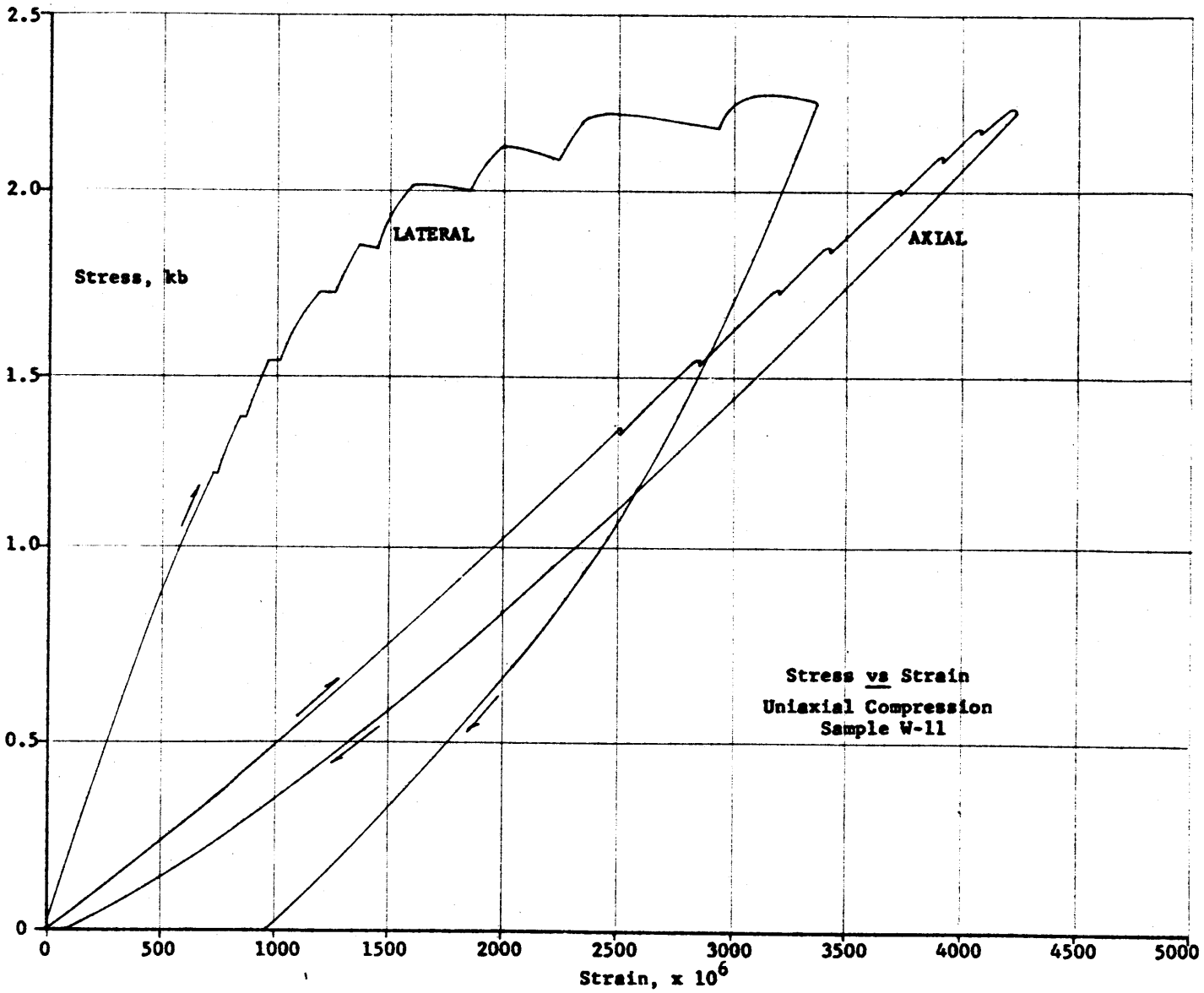
2.5
2.0
1.5
1.0
0.5
0
Stress, kb
LATERAL
AXIAL
Stress vs Strain
Uniaxial Compression
Sample W-11
0
500
1000
1500
2000
2500
3000
3500
4000
4500
5000
Strain, x 10^6

Figure 8

with stress. On the return curve, i.e., decreasing stress, there was essentially no detectable time-dependent deformation. After the stress had been completely removed, there was a substantial permanent lateral strain (about 0.1 per cent or of the order of one-third the maximum lateral strain), but little or no permanent axial strain.

The volumetric strain, $\frac{\Delta V}{V}$, was calculated from the axial and lateral strains. In this study, the lateral strain gages extended nearly halfway around the circumference of the sample. This is necessary for determining the volumetric strain of an anisotropic material, (Appendix 7). The plot of volumetric strain vs uniaxial compressive stress corresponding to the stress-strain diagram of Figure 8 is presented in Figure 9.

In general, the volume decreased rather rapidly during the initial stress build-up and then decreased at a rather constant rate with stress up to about 50 per cent of the fracture strength. From this point, to about 75 per cent of the fracture strength, the rate of volume decrease decreased with increasing stress. At about 75 per cent of the fracture strength, the volume was a minimum. It then increased with further increase in the applied stress. At just below the fracture strength the volumetric strain passed through zero and became positive. The greater part of this increase in volume was retained when the stress was

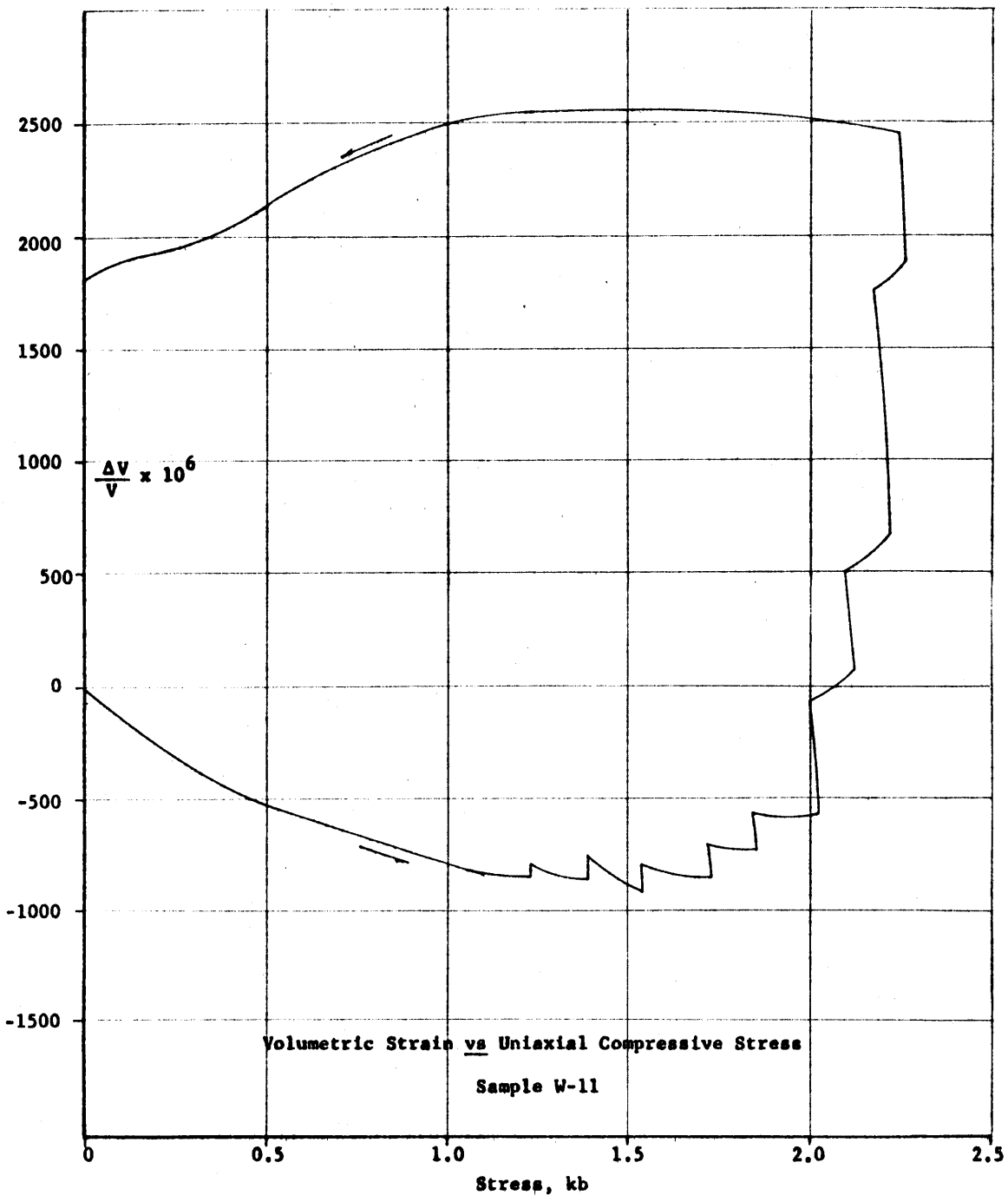
2500
2000
1500
1000
500
0
-500
-1000
-1500
$\frac{\Delta V}{V} \times 10^6$
0
0.5
1.0
1.5
2.0
2.5
Stress, kb
Volumetric Strain vs Uniaxial Compressive Stress
Sample W-11

Figure 9

TABLE 4

Results of Discontinuous Uniaxial Compression Tests

Sample	Maximum Stress (kb)	Maximum Young's Modulus (mb)	Slope of Linear Portion of $\frac{\Delta V}{V}$ vs σ_3 (mb^{-1})	Permanent Volumetric Strain ($\times 10^{-6}$)	Stress at Departure From Linearity (kb)
W-8	1.52	0.580	0.64	225	0.90
W-9	1.07	0.562	0.79	50	0.95
W-11	2.28	0.582	0.60	1800	1.10
W-12	2.28	0.568	0.76	1600	1.15
W-14	2.18	0.576	0.71	1800	0.92
		(0.574 ± 0.012)	(0.70 ± 0.10)		(1.00 ± 0.15)

completely removed. At stresses greater than that at which the plot of $\frac{\Delta V}{V}$ vs σ_3 departs from the linear portion, there was a pronounced increase in volume during the five-minute waiting periods.

The results of the discontinuous uniaxial compression tests are presented in Table 4. The maximum error, (Appendix 8), of the maximum stress and maximum Young's modulus are about 2 and 4 per cent, respectively. The maximum error of the slope of the linear portion of $\frac{\Delta V}{V}$ vs σ_3 and the permanent volumetric strain are about 8 and 6 per cent, respectively. The maximum error of the stress at the departure of the $\frac{\Delta V}{V}$ vs σ_3 curve from linearity is approximately 10 per cent.

Cyclic Tests

In these tests the sample was discontinuously stressed to a certain magnitude and then unloaded. It was then again stressed in similar manner but to a greater stress. This cyclic procedure was repeated until the sample had been stressed to about 90 per cent of the fracture strength. Figure 10 are the stress-strain curves obtained from these cyclic tests. Both the axial and lateral strain were recorded as a function of stress.

The volumetric strain was computed from the axial and lateral strains. The plots of $\frac{\Delta V}{V}$ vs σ_3 are presented in Figure 11.

All the plots of $\frac{\Delta V}{V}$ vs σ_3 show a rather rapid decrease in volume during the initial stress build-up. After this rapid decrease, the variation of $\frac{\Delta V}{V}$ vs σ_3 was essentially linear up to the maximum stress of the previous cycle. For example, the $\frac{\Delta V}{V}$ vs σ_3 plot for the cycle to 1.38 kb remains linear up to approximately 1.03 kb, the maximum stress to which the sample was previously cycled. The slope of the linear portion of the curves decreased markedly for the last two cycles.

During the stress release, the plots of $\frac{\Delta V}{V}$ vs σ_3 were linear during a substantial amount of the unloading portion of the curve. The last three cycles showed a pronounced permanent volumetric strain after the load was completely released.

The results of the cyclic uniaxial tests are presented in Table 5. The maximum errors, (Appendix 8), are the same as reported for the discontinuous uniaxial compression tests.

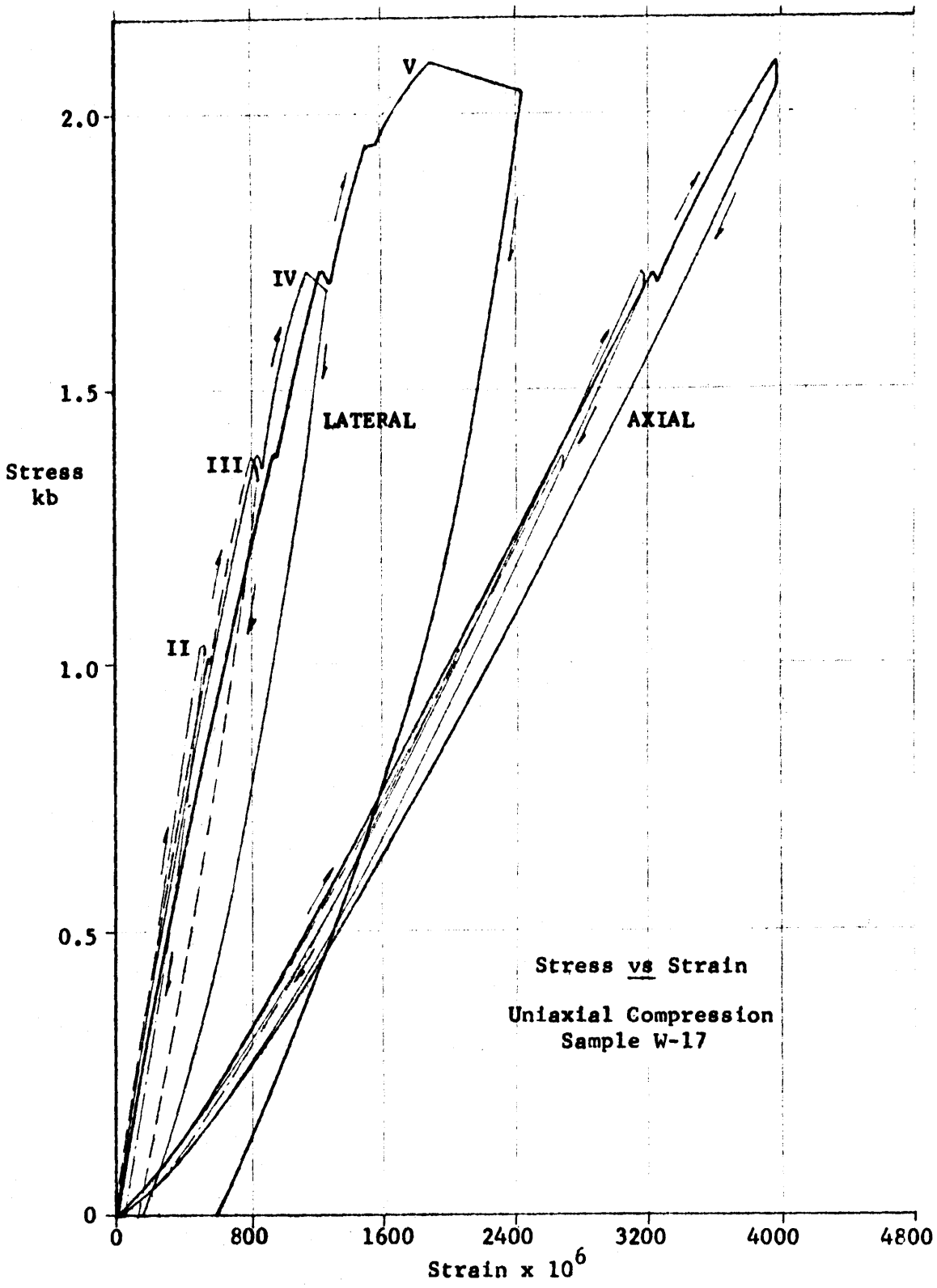

Axial strains are negative

Figure 10

TABLE 5

Results of Discontinuous Cyclic Uniaxial Compression Tests

Sample W-17

Cycle	Maximum Stress (kb)	Maximum Young's Modulus (mb)	Slope of Linear Portion of $\frac{\Delta V}{V}$ vs σ_3 (mb^{-1})	Permanent Volumetric Strain ($\times 10^{-6}$)	Stress at Departure From Linearity (kb)
1	0.69	0.558	---	50	---
2	1.03	0.572	0.74	100	---
3	1.38	0.565	0.74	160	1.0
4	1.72	0.593	0.47	350	1.3
5	2.11	0.558	0.30	1200	1.6
		(0.572 ± 0.021)			

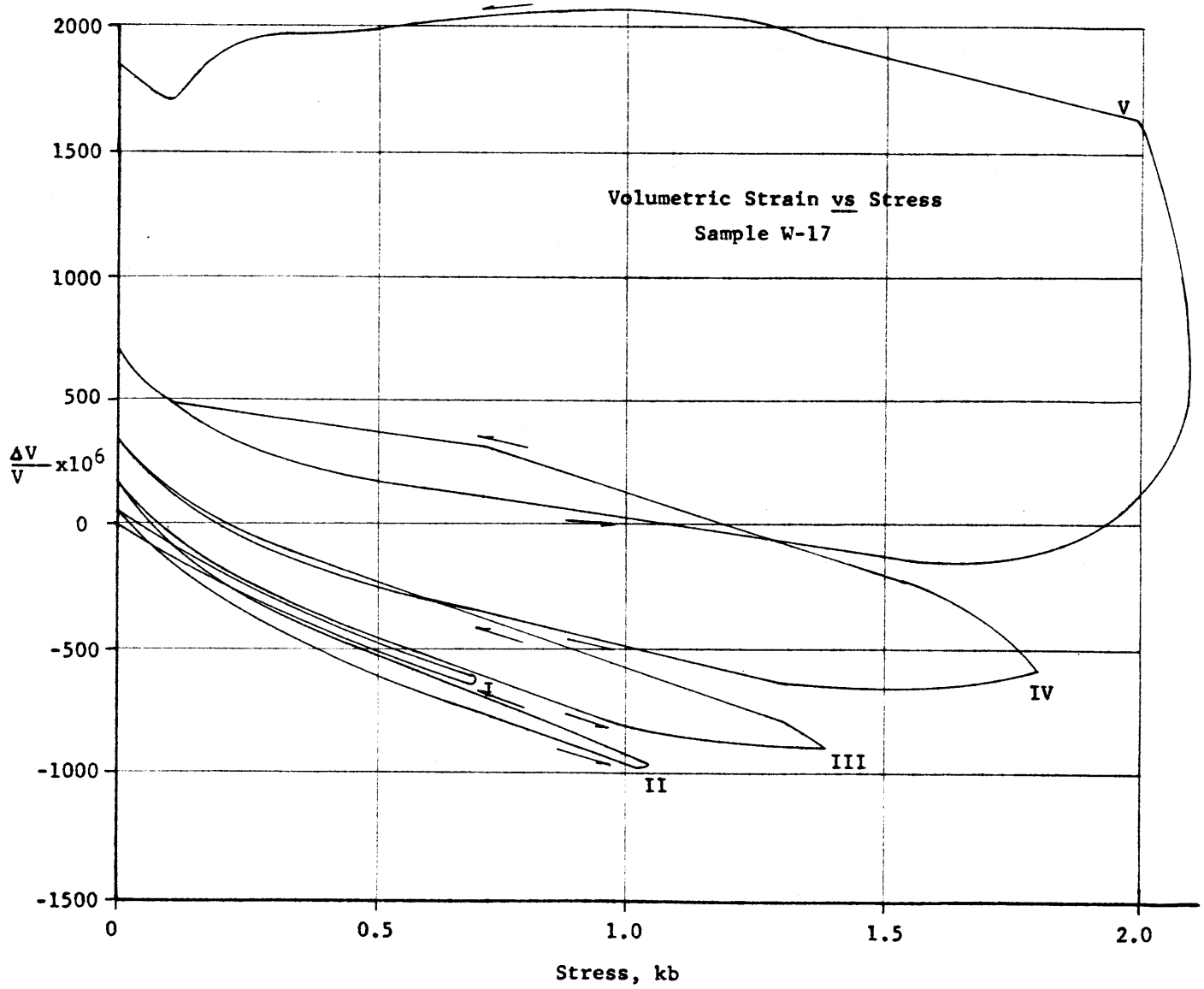
Volumetric Strain vs Stress
Sample W-17
2000
1500
1000
500
0
-500
-1000
-1500
ΔV/V x10^6
0
0.5
1.0
1.5
2.0
Stress, kb
I
II
III
IV
V

Figure 11

Tests Indicating Effect of Strain Rate

The stress vs strain and volumetric strain vs stress curves for the samples stressed discontinuously have been presented (Figures 10 and 11, respectively). For these tests, the average axial strain rate was about 10^{-4} min^{-1}. The $\frac{\Delta V}{V}$ vs σ_3 curves for a sample which was cyclically stressed at an axial strain rate of about 10^{-3} min^{-1} to ever-increasing values of the maximum stress are presented in Figure 12.

Compared with the pronounced hysterisis of the $\frac{\Delta V}{V}$ vs σ_3 curves for the discontinuous tests, the sample stressed at the faster strain rate experienced relatively little non-elastic deformation.

The results of the cyclic tests conducted at an axial strain rate of about 10^{-3} min^{-1} are presented in Table 6. The maximum errors, (Appendix 8), are the same as reported for the discontinuous uniaxial compression tests.

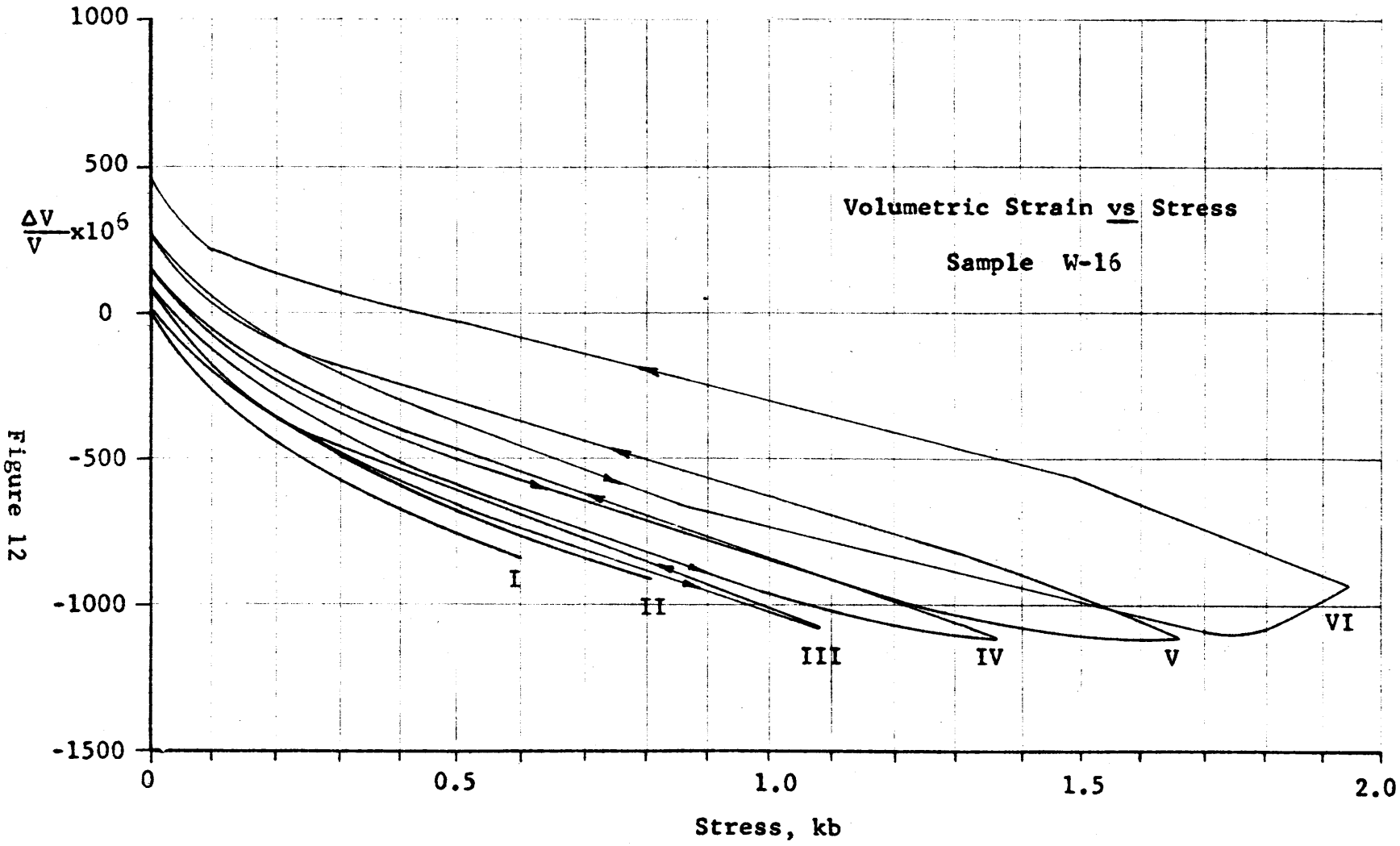
Volumetric Strain vs Stress
Sample W-16
$\frac{\Delta V}{V} x10^6$
1000
500
0
-500
-1000
-1500
0
0.5
1.0
1.5
2.0
Stress, kb
I
II
III
IV
V
VI

Figure 12

TABLE 6

Results of Continuous Cyclic Uniaxial Comprssion Tests

Sample W-16

Cycle	Maximum Stress (kb)	Maximum Young's Modulus (mb)	Slope of Linear Portion of $\frac{\Delta V}{V}$ vs σ_3 (mb^{-1})	Permanent Volumetric Strain ($\times 10^{-6}$)	Stress at Departure From Linearity (kb)
1	0.54	---	---	0	---
2	0.81	0.585	---	0	---
3	1.09	0.570	0.72	50	---
4	1.37	0.582	0.74	60	1.05
5	1.66	0.582	0.71	85	1.25
6	1.94	0.583	0.65	190	1.70
		(0.577 ± 0.008)			

Discussion of Experimental Results

The results of the uniaxial compression tests have provided insight into the stress at the onset of crack growth, the direction of propagation, and the effect of new cracks on the subsequent deformational behavior of the sample.

The discussion of the experimental results is divided into two parts. The first contains detailed interpretations of the stress vs strain and volumetric strain vs stress curves in terms of the mechanics of crack growth. This first section follows the same order of presentation as in the preceding section. The second part is a description of the thin and polished sections of the fractured specimens.

Discontinuous Tests

The stress-strain diagram , Figure 8, is characteristic of this type of test. The stress vs axial strain curves show a generally linear behavior, little or no permanent strain, and a moderate hysteresis loop. The stress vs lateral strain curves, on the other hand, show that the strain increased markedly with stress, especially near the fracture strength, and that there was a large hysteresis loop and permanent strain.

The characteristics of the volumetric strain vs stress diagram, shown in Figure 9, are felt to be significant and are interpreted as follows: Up to about 0.55 kb the volume decreased rather rapidly. This was due to the closing of cracks oriented so as to close under the applied stress. Similar effects due to the closing of cracks have been reported by various investigators: Brace (1965) explained the initially low value of Young's modulus and high compressibility, characteristic of certain rock types, as due to the closing of cracks under low values of the applied stress, and Birch (1961) accounted for the rapid increase in the velocity of sound with applied pressure as due to a decrease in porosity.

Above approximately 0.55 kb the variation of the volumetric strain with stress was essentially linear up to a stress of about 1.10 kb. Walsh (1965b) has studied the case of an isotropic crack-filled solid. When such a material is stressed uniaxially, one does not obtain the intrinsic values of Young's modulus and Poisson's ratio because of the frictional sliding of opposing crack faces. However, according to Walsh's analysis, the volumetric strain experienced by the sample during a uniaxial stress increase is one-third that experienced by the intrinsic material during a bulk compressibility test when the confining pressure was increased by the same amount. The intrinsic bulk

compressibility of Westerly granite is about 2 mb^{-1} (Brace, 1965). Therefore, the slope of the linear portion of the $\frac{\Delta V}{V}$ vs σ_3 plot should have a slope equal to 0.66 mb^{-1}. The average of the slopes for 5 tests was 0.70 ± 0.10 mb^{-1}, (Table 4).

The onset of crack growth occurred at the point where $\frac{\Delta V}{V}$ vs σ_3 departed from the linear portion of the curve. For the Westerly granite, the average value of the axial stress at the onset of crack growth was 1.00 ± 0.15 kb or roughly 50 per cent of the fracture strength. This fact has important implications with regard to the Griffith theory of fracture. The Griffith theory or its present modification (McClintock and Walsh, 1962) cannot be expected to predict the compressive strength of materials if crack growth occurs in such materials at stresses less than the fracture strength.

As the stress was increased, the departure of the $\frac{\Delta V}{V}$ vs σ_3 curve from the tangent to the linear portion increased. Thus, crack growth continued as the stress was raised. The fact that the growth of cracks was time-dependent was established by noting the increase in volume during the five-minute intervals of essentially constant stress. In room temperature tests on silicate materials, such as Westerly granite, this increase in volume could only be accounted for by the growth of cracks (Christie et al., 1964).

As the fracture strength was approached, the volume increased rapidly with increasing stress. This volume increase represents the increase in the amount of crack growth which occurred prior to fracture.

There was a significant permanent increase in volume of the sample after the load had been completely removed. This was a result of the extensive crack growth which occurred during the deformation of the sample. Referring to the stress-strain diagrams, one notes that the permanent change in volume was almost entirely accounted for by a permanent increase in the cross-sectional area of the specimen, i.e., there was little or no permanent axial strain. This suggests that the predominant direction of crack growth was vertical, i.e., parallel to the direction of the applied stress. The fact that crack growth was vertical was established by performing a compressiblity test on the sample before and after the uniaxial test. It was found (Chapter III) that the linear compressibility in the axial direction was essentially unchanged but the lateral compressibility was much greater subsequent to the uniaxial test.

Cyclic Tests

The cyclic uniaxial test, with each cycle proceeding to a higher stress level than the preceding test, provided insight into the effect of crack growth on the deformational

behavior of the material. The stress vs strain diagrams, and the volumetric strain vs stress diagrams, are presented in Figures 10 and 11, respectively.

The maximum value of Young's modulus was computed from the slope of the stress vs axial strain diagrams. The maximum values of Young's modulus for each cycle are presented in Table 5. It is interesting to note that Young's modulus was nearly the same for each cycle even though extensive crack growth had occurred as shown by the plots of $\frac{\Delta V}{V}$ vs σ_3.

Unlike Young's modulus, certain characterisitics of the plots of volumetric strain vs stress changed with each cycle. As anticipated, from the results of the discontinuous tests, the plots of $\frac{\Delta V}{V}$ vs σ_3 for the cycles up to 0.69 and 1.03 kb indicated no crack growth. The $\frac{\Delta V}{V}$ vs σ_3 plot for the cycle up to 1.38 kb departed from the linear portion at approximately 1.0 kb, indicating the onset of crack growth. The plot of $\frac{\Delta V}{V}$ vs σ_3 for the next cycle, however, departed from the linear portion at the maximum stress to which the sample had been previously stressed, i.e., about 1.3 kb. Similarly, the curve for cycle to 2.11 kb departed from the linear portion at about 1.6 kb.

These results indicate that new crack growth did not occur until the previous maximum stress had been exceeded. Therefore, the average axial strain rate of about 10^{-4} min^{-1}

was slow enough to permit almost complete crack growth to occur at each stress level.

When the sample was stressed to a value less than required to initiate crack growth, the slope of the linear portion of the $\frac{\Delta V}{V}$ vs σ_3 curve is approximately equal to one-third the intrinsic bulk compressibility, (Table 5). However, once crack growth had occurred, the slope of the linear portion decreased with each cycle. This means that the lateral strains at each stress level (above approximately 0.55 kb) were greater than in the previous cycle.

The compressibility tests (Chapter III), performed between each of these uniaxial cycles, show that the new crack growth was essentially vertical, i.e., parallel to the direction of uniaxial compression, and that crack growth was more extensive at the conclusion of each subsequent cycle.

Thus, the evidence indicates that during the tests to 1.38 kb and above, the sample contained newly-formed vertical cracks which open during the stress build-up and that new crack growth did not occur until the maximum stress of the preceding tests had been exceeded.

The actual configuration of these vertical cracks is not absolutely clear. It is important in choosing a model for theoretical studies to know if the vertical cracks are

isolated or if they have grown out of inclined cracks as suggested by Brace and Bombolakis (1963). Observation of the thin and polished sections (presented later in this section) does not provide conclusive evidence. However, the plots of $\frac{\Delta V}{V}$ vs σ_3 suggest that some vertical cracks have grown out of inclined cracks. The evidence for this conclusion can be better appreciated after considering the deformation of these two types of cracks when subjected to a uniaxial compressive stress.

Consider first the case of an isolated crack which is parallel to the direction of the uniaxial compressive stress. For purposes of discussion, such a crack may be approximated as a narrow ellipse as shown in Figure 13.

Inglis (1913) has shown that the maximum lateral displacement, δ_L, of a crack so oriented is related to the crack dimensions, Young's modulus, and the applied stress according to

$$\delta_L = A\frac{\sigma}{E} \cdot \frac{b}{a} \quad ;$$

where A is a constant of proportionality of about unity.

The deformation of such a crack is completely reversible. If the difference between the actual and intrinsic volumetric strain during the linear portions of the $\frac{\Delta V}{V}$ vs σ_3 curves is a result of the opening of such cracks, then one

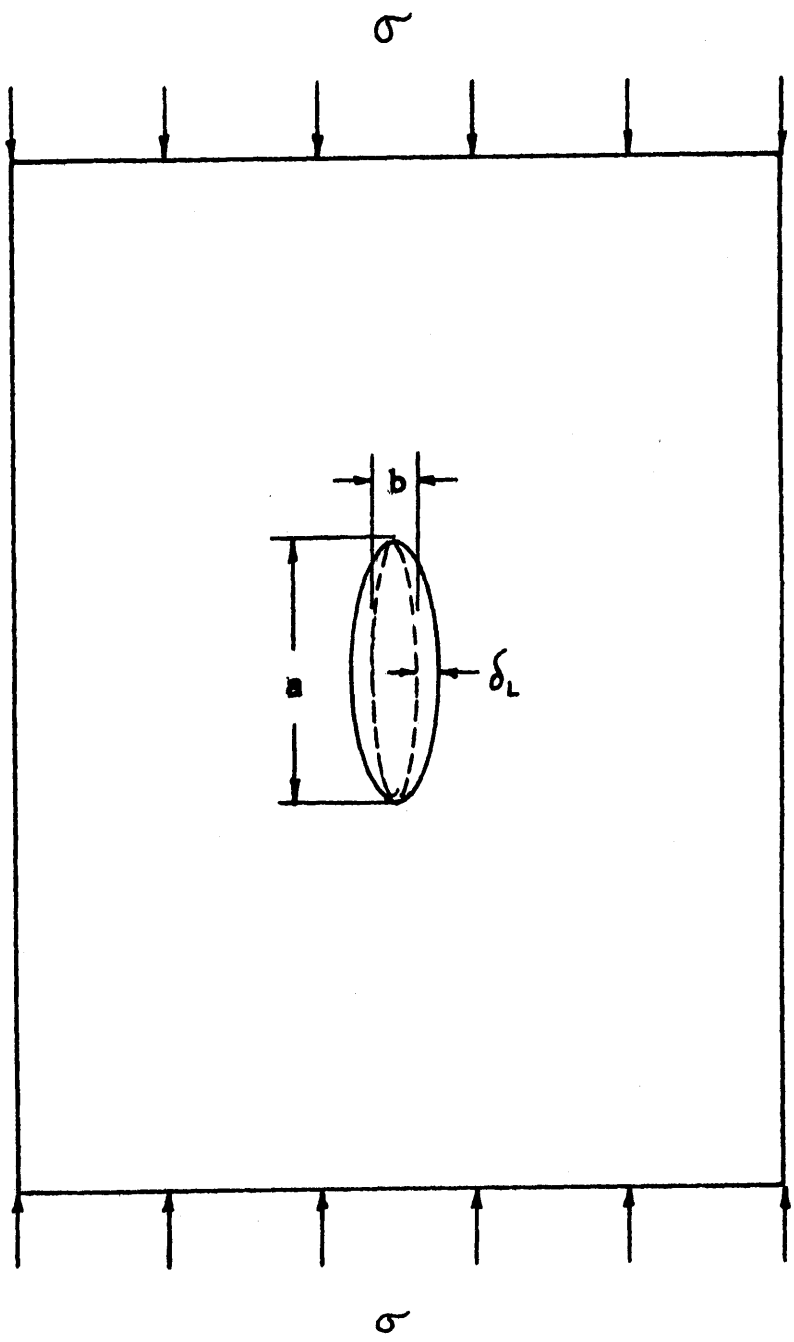

Elliptical Crack in Uniaxial Compressive Stress Field

Figure 13

would expect a smooth curve as the stress was released. In addition, the slope of the linear portion during increasing stress of each cycle should agree with the slope of the descending curve of the preceding cycle.

The second case, of vertical cracks which have grown out of inclined cracks, is more complex and no analytic solution exists which provides the deformation of such a crack when subjected to stress. When the applied stress is very small the inclined portion of such a crack would be open, (Figure 14a). As the stress is increased, the inclined portion of the crack closes until the crack surfaces are in frictional contact (Figure 14b). As the stress is further increased, frictional sliding may occur so that the vertical portions of the crack open, (Figure 14c). If the inclined portion is at an angle such that frictional sliding is impossible, the vertical portions of the crack might behave as isolated vertical cracks. The frictional stresses along the surfaces of the inclined crack change direction when the stress is released. As a result, the deformation of these cracks is not reversible simply by unloading and the vertical portions remain open at stresses less than that required to open them during the stress increase. Eventually the stress reaches a point at which the inclined portions of the crack open and the vertical segments are essentially as they were prior to the test. The permanent volumetric strain would be a result of the growth of new cracks and the incomplete closing of vertical cracks which had formed during an earlier cycle.

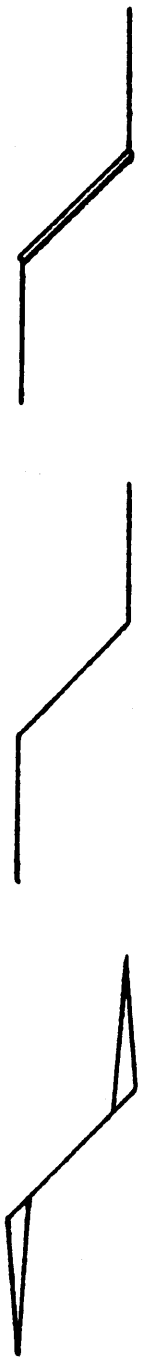

a.

b.

c.

Schematic Behavior of an Inclined Crack with Vertical Extensions Subjected to Uniaxial Compression

Figure 14

The plots of $\frac{\Delta V}{V}$ vs σ_3 (Figure 11) do not show the features which would be expected if the material contained only isolated vertical cracks. The slope of linear portions during increasing stress was generally greater than the slope of the descending curve of the preceding cycle and the curves during decreasing stress were not continuous, especially for the last two cycles. The frictional sliding associated with the inclined portion of the second type of crack would account for these characteristics.

Tests Indicating the Effect of Strain Rate

In general, the plots of $\frac{\Delta V}{V}$ vs σ_3 for the samples stressed at an axial strain-rate of about 10^{-4} min^{-1} show a hysteresis loop and permanent volumetric strain (Figures 9 and 11). These characteristics are much less pronounced during the tests at an axial strain rate of approximately 10^{-3} min^{-1} (Figure 13).

Direct comparison can be made between the results of the two samples which were cyclically stressed to ever-increasing values of the maximum stress. The results of the samples stressed at average axial strain-rates of 10^{-4} min^{-1} are presented in Tables 4 and 5, respectively. The effect of axial strain-rate on the extent of crack growth is indicated by the difference in slopes of the linear portions of the $\frac{\Delta V}{V}$ vs σ_3 curves and the permanent volumetric strain.

The slope of the linear portion of the $\frac{\Delta V}{V}$ vs σ_3 curves for the faster tests remained essentially constant. In contrast, the slope of the linear portions for the slower tests decreased markedly, especially after the third cycle. This decrease in slope is attributed to the opening of vertical cracks, either isolated or associated with inclined cracks, and indicates that crack growth was more extensive during the slower tests.

The maximum stress of the cycles at the different strain rates did not correspond exactly. However, it is apparent that a considerably greater amount of permanent volumetric strain occurred during the tests conducted at an average axial strain rate of 10^{-4} min^{-1}. This is additional evidence that crack growth was more extensive during the slower tests.

Description of Fractured Samples

After the uniaxial compression tests, the samples were cast into a mold (Stycast 1916) and sawed in half normal to the fracture surface so that both a thin section and a polished section could be obtained from each sample. In the partially fractured samples the orientation of the potential fracture surface was indicated by the surface cracks.

There was pronounced crack growth along the edge of the thin sections which corresponded to the region of the surface cracks observed during the test. However, it was impossible to distinguish between the crack growth which occurred during the test and that due to preparation of the thin section. There was no discernable crack growth in the central region of the partially fractured specimens.

The details of crack growth and partial fractures were best shown by the thin and polished sections of sample W-4. Even though the sample completely fractured, the polished end pieces clearly revealed the development of partial fractures, as shown in Figure 15. The zig-zag white lines are the partial fractures filled with polishing abrasive. The darkening of the sample in the region of the fracture is probably due to intrusion of the casting material. An enlarged view of the fracture region is shown in Figures 16 and 17.

Figure 16 is particularly interesting since it shows the development of two partial fractures approximately parallel with the fracture surface. In addition, the partial fractures and the fracture surface are roughly equally-spaced, reminiscent of parallel, equi-distant faults. The partial fractures are composed of inclined and near-vertical segments. The most common inclination, from vertical, of the inclined segments is about 40 degrees. On the whole, the inclined segments are <u>en échelon</u>.

Photographs of the thin section made from the other half of the end piece shown in Figure 16 are presented in Figure 18. They were obtained along a traverse of the two partial fractures. The direction of σ_3 is vertical. Exact correlation between the thin and polished sections cannot be expected because of the intervening material removed during sawing and polishing. Even so, agreement is good and indicates that the shape of the partial fractures did not change appreciably over a distance of about $\frac{1}{16}$ of an inch. This distance is equal to about three times the average grain diameter.

It can be seen that the partial fractures follow a rather tortuous path through and around the individual grains. The inclined segments are sometimes along grain boundaries as shown by the manner in which the partial fracture on the left passes around the grain in the upper third of Figure 18. The linear nature of the inclined trans-granular cracks suggests that they existed prior to the uni-axial test since we have no reason to assume that, in compression, a crack will grow in a direction other than nearly parallel with σ_3. This is shown, for example, by the manner in which the partial fracture on the right hand side passes through a grain in the lower third of Figure 18. Photographs of a partial fracture in sample W-16 are shown in Figure 19. The direction of σ_3 is vertical. Here, particularly, the inclined segments are trans-granular and linear.

One is restricted in drawing conclusions on the development of a fracture without knowledge of the third demension. However, the agreement between the thin and polished sections, with regard to the shape of the partial fractures, suggests that the views shown in Figure 18 are, in general, representative, at least for a distance of a few grain diameters.

For additional descriptions of fractured specimens the reader is referred to the Discussion of Experimental Results, Chapter IV. The interpretation of the features observed in the fractured material is presented in Chapter V, CONCLUSIONS.

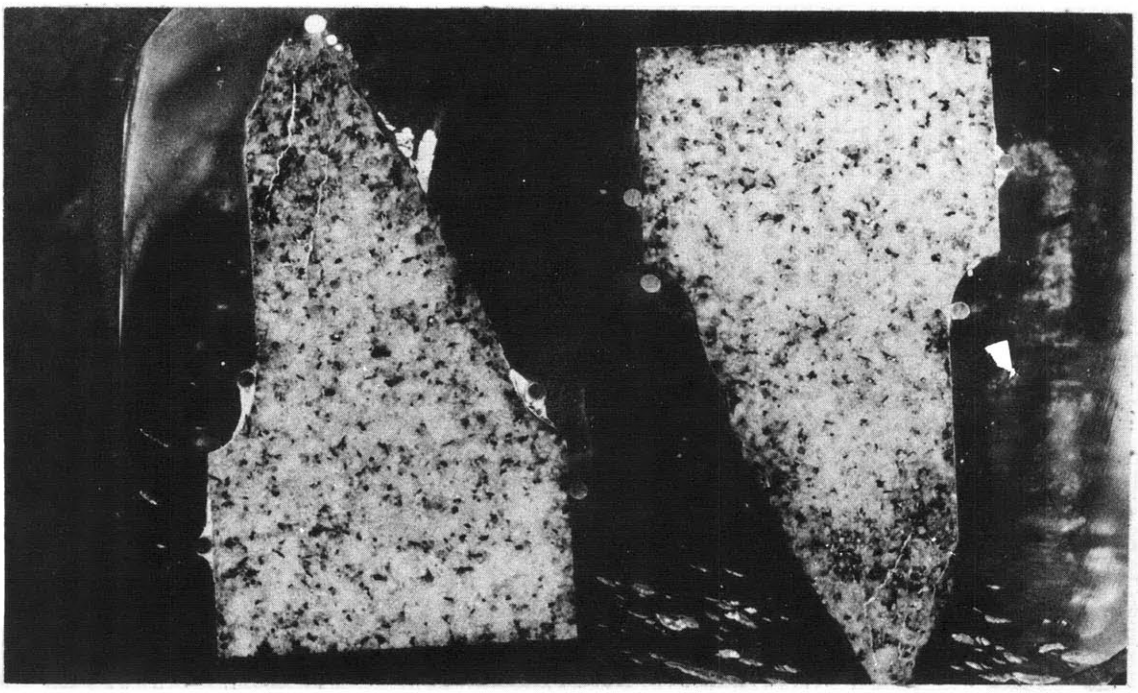

Polished End Pieces

Sample W-4

Figure 15

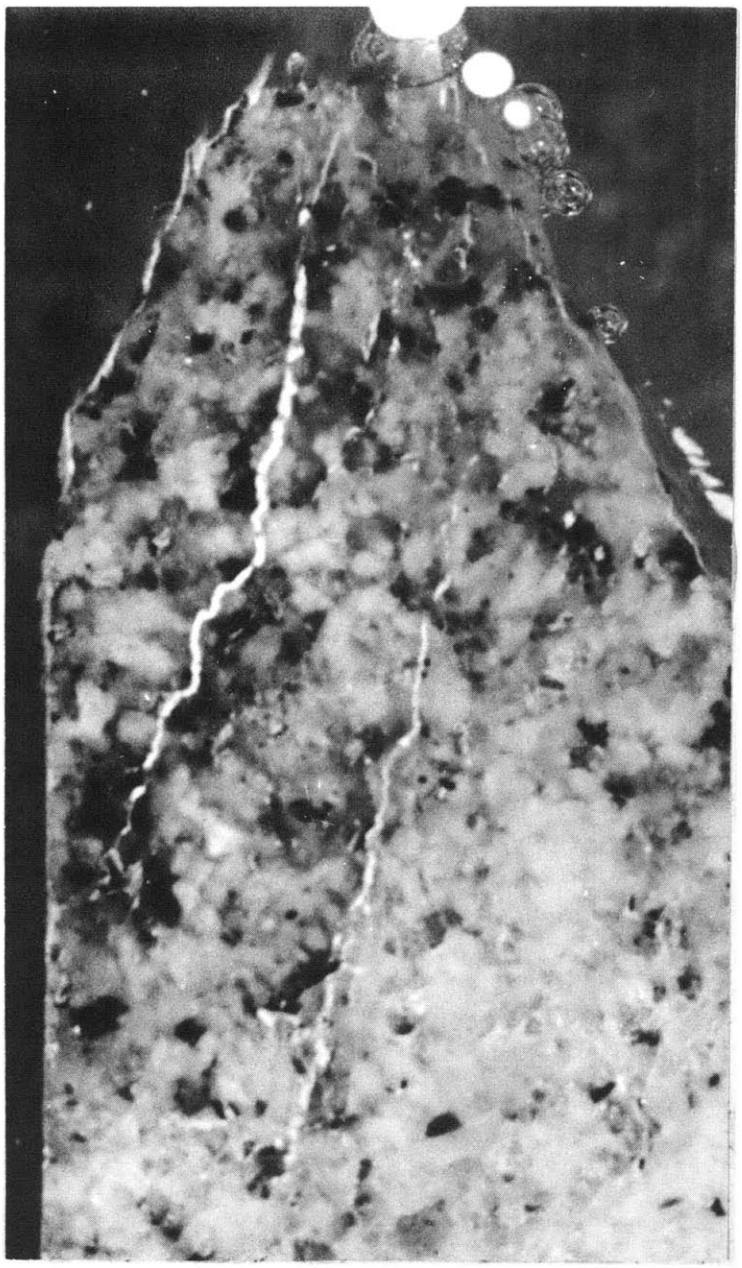

Detail of Crack Growth

Sample W-4

Figure 16

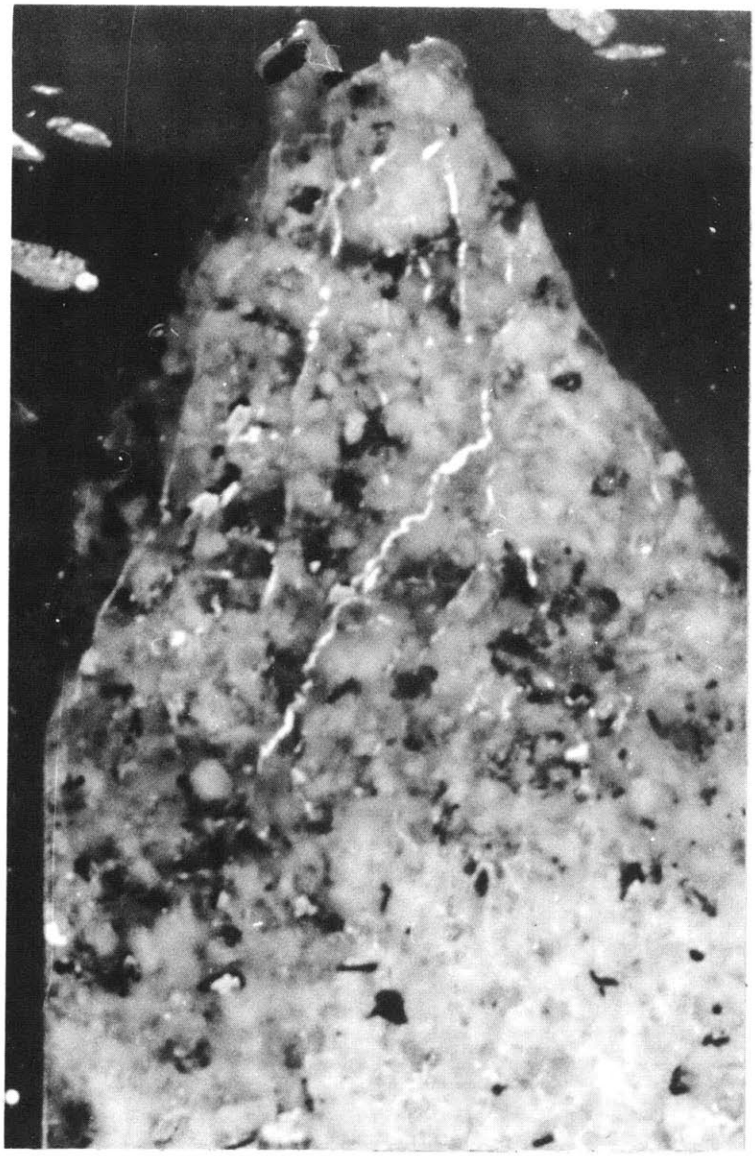

Detail of Crack Growth

Sample W-4

Figure 17

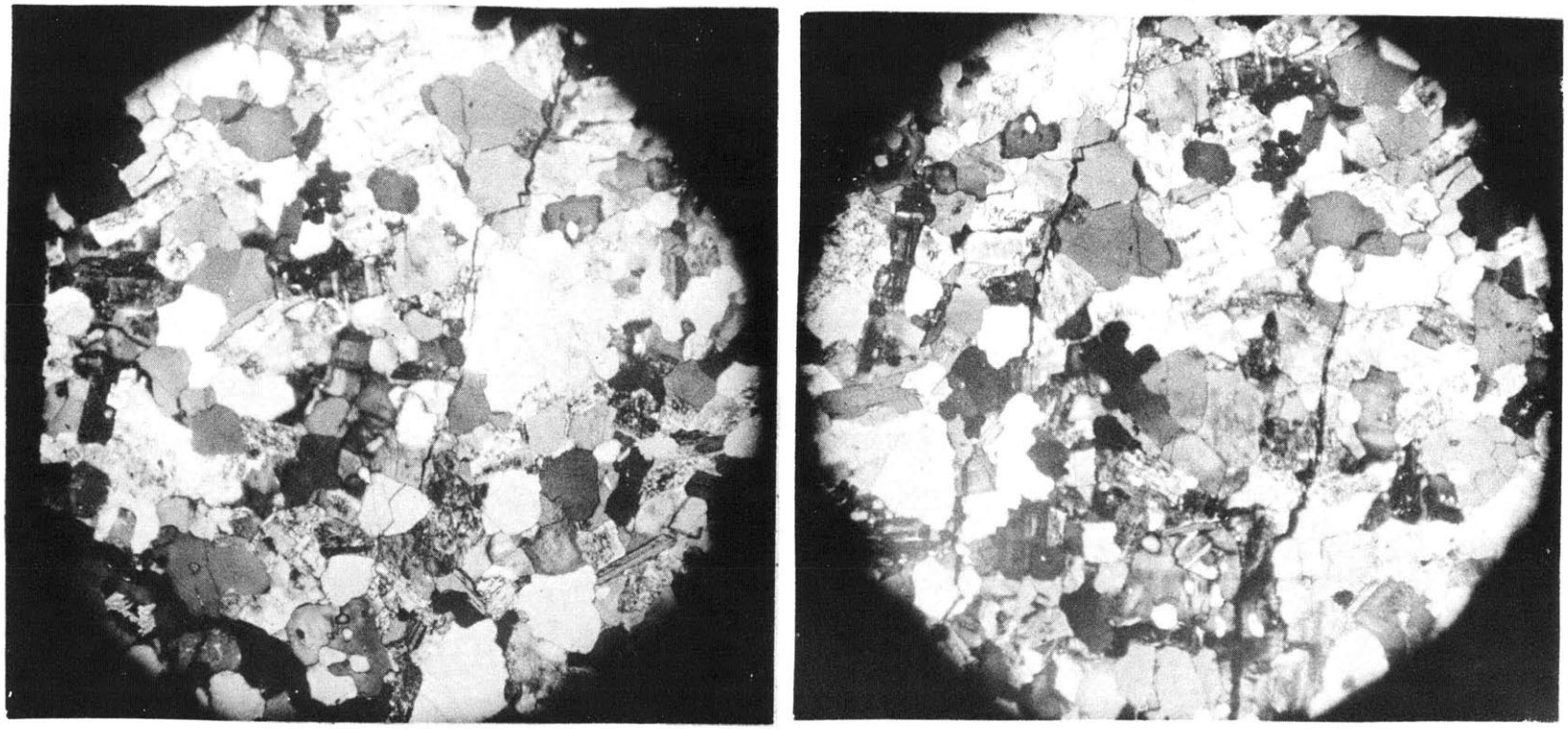

a b

Microscopic View

Sample W-4

Figure 18

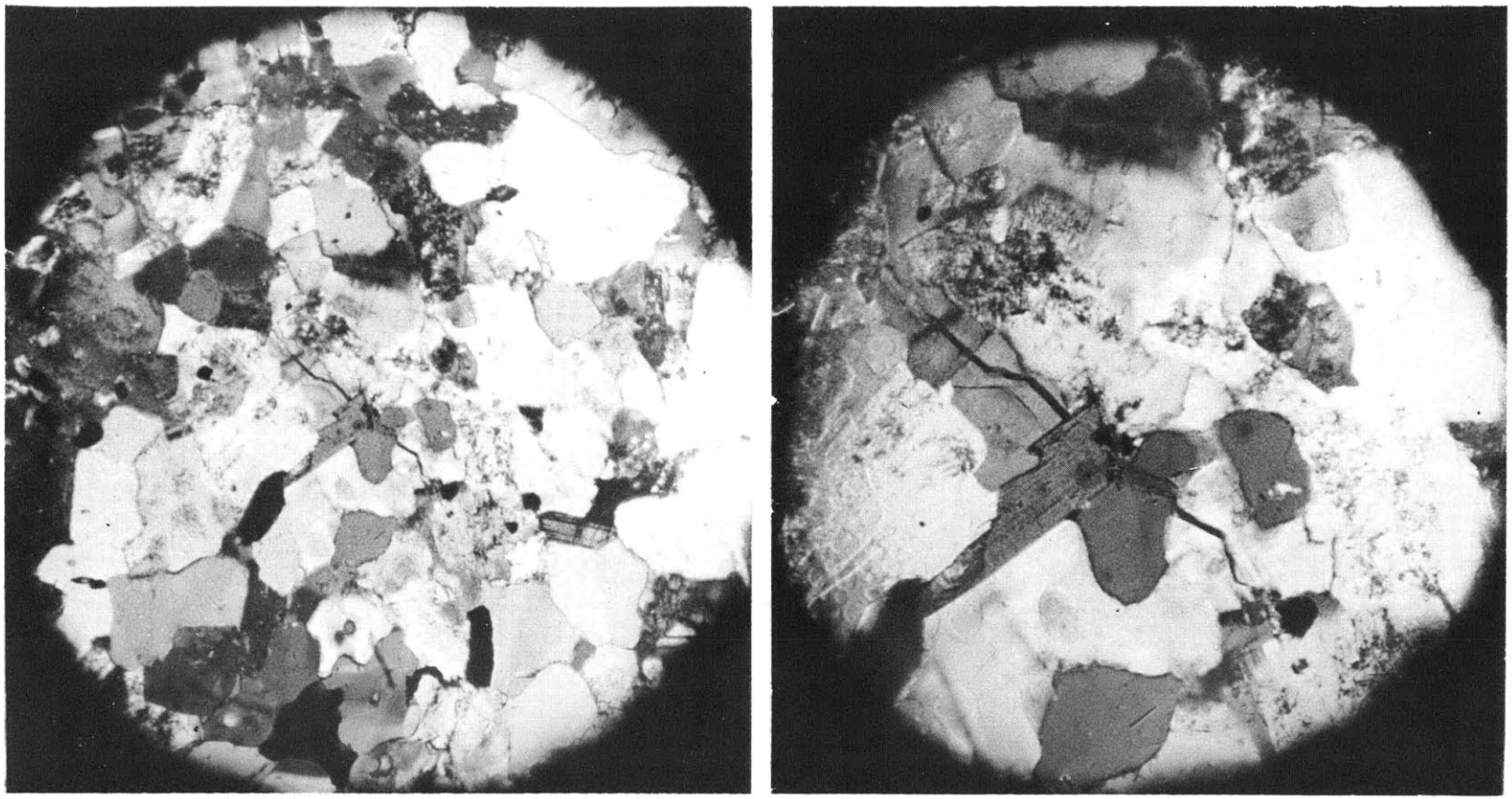

a b

Microscopic View

Sample W-16

Figure 19

COMPRESSIBILITY TESTS

Introduction

Walsh (1965a) made a theoretical study of the effect of cracks on the compressibility of rocks. He considered rock to be an elastic isotropic material containing randomly-oriented narrow cracks. With this model he derived an expression for the effective compressibility in terms of the compressibility of the solid material and the rate of change of porosity with external pressure. His analysis led to the result that the porosity of a rock containing narrow cracks could be determined from the compressibility curve by extending the linear portion of the curve back to zero pressure and noting the intercept on the volumetric strain axis, (Appendix 9). The linear portion of the compressibility curve represents the compressibility of the solid material.

Brace (1965) measured the linear compressibility of several rocks up to 10 kb. For the Westerly granite he found that the initial compressibility was greatest normal to the direction of the longest grain boundaries. Considering grain boundaries as narrow cracks, Brace found that the relative initial linear compressibility was related to the average grain boundary length according to Walsh's analysis.

Observation of the thin sections used by Brace in determining the grain boundary pattern revealed the existance of numerous trans-granular cracks. The thin sections were mapped and it was found that the cracks had a preferred orientation, (Appendix 10). The preferred orientation could qualitatively account for the directional characteristics of the initial linear compressibility determined by Brace. In particular, the most compressible direction was most nearly normal to the preferred direction of cracks.

The results of Walsh and Brace suggested that the compressibility test would be a useful technique in determining two characteristics of crack growth which occur during the uniaxial compression tests. The direction of crack growth could be established by comparing the linear compressibilities before and after a uniaxial test. The compressibility should be greater normal to the direction of crack growth than it was prior to the uniaxial test. In addition, support for the idea that the permanent volumetric strain associated with uniaxial compression tests is caused by new crack growth could be established by measuring the increase in porosity due to cracks. The increase in porosity should agree with the permanent volumetric strain if the pressure is increased sufficiently to close all the new cracks.

It was decided to subject the sample to several uniaxial compressive tests with each test carried to a higher

stress. The presence of new cracks could then be determined by comparing the compressibility of the undeformed rock with the compressibilities obtained after each uniaxial test.

Experimental Procedure

The samples were circular cylinders with a reduced central section and of the same dimensions as used during the uniaxial compression tests (Appendix 4). Axial and lateral strain gages were attached directly to the specimen and the entire sample was jacketed with silicone rubber (Appendix 11). The sample was placed in the triaxial chamber shown in Figure 20 which was filled with kerosene or machine oil.

The linear compressibility of the virgin sample was measured to 1 kb. The silicone rubber was then removed from the heads of the specimen and the sample was subjected to a uniaxial compressive stress of 0.69 kb. The heads were rejacketed and the second compressibility test was run. This process was repeated five times. The maximum uniaxial stress of each subsequent cycle was increased by approximately 0.35 kb. The maximum pressure of the compressibility tests was 1 kb. This value was chosen to avoid the difficulties associated with higher pressures and because Brace (1965) found that most of the porosity due to narrow cracks was eliminated at 1 kb.

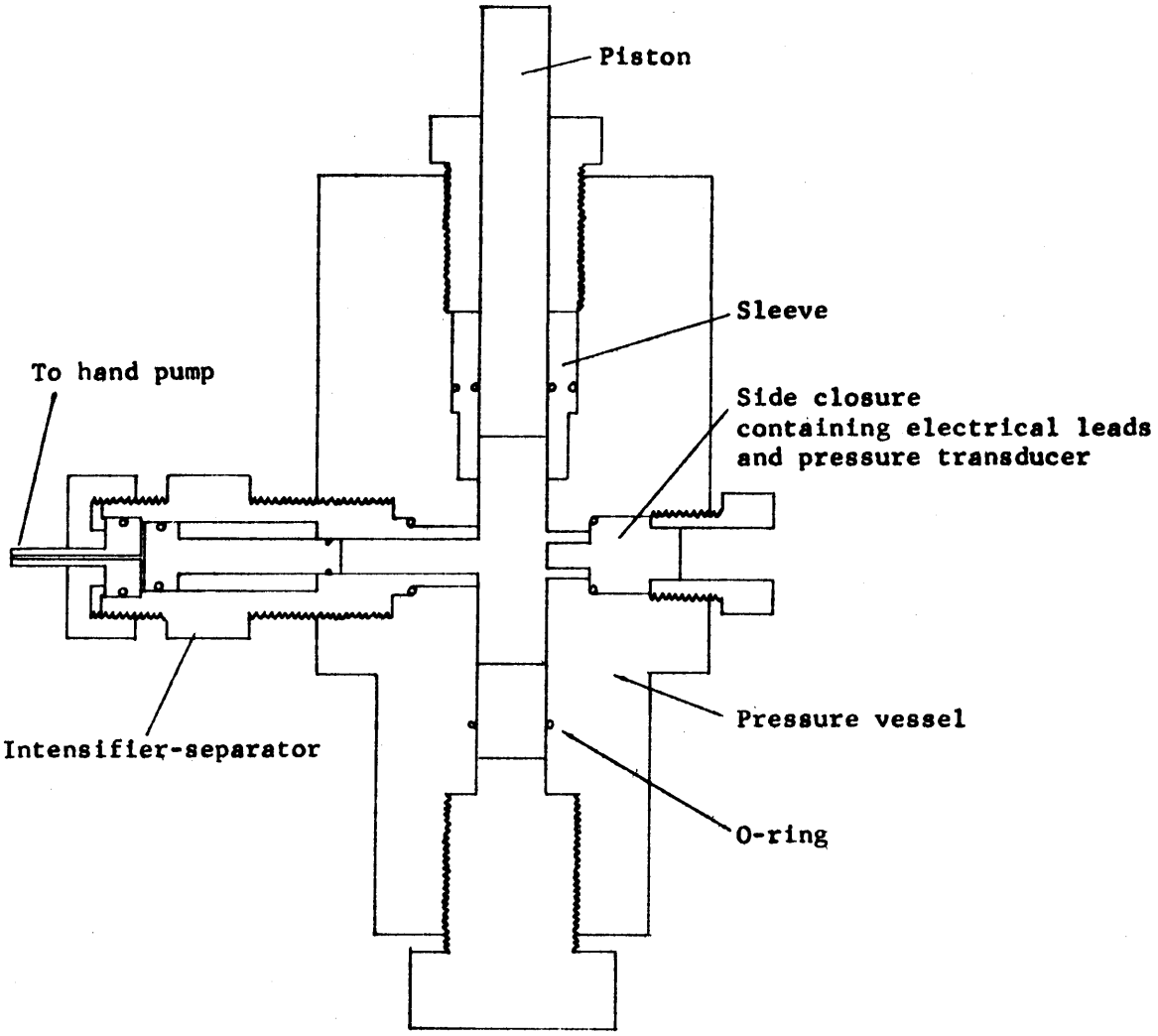

Triaxial Chamber

(Taken from Brace, 1964)

Figure 20

Experimental Results

The virgin compressibility curve to 1 kb for sample W-17 is shown in Figure 21. The minimum linear compressibilities are 0.81 mb^{-1} and 0.96 mb^{-1} in the axial and lateral direction, respectively. This corresponds to a bulk compressibility of 2.7 mb^{-1}. The compressibility of the solid material is about 2.0 mb^{-1}, (Brace, 1964), which corresponds to a linear compressibility of $\frac{2.0}{3}$ mb^{-1} or 0.67 mb^{-1}. The linear strain due to crack closure at 1 kb is found by subtracting 670 x 10^{-6} from the total linear strain. Prior to the uniaxial compression tests the linear strains due to crack closure at 1 kb were 400 x 10^{-6} and 590 x 10^{-6} in the axial and lateral directions, respectively. These values correspond to a volumetric strain of

$$400 \times 10^{-6} + 2(590 \times 10^{-6}) = 1580 \times 10^{-6} .$$

Therefore, for the virgin material, the decrease in porosity at 1 kb is about 0.00158.

The stress vs strain and volumetric strain vs stress curves of the uniaxial tests on sample W-17 are shown in Chapter II, Figures 10 and 11, respectively. The compressibility curves obtained after the uniaxial test to 2.11 kb is presented in Figure 21 for comparison with the original compressibilities. The results of the compressibility tests are presented in Table 7. The uniaxial stress to

which the sample had been subjected prior to the compressibility test is given in the first column. The linear strains due to the closing of cracks are presented in the second and third columns. The maximum error (Appendix 7) of the linear strains is about 2 per cent. The porosity due to cracks which close at 1 kb, n_c, is presented in the fourth column. The maximum error of n_c is about 6 per cent. The difference between the porosity of the deformed samples and the virgin sample is presented in the fifth column. The sensitivity is about 50×10^{-6}. The cumulatative volumetric strain, $(\frac{\Delta V}{V})_p$, of the sample prior to the compressibility test is presented in the next column. This is found by summing the permanent volumetric strains of the uniaxial compression tests and subtracting the permanent volumetric strains which occurred during the preceding compressibility tests. The sensitivity is about 50×10^{-6}. The minimum values of the linear compressibilities in the axial and lateral directions are given in the last two columns, respectively. These values were found by measuring the slope of the linear compressibility curves near 1 kb. The maximum error is about 4 per cent.

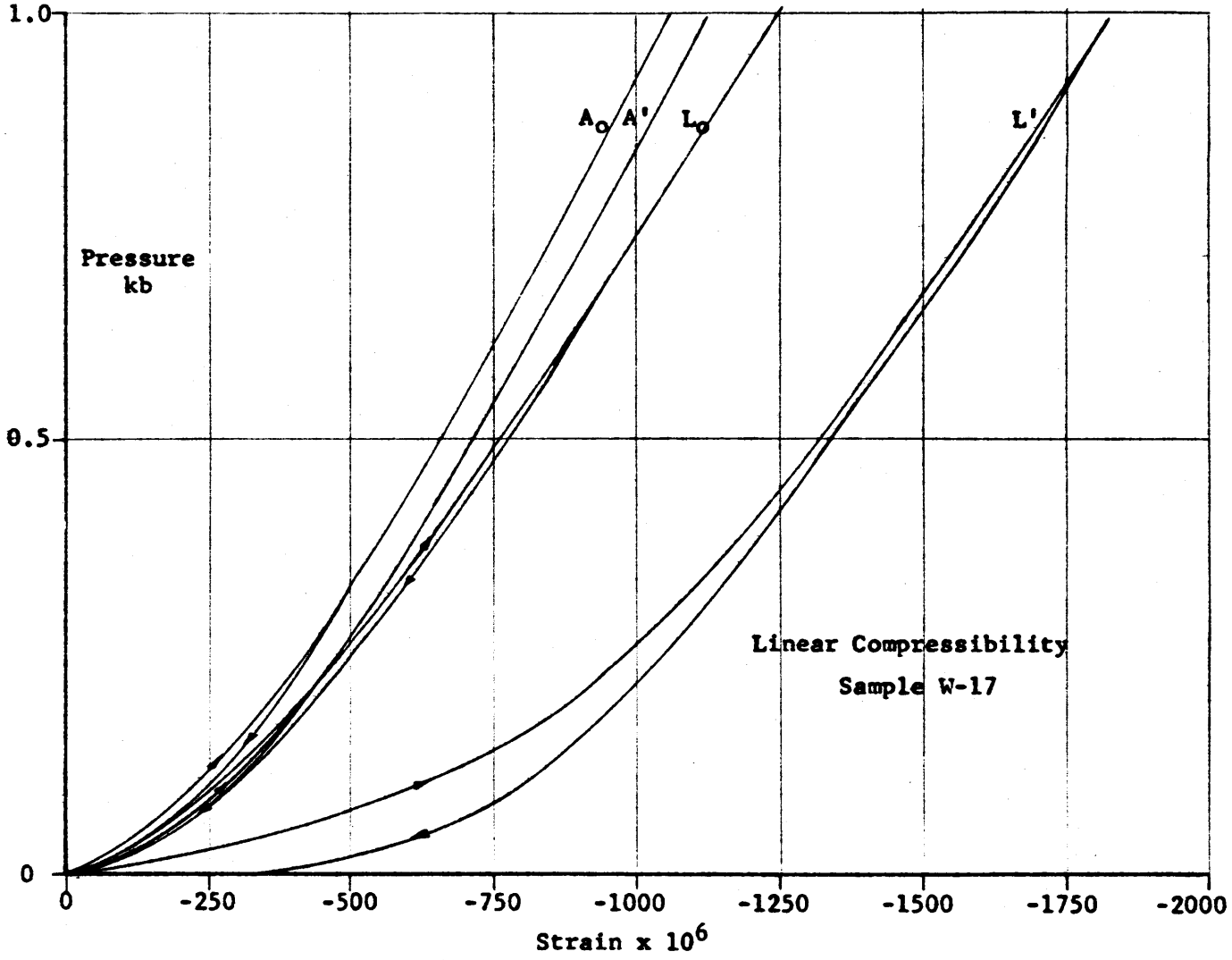

Figure 21

Subscript $_o$ denotes original compressibility
Primes denote compressibility after uniaxial test to 2.11 kb

TABLE 7

Results of Compressibility Tests

Sample W-17

Maximum Uniaxial Stress (kb)	Linear Strain Due to Crack Closure ($\times 10^{-6}$)		Porosity ($\times 10^{-6}$)		Cumulatative Permanent Volumetric Strain ($\times 10^{-6}$)	Minimum Linear Compressibility (mb^{-1})	
	Axial	Lateral	n_c	n_c-1580		Axial	Lateral
0	400	590	1580	---	---	0.82	0.96
0.69	400	580	1560	-20	50	0.82	0.96
1.03	420	600	1620	40	110	0.81	0.93
1.38	430	640	1710	130	230	0.81	0.95
1.72	430	810	2050	470	420	0.81	0.94
2.11	450	1160	2770	1190	1350	0.82	0.95

Discussion of Experimental Results

The continual increase in porosity of the samples uniaxially stressed to more than 1 kb suggests that additional crack growth occurred during each uniaxial test, especially during the cycles to 1.38, 1.72, and 2.11 kb. This evidence supports the idea presented in Chapter II that crack growth occurs at stresses less than the fracture strength.

The marked increase in the lateral strain, with little or no increase in the axial strain, due to crack closure at 1 kb, indicates that the direction of crack growth was parallel to the direction of uniaxial compression.

The agreement, within experimental accuracy, of the increase in porosity and cumulative volumetric strain indicates that the porosity due to crack growth which occurred during the uniaxial compression tests is removed by the application of a hydrostatic pressure of 1 kb. Additional support that the new cracks closed at 1 kb is given by the nearly constant values of the minimum compressibility. The compressibility of the deformed samples should be greater than of the virgin sample if the cracks remained open.

CONFINED COMPRESSION TESTS

Introduction

The Onset of Crack Growth and the McClintock-Walsh Modification

Brace and Bombolakis (1963) found that critically oriented cracks grow into a stable position in a uniaxial compressive stress field. They concluded that the Griffith theory could not predict the strength of rocks unless the stress at which crack growth is initiated is nearly the same as the fracture strength.

The results of the uniaxial compressive tests on Westerly granite in this study (Chapter II) show that crack growth occurs at stresses far less than the compressive strength. Volumetric strain vs axial stress calculations for Frederick diabase and Cheshire quartzite (unpublished data of Brace, 1963), marble and soapstone (Bridgman, 1949) and basalt and monzonite (Matsushima, 1961) indicate similar behavior. Therefore, for these rock types at least, one would not expect the Griffith theory or its present modification to predict the fracture strength.

However, one might expect the McClintock-Walsh modification to predict the stress difference required to initiate crack growth. The extension of the McClintock-

Walsh modification to predict the stress difference required to initiate crack growth is presented in Appendix 12. The predicted stress difference depends on the value of the coefficient of friction of the crack surfaces.

Reported values of the coefficient of friction of rock on rock are 0.9 (Paterson, 1958), 0.47 to 0.86 (Jaeger, 1959) and 0.4 to 0.77 (Handin, 1964). In a study of the effect of cracks on the uniaxial compression of rocks, Walsh (1965b) calculated that, for Westerly granite, the coefficient of friction on crack surfaces is $0.65 \pm .05$.

The behavior of the cracks, prior to their propagation, should be the same during elastic uniaxial tests (which Walsh considered) as during confined compressive tests. Therefore, on confined compression tests on Westerly granite one would expect the observed stress difference required to initiate crack growth to agree best with the McClintock-Walsh modification with a coefficient of friction of 0.65, providing the friction coefficient is independent of pressure.

The pdV Work Associated with Crack Growth

The work per unit volume required to fracture a specimen is given by the area under the maximum stress difference vs axial strain diagram, i.e., $\int(\sigma_3 - \sigma_1)d\epsilon_{11}$. The plots

$\frac{\Delta V}{V}$ vs σ_3 for the uniaxial compression tests show that there is a significant increase in volume as a result of the growth of cracks. If crack growth in confined compression tests also produces a pronounced increase in volume, then an appreciable percentage of the work required to fracture a specimen may go into work against the pressure medium.

Consideration of the work done against the pressure medium, i.e., pdV work , may be important in attempting to establish a fracture criterion. If, in confined compression tests, there is a large discrepancy between the fracture stress and the stress difference required to initiate crack growth, such as exists during uniaxial compression tests, then part of this discrepancy may be due to the pdV work.

Experimental Procedure

The samples were circular cylinders with a reduced central section and of the same dimensions as used during the uniaxial tests (Appendix 4). Axial and lateral strain gages were attached and the heads of the sample were covered with copper foil (Appendix 11). The throat region of the sample was jacketed in silicone rubber. The sample was positioned in the triaxial chamber shown in Figure 20 which was filled with machine oil or kerosene. The leads from the

strain gages and manganin coil were led out through a plug in the side of the chamber.

The ram was brought in contact with the sample prior to raising the confining pressure to prevent the expulsion of the ram and to minimize pressure changes during the test. The confining pressure was increased to the desired level by means of an intensifier. The axial stress in the sample was increased by advancing the ram and was held essentailly constant for intervals of a few minutes during the test. The force applied by the ram was measured by a load cell. The output from the strain gages and load cell were recorded on a three-channel recorder (Appendix 6). The change in resistance of the manganin coil was measured with a Wheatstone bridge (Appendix 6). In order to obtain partially fractured specimens the axial stress was decreased when the strains indicated that fracture was impending. However, this was not always possible.

The force of the ram was balanced by friction at the O-rings, the pressure medium, and the axial stress in the sample:

$$F = f + \bar{\sigma}_1 (A_R - A_T) + \bar{\sigma}_3 A_T \,, \quad \text{(Equation 1)}$$

where F = force applied by the ram
f = frictional force at O-rings
A_R = cross-sectional area of the ram
A_T = cross-sectional area of the reduced section of the sample

and σ_3, σ_1 are the maximum and minimum compressive stresses, (Appendix 13).

The variation of the frictional force at the O-rings with pressure was found to be $(0.017)(A_R)(\sigma_1)$ above 1 kb (Appendix 14). The frictional force was negligible below 1 kb.

Substitution of the appropriate dimensions into Equation 1 gives the maximum stress difference in terms of the ram load, confining pressure, and friction at the O-rings:

$$(\sigma_3 - \sigma_1) = 5.92(F - f)in^{-2} - 4.65\,\sigma_1$$

(Equation 2)

The volumetric strain was computed as a function of maximum stress difference from the axial and lateral strain vs maximum stress difference curves (Appendix 7). The stress difference required to initiate crack growth was determined from the $\frac{\Delta V}{V}$ vs $(\sigma_3 - \sigma_1)$ plots by noting the point at which curve departed from linearity.

The total work required to fracture the specimen was determinined by measuring the area with a planimeter under the curve of $(\sigma_3 - \sigma_1)$ vs $\epsilon_{\prime\prime}$. The records of the confined compression tests consisted of traces of $\bar{\epsilon}_1$ vs F and $\epsilon_{\prime\prime}$ vs F. Typical records are shown in Figures 22 and 23. From

Equation 2

$$\Delta(\sigma_3 - \sigma_1) = 5.92\ \Delta F\ in^{-2} \qquad \text{(Equation 3)}$$

Therefore, the work per unit volume of the sample represented by a unit area of the trace of $\epsilon_{\parallel}$ vs F was found according to

$$\frac{W}{in^3\ in^2} = (5.92\ \frac{\Delta F\ in^{-2}}{in})(\frac{\Delta \epsilon_{\parallel}}{in}) \ .$$

(Equation 4)

For example, if one inch on the strain axis represents 4000×10^{-6} and one inch on the force axis represents 5000 pounds, then the work per unit volume represented by one square inch equals

$$\frac{W}{in^3} = (5.92(5000\ \frac{\#}{in^2})(4000 \times 10^{-6}) = 118.4\ \frac{in\#}{in^3} = 0.818 \times 10^{-2} kb$$

In order to determine the work per unit volume done against the pressure medium the volumetric strain associated with crack growth was found by noting the difference between the volumetric strain at fracture and the volumetric strain which would have existed if crack growth had not occurred. The latter was found by extending the straight line portion of the $\frac{\Delta V}{V}$ vs $(\sigma_3 - \sigma_1)$ plot to the value of $(\sigma_3 - \sigma_1)$ at fracture. The work against the pressure medium was found by multiplying the pressure times the volumetric strain caused by crack growth.

Experimental Results

Typical examples of the strain vs ram-force traces obtained during the combined compression tests are shown in Figures 22 and 23. The zig-zag nature of the initial portion of each trace is a result of alternately applying the confining pressure and advancing the ram. The trace of the axial and lateral strains are indicated on the record by AXIAL and LATERAL, respectively. The intervals during which the stress was held essentially constant for a few minutes are recognized by the offsets along the curve.

The maximum stress difference was found at several points by subtracting the frictional force from the load on the ram and substituting into Equation 2. The plots of $\frac{\Delta V}{V}$ vs $(\sigma_3 - \sigma_1)$ were drawn by measuring, on the trace, the axial and lateral strains, computing $\frac{\Delta V}{V}$, and plotting this value against the corresponding value of $(\sigma_3 - \sigma_1)$. Typical examples of the plots of $\frac{\Delta V}{V}$ vs $(\sigma_3 - \sigma_1)$ are presented in Figures 24 and 25. The slope of the linear portion of $\frac{\Delta V}{V}$ vs $(\sigma_3 - \sigma_1)$ was determined for comparison with the slopes during uniaxial compression tests.

The stress difference required to initiate crack growth, $(\sigma_3 - \sigma_1)'$, was determined from the plots of $\frac{\Delta V}{V}$ vs $(\sigma_3 - \sigma_1)$ by noting when the curve departed from linearity. The maximum error of $(\sigma_3 - \sigma_1)'$ is about 10 per

cent. In order to test if the McClintock-Walsh modification of the Griffith theory predicts the stress difference required to initiate crack growth, the corresponding values of $(\sigma_3 - \sigma_1)'$ and σ_1 were divided by the stress required to initiate crack growth in a uniaxial compression test, σ_3'. The results of these computations are presented in Table 8. The values of $\frac{(\sigma_3 - \sigma_1)'}{\sigma_3'}$ are plotted against the values of $\frac{\sigma_1}{\sigma_3'}$ in Figure 26. The maximum error is 20 per cent for the ordinate and 13 per cent for the abscissa (Appendix 8). Agreement is best with the McClintock-Walsh modification which incorporates a coefficient of friction of about 0.7. The work per unit volume done against the pressure medium, $p(\frac{\Delta V}{V})$, was found by multiplying the pressure times the volumetric strain due to crack growth. The total work required to fracture the specimen was found by measuring the area under the maximum stress difference vs axial strain curve and multiplying by the work per unit area. The maximum error of the work done against the confining pressure and total work are 9 and 7 per cent, respectively, (Appendix 8). The values of the pdV work and total work and the ratios of the two are presented in Table 8.

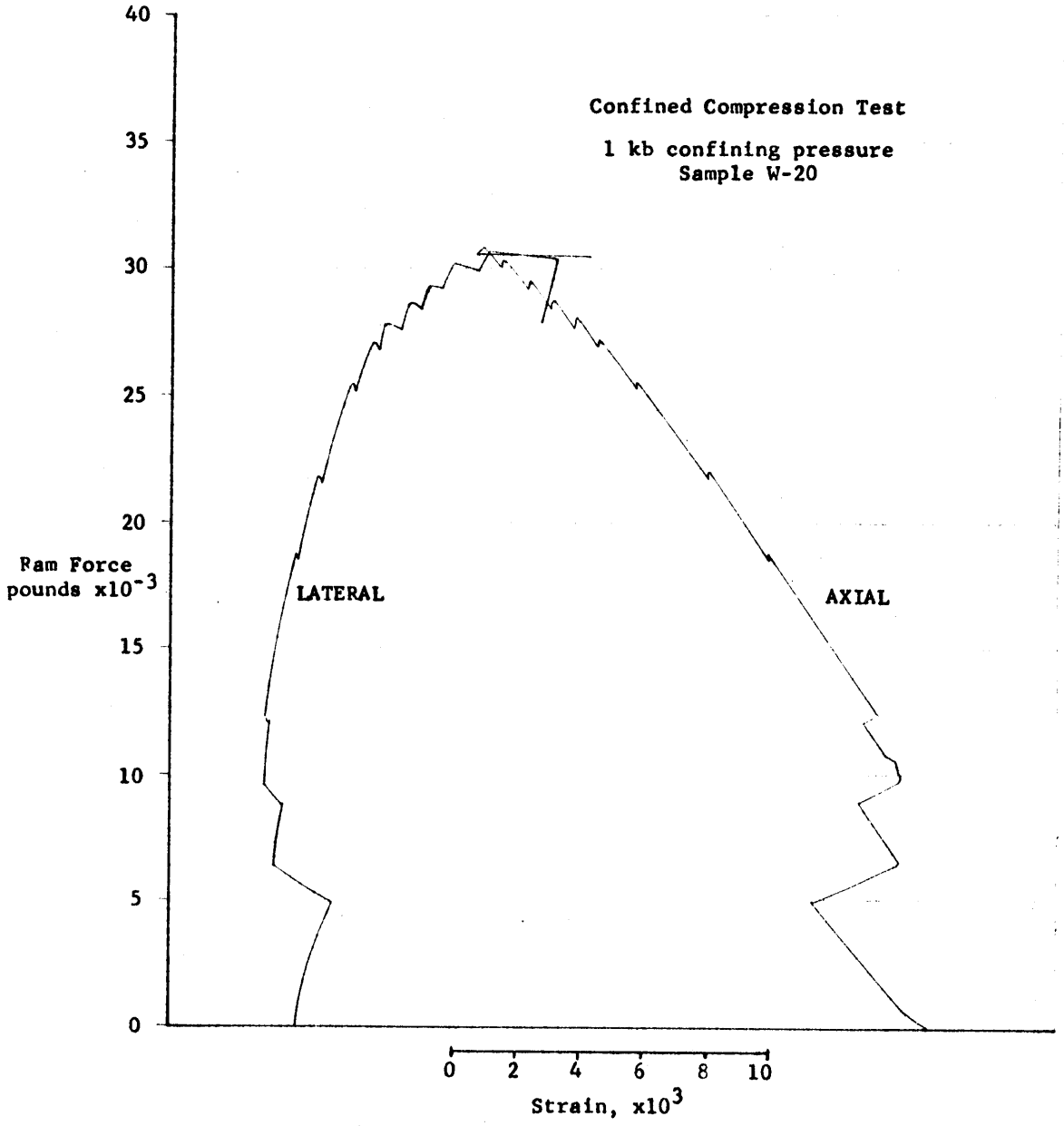
Confined Compression Test
1 kb confining pressure
Sample W-20
Ram Force
pounds x10-3
40
35
30
25
20
15
10
5
0
LATERAL
AXIAL
0
2
4
6
8
10
Strain, x10^3

Figure 22

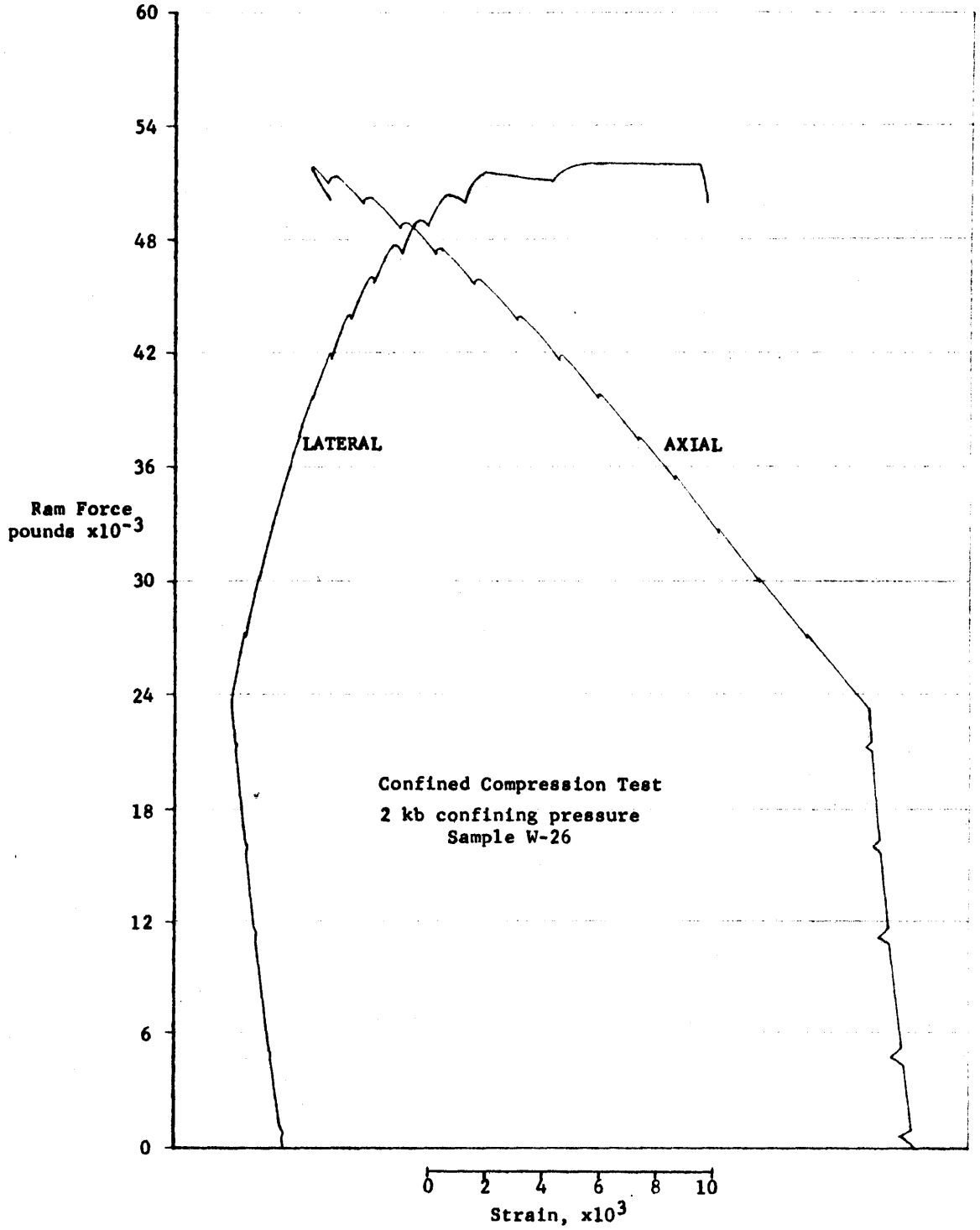
60
54
48
42
36
30
24
18
12
6
0
Ram Force
pounds x10^-3
LATERAL
AXIAL
Confined Compression Test
2 kb confining pressure
Sample W-26
0
2
4
6
8
10
Strain, x10^3

Figure 23

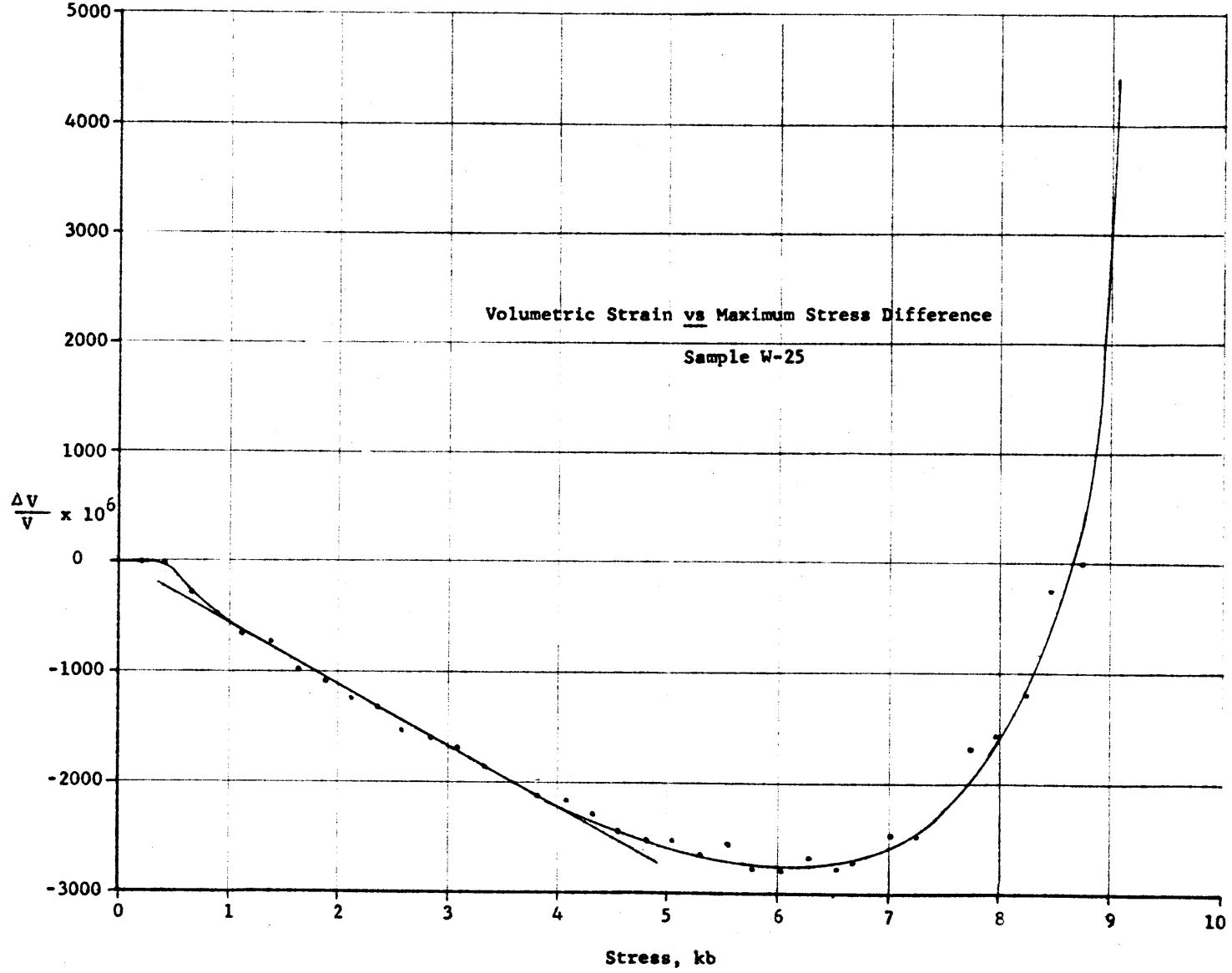
Volumetric Strain vs Maximum Stress Difference
Sample W-25
$\frac{\Delta V}{V} \times 10^6$
5000
4000
3000
2000
1000
0
-1000
-2000
-3000
0
1
2
3
4
5
6
7
8
9
10
Stress, kb

Figure 24

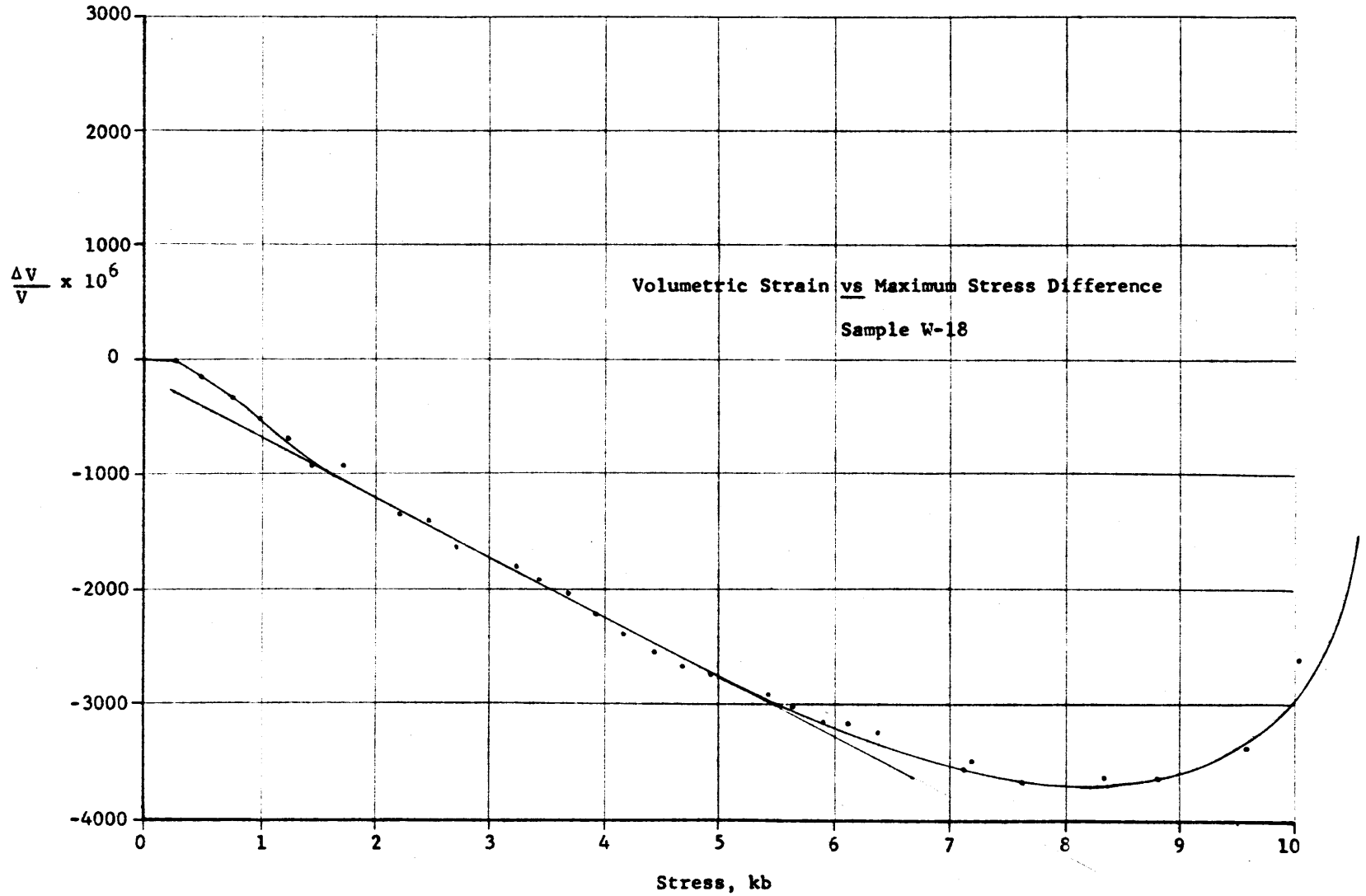
Volumetric Strain vs Maximum Stress Difference
Sample W-18
$\frac{\Delta V}{V} \times 10^6$
3000
2000
1000
0
-1000
-2000
-3000
-4000
0
1
2
3
4
5
6
7
8
9
10
Stress, kb

Figure 25

TABLE 8

Results of Confined Compression Tests

Sample	Confining Pressure (kb)	Strength $(\sigma_3-\sigma_1)_{max}$ (kb)	Onset of Crack Growth $(\sigma_3-\sigma_1)'$ (kb)	Slope of $(\frac{\Delta V}{V})$ vs $(\sigma_3-\sigma_1)$ (kb x 10^{-6})	$\frac{(\sigma_3-\sigma_1)'}{\sigma_3'}$ (σ_3'=1.0±0.1 kb)	$\frac{\sigma_1}{\sigma_3'}$	pdV Work (10^{-2} kb)	Total Work (10^{-2} kb)	$\frac{\text{pdV Work}}{\text{Total Work}}$
W-18	1.5	10.52	5.20	520	5.20	1.5	1.37	11.05	0.12
W-20	1.0	7.88	3.86	520	3.86	1.0	0.91	5.89	0.15
W-22	1.6	10.67	5.03	510	5.03	1.6	1.52	12.66	0.12
W-23	1.5	10.62	5.15	520	5.15	1.5	2.10	12.73	0.16
W-24	2.0	*	6.25	570**	6.25	2.0	*	*	
W-25	1.0	9.28	3.90	570	3.90	1.0	1.33	9.22	0.14
W-26	2.0	11.80	6.50	450**	6.50	2.0	2.20	12.87	0.17
W-28	0.5	6.30	2.20	700	2.20	0.5	0.46	3.97	0.12

*Jacket leaked at $(\sigma_3-\sigma_1)$ = 8.6 kb.

**Linear portion was discontinuous.

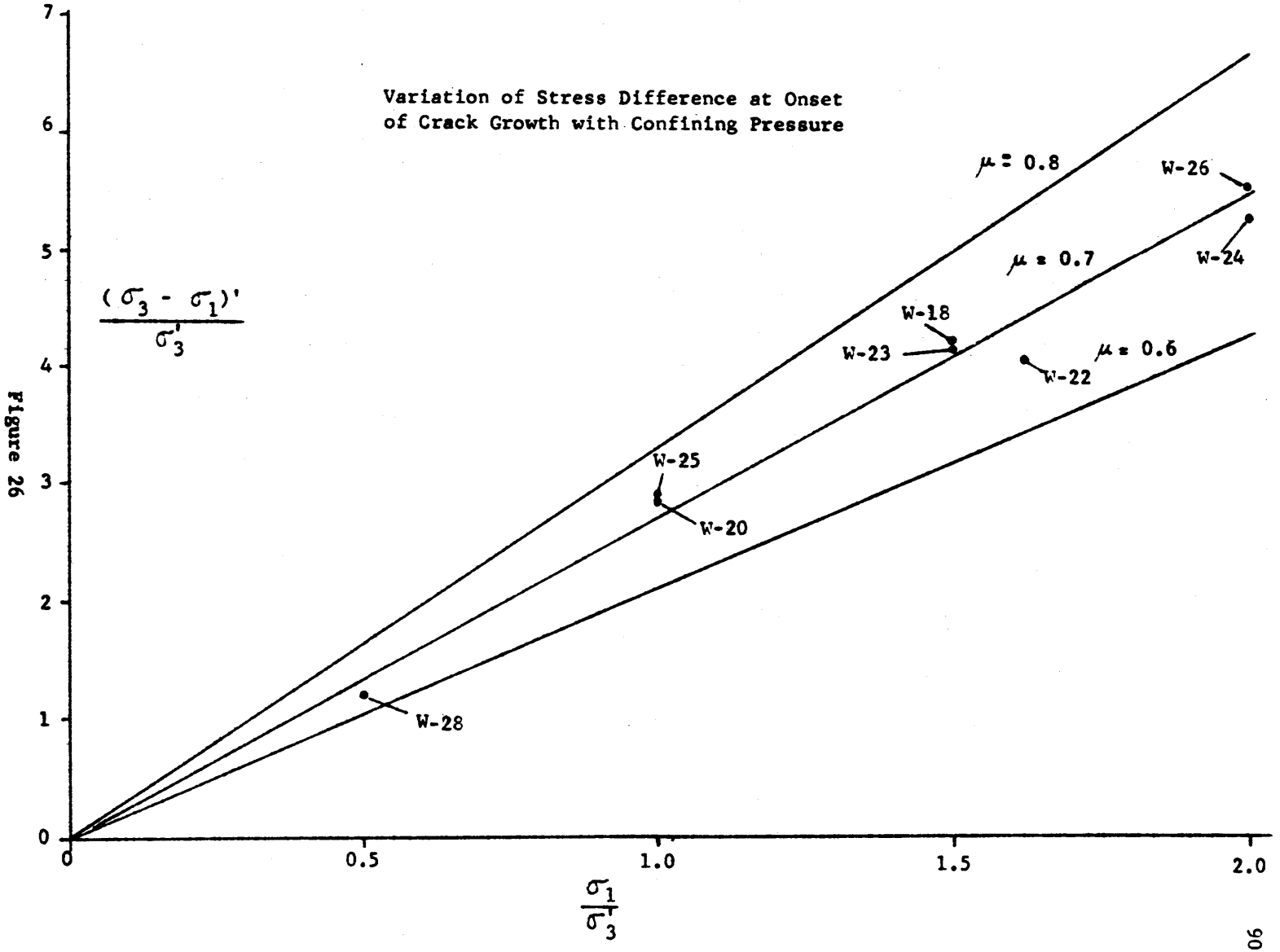
Variation of Stress Difference at Onset of Crack Growth with Confining Pressure
$\frac{(\sigma_3 - \sigma_1)'}{\sigma_3'}$
$\frac{\sigma_1}{\sigma_3'}$
μ = 0.8
μ = 0.7
μ = 0.6
W-26
W-24
W-18
W-23
W-22
W-25
W-20
W-28
0
0.5
1.0
1.5
2.0
1
2
3
4
5
6
7

Figure 26

Discussion of Experimental Results

The discussion of the experimental results is concerned with three topics: (1) the ability of the McClintock-Walsh modification to predict the maximum stress difference required to initiate crack growth, (2) the importance of the work done against the pressure medium, and (3) the description of the fractured specimens.

(1) Stress Difference Required to Initiate Crack Growth

The results of the confined compression tests presented in Table 8 and, in particular, in Figure 26, show that, for Westerly granite, the analysis of McClintock and Walsh predicts the maximum stress difference required to initiate crack growth. It is significant that the experimental results agree best with the McClintock-Walsh analysis which incorporates a coefficient of friction of about 0.7. As described on page Walsh (1965b) computed a coefficient of friction of 0.65 ± 0.05 from uniaxial tests on Westerly granite. This agreement with the curve for a coefficient of friction of about 0.7 is additional evidence that the analysis of McClintock and Walsh does predict the onset of crack growth as a function of confining pressure. The fact that the variation of $(\sigma_3 - \sigma_1)'$ with σ_1 was linear suggests that the coefficient of friction did not change appreciably up to 2 kb.

(2) Work Done Against the Pressure Medium

Comparison of the values of pdV work and total work, presented in Table 8, show that the work done against the pressure medium accounted for 12 to 17 per cent of the total work required for fracture. In general, the magnitude of the pdV work increases with pressure: 0.46, 1.12, 1.72, and 2.20 x 10^{-2} kb at σ_1 = 0.5, 1.0, 1.5, and 2.0 kb, respectively. (The values of 1.12 and 1.72 x 10^{-2} kb are the average values at σ_1 = 1.0 and 1.5 kb, respectively.) However, the ratio of pdV work remained constant, at least within experimental accuracy.

It should be realized that there is a certain amount of indeterminant error involved in calculating the maximum volumetric strain used in determining the pdV work. At just before fracture, surface cracks may develop directly beneath a strain gage which could result in a strain reading not representative of the entire sample. The assumption that the diametrical strain varies continuously around the sample would no longer be true and an erroneous volumetric strain would be obtained. Fortunately, anomalous behavior of the strain gages was apparent from observation of the graphical trace and the above-mentioned error was minimized by computing the maximum volumetric strain from the output of the strain gages just prior to when their behavior was suspect.

(3) Description of the Fractured Specimens

It was relatively easy to obtain partially-fractured samples during the confined compression tests. This was done by immediately lowering the applied load when anomalous behavior of the strain gages indicated that fracture was imminent.

Sample W-26 was tested under a confining pressure of 2 kb. As shown by the LATERAL curve in Figure 23, the lateral strain became excessive and the load was released. The surface of the sample was pitted due to the loosening of grains. In addition, there were two well-defined partial fractures as shown in Figure 27. The inclination of each partial fracture was about 35 degrees from the vertical. Examination of the polished section revealed a partial fracture which incorporated three inclined biotite flakes. This is shown in Figure 28a. Observation of the outline of the grains indicates that the partial fracture grew predominantly along grain boundaries. Figure 28b shows the crack growth between the upper two biotite grains of Figure 28a. It appears that there are several, small, near-vertical cracks associated with the main crack connecting the two grains. This association of subsidiary near-vertical cracks with a major crack was frequently noted.

Figures 29 and 30 are nearly perpendicular views of sample W-20. The test was conducted at a confining pressure

of 1 kb and stopped when the resistance of the axial strain gage began to increase rapidly. Observation of Figure 31 explains the anomalous behavior of the strain gage: A partail fracture extends about halfway through the sample and has cut the axial strain gage. The amount of displacement along the partial fracture is indicated by the offsets of the grid of the gage. The inclination of the partial fracture is about 30 degrees. Close inspection of Figure 31 reveals that the surface expression of the partial fracture is composed of vertical and inclined segments. Figure 32 shows an enlarge view of abrasive-filled en échelon cracks which occur along a portion of the partial fracture. Figure 32b, in particular, shows the numerous near-vertical cracks frequently found between the inclined segments of partial fractures.

Sample W-23 was tested under a confining pressure of 1.5 kb. Figure 33 is a view of the thin section. The direction of maximum compression is vertical. The detail of crack growth is shown quite clearly in Figure 33b. Here, again, are the numerous near-vertical cracks between the inclined cracks. Some of the cracks end at the grain boundary, reminiscent of cracks introduced at the ends of compression specimens due to the elastic mismatch between the steel platens and the sample. It is interesting that the upper inclined crack shows no appreciable change in orientation when crossing the grain boundary.

Sample W-18 was tested under a confining pressure of 1.5 kb. No partial fractures were observed but an interesting crack array was found in one grain, as shown in Figure 34. The inclination of the array is about 25 degrees from the direction of maximum compression, σ_3. The average inclination of the non-vertical cracks is about 40 degrees from the direction of σ_3. The typical appearance of the completely broken samples is shown in Figure 35. The inclination of the faults in each test was about 30 degrees.

The features observed during the examination of the fractured material are interpreted in Chapter V, CONCLUSIONS.

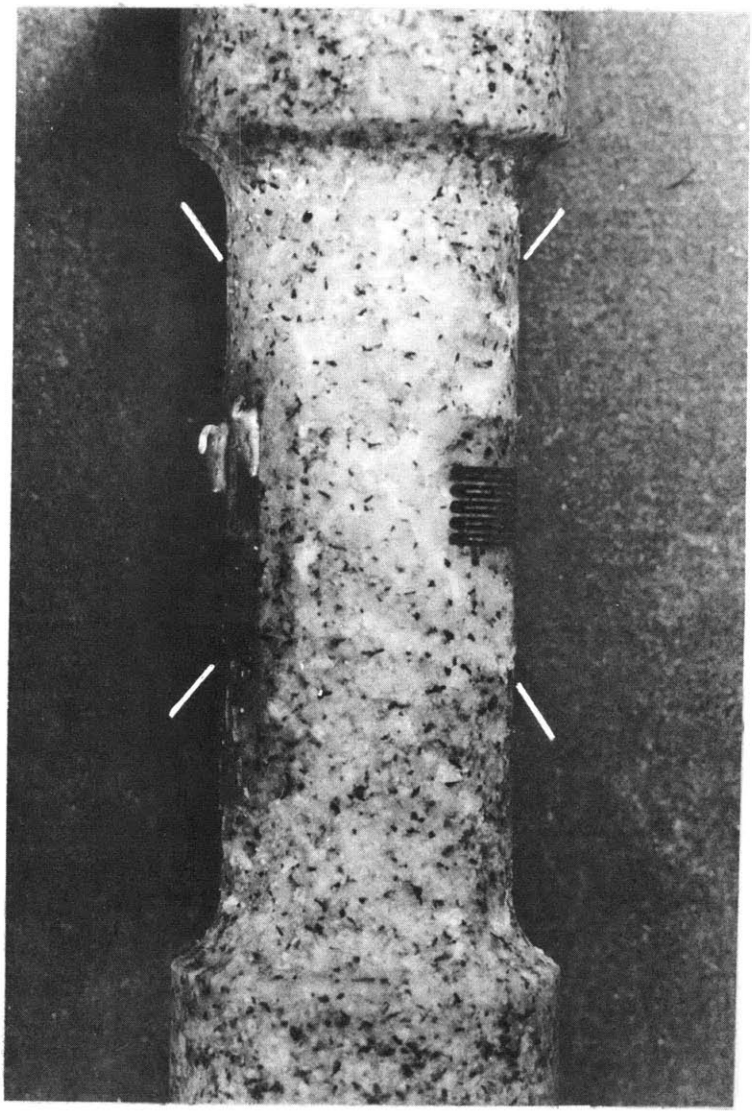

Partial Fracture

Sample W-26

Figure 27

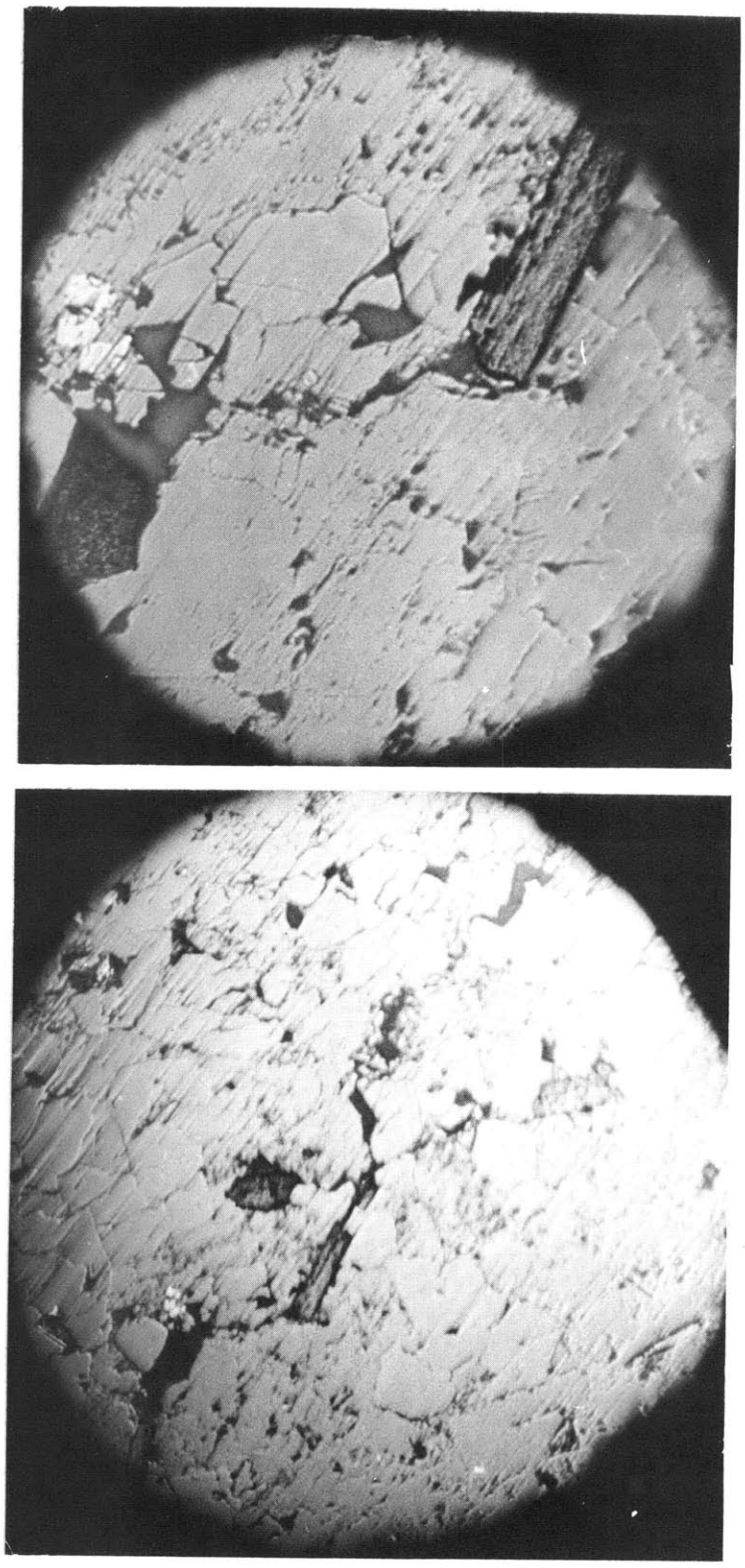

b

a

Detail of Crack Growth

Sample W-26

Figure 28

Partial Fracture

Sample W-20

Figure 29

Partial Fracture

Sample W-20

Figure 30

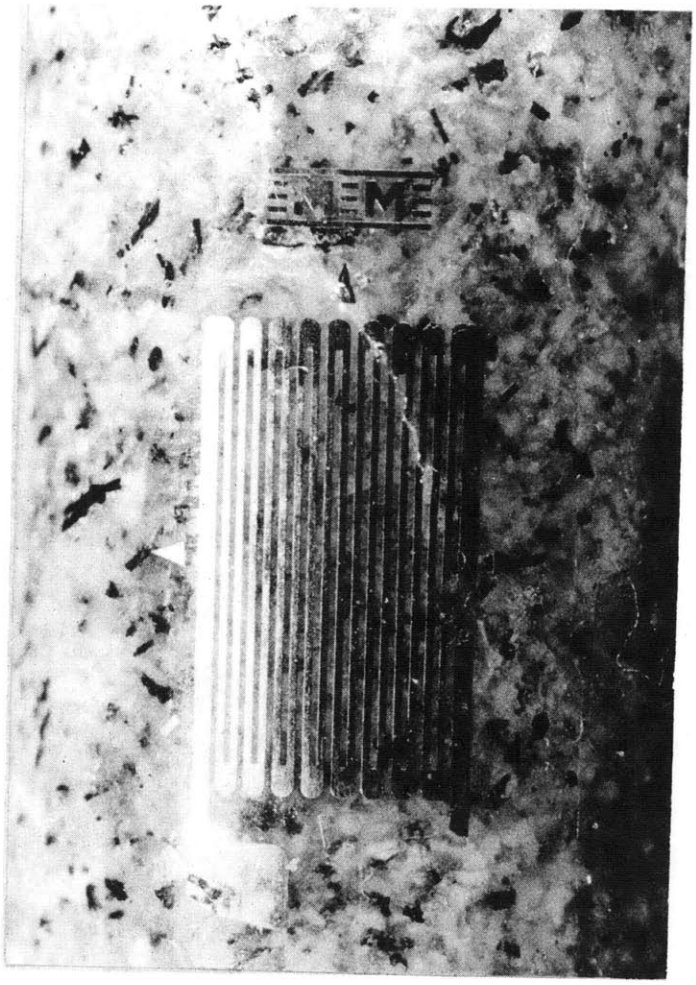

Partial Fracture

Sample W-20

Figure 31

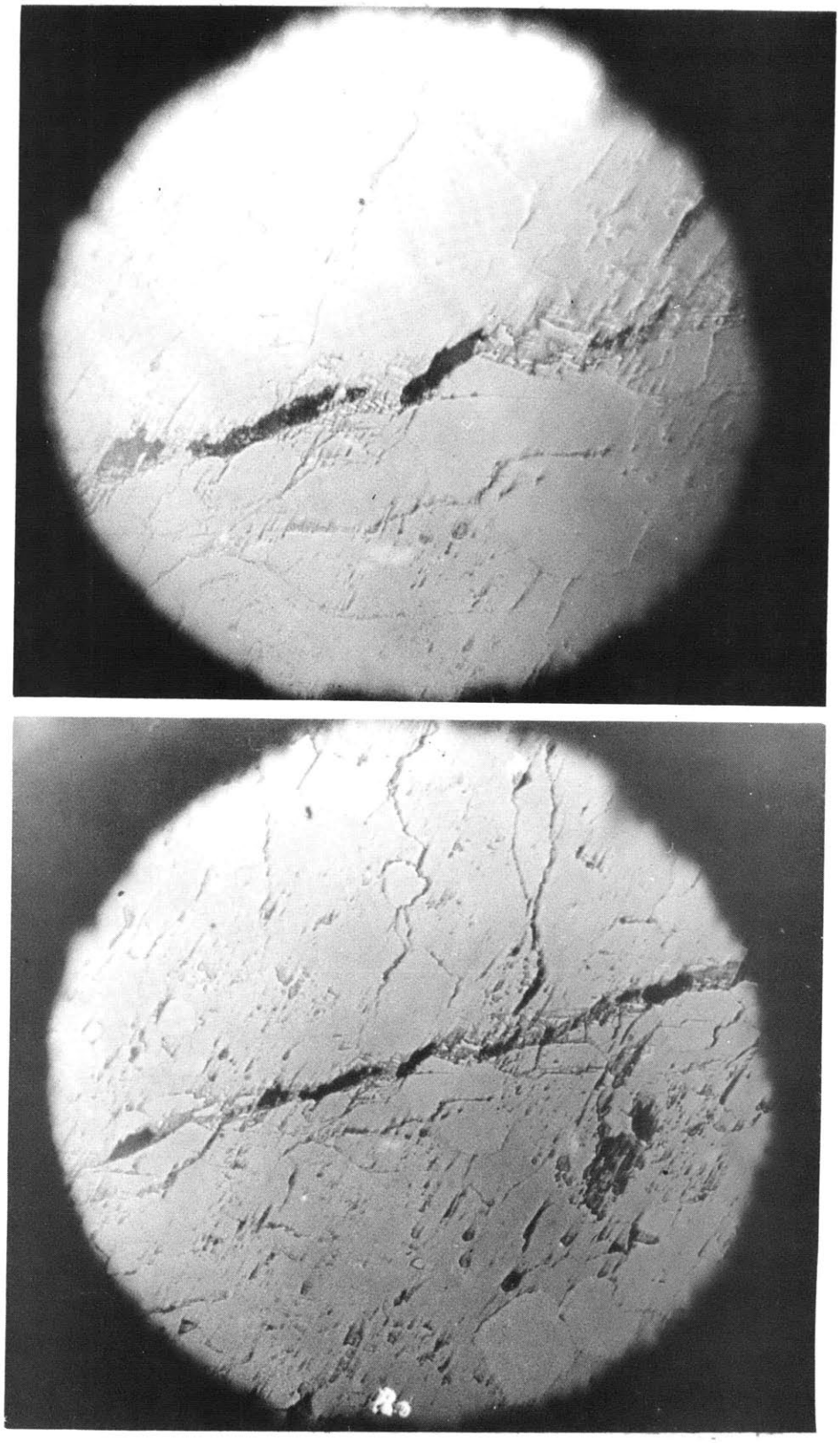

a b

Detail of Crack Growth

Sample W-20

Figure 32

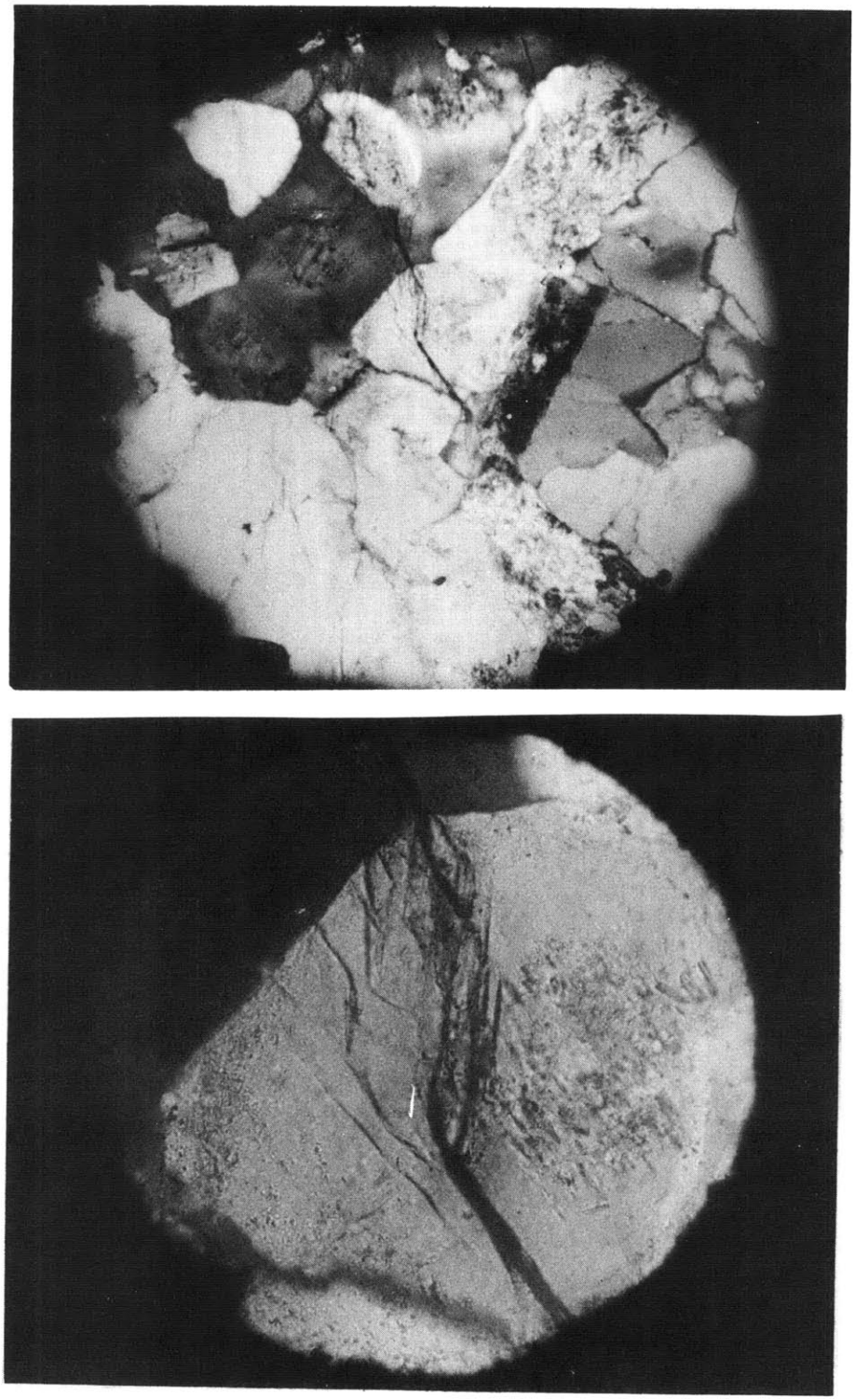

a

b

Detail of Crack Growth

Sample W-23

Figure 33

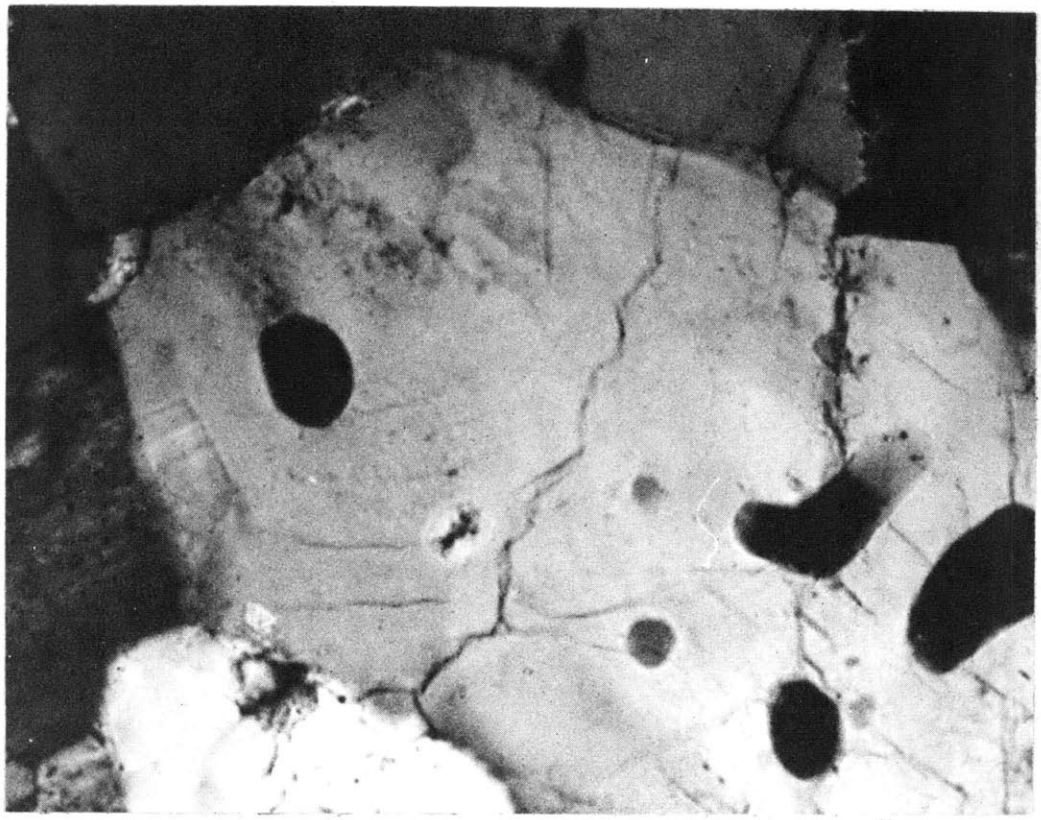

Detail of Crack Growth

Sample W-18

Figure 34

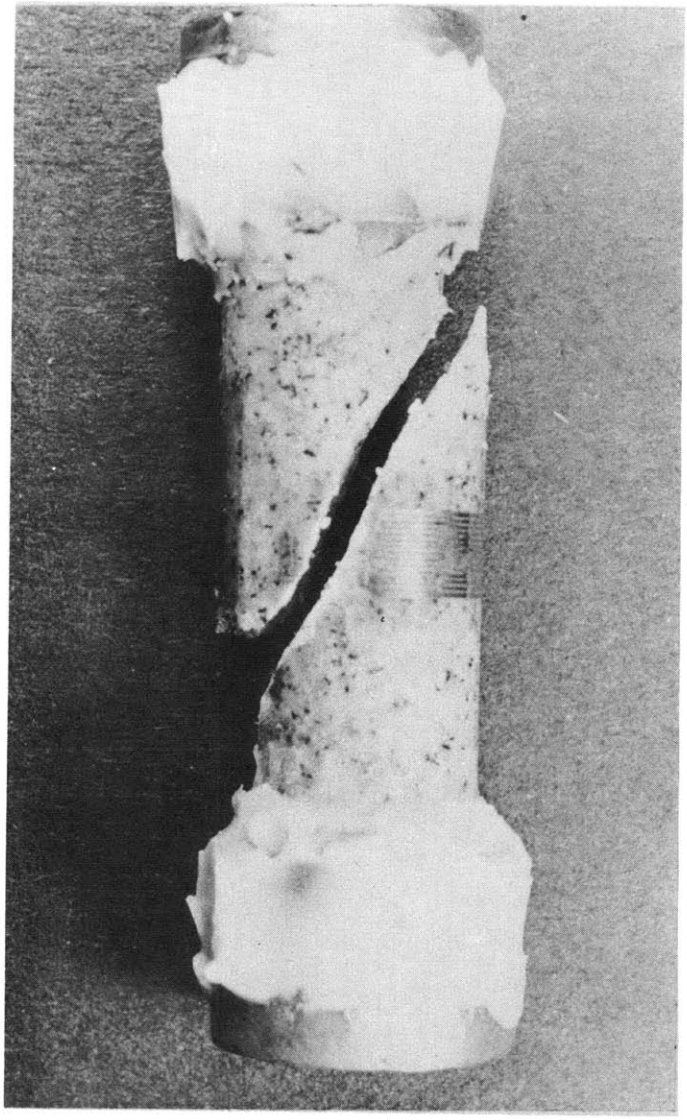

Fractured Sample

Figure 35

CONCLUSIONS

Introduction

This study has been oriented toward obtaining a more thorough understanding of the mechanics of crack growth during brittle fracture. This has necessitated the use of several types of experiments and techniques of data interpretation, some of which were developed during this investigation. It is appropriate that these experimental and interpretative techniques be evaluated as part of the conclusions of this study. This is done in the first part of this chapter.

The implications of the results of this study with regard to the process of brittle fracture is presented in the second half of this chapter. This includes the microscopic and macroscopic picture of brittle compressive fracture as existed when this investigation was begun, the change in this picture as a result of this study and suggestions for further investigation.

PAGES (S) MISSING FROM ORIGINAL

Page 106 does not exist in the original document

Evaluation of Experimental and Interpretative Techniques

Stiffening Element

The modification of the hydraulic ram was very beneficial. The ability to obtain partially fractured specimens, with strains greater than obtained at complete fracture in a conventional loading system, (Brace, 1964), is an indication of the value of the stiffening element when studying the growth of cracks. Another advantage of the particular stiffening element used in this study was the simplicity of design and small cost. Two obvious disadvantages are the limitations of sample size and restriction to uniaxial compression tests.

Sample Shape

The sample shape was a modification of one used previously (Brace, 1964). The samples were relatively easy to prepare and were economical of material. Unfortunately, there is, theoretically, a stress concentration of about 1.25 (Peterson, 1953), at the fillets. However, the value of Young's moduli and compressive strengths agreed with the results of Brace (1964). In addition, observation of the sample during uniaxial compression tests showed that

crack growth generally began in the throat region of the sample, well removed from the fillets.

Determing Onset of Crack Growth with the Plot of $\frac{\Delta V}{V}$ vs $(\sigma_3 - \sigma_1)$

Earlier attempts at detecting crack growth employed sonic techniques (Obert and Duvall, 1945) and the erratic behavior of strain gages due to crack growth directly beneath the gage (Blakey and Beresford, 1953). The disadvantage of the sonic method is that crack growth at the ends of the specimen in contact with the platens would be detected in addition to the cracks which grow in the central region of the sample. The limitation of Blakey's method is that it detects only those cracks which occur directly beneath the strain gage.

The calculation and graphical presentation of the volumetric strain as a function of stress has proven to be a very good method for detecting the onset of crack growth. Many of the conclusions derived from this study are based on this technique and it was of great value in understanding qualitatively how cracks grow. The reported error in determining the maximum stress difference at the onset of crack growth is about 10 per cent. This value was judged from how accurately one is able to decide on the stress difference at which the $\frac{\Delta V}{V}$ vs $(\sigma_3 - \sigma_1)$ curve departs from linearity.

However, the reproducibility is much better than this, as shown in Figure 26, and so the reported error of 10 per cent is felt to be conservative.

Use of Compressibility Test in Determining New Crack Growth

Walsh's (1965a) analysis of the effect of narrow cracks on the compressibility of rocks has proven to be very beneficial in determining the orientation of new crack growth. Direct observation of the polished sections of the deformed samples supported the results of the compressibility tests which indicated that the predominant direction of crack growth is parallel with the direction of maximum compression. In addition, the increase in porosity as determined from the compressibility tests agreed quite well with the permanent volumetric strain obtained during the uniaxial compression tests, (Chapter III, Table 7). Thus the technique for determining the porosity due to narrow cracks as suggested by Walsh is valid and offers a convenient method for studying new crack growth.

The Process of Brittle Fracture

Microscopic

Brace (1964) correlated the microscopic process of fracture with certain characteristics of the stress vs

axial strain curve. His stress-strain curve is reproduced here (Figure 36) to aid in the following discussion. The stress at which Young's modulus begins to decrease is designated as the beginning of region III. From examination of the polished sections of rocks stressed to region III, Brace found that the initial stage of brittle fracture was a detachment of grains along their boundaries so that just prior to fracture there were numerous loosened sections of grain boundaries of various lengths and orientation. During region IV Brace reported that cracks begin to grow out of certain of the grain boundaries which opened during region III. The final stage consists of a through-going fracture which forms out of systems of these cracks, especially en échelon arrays of loosened grain boundaries and cracks. As a fault grows out of an en échelon array of cracks it must break through the intervening material between the individual cracks. Brace reasoned that this results in the pulverized material associated with a fault.

Some of the results of this study differ from the observations of Brace. Measurement of the linear compressibilities before and after the uniaxial tests indicate that the predominant orientation of new cracks was parallel with the direction of maximum stress. Had grain boundaries opened at various orientations, as suggested by Brace, then the axial compressibility would have increased.

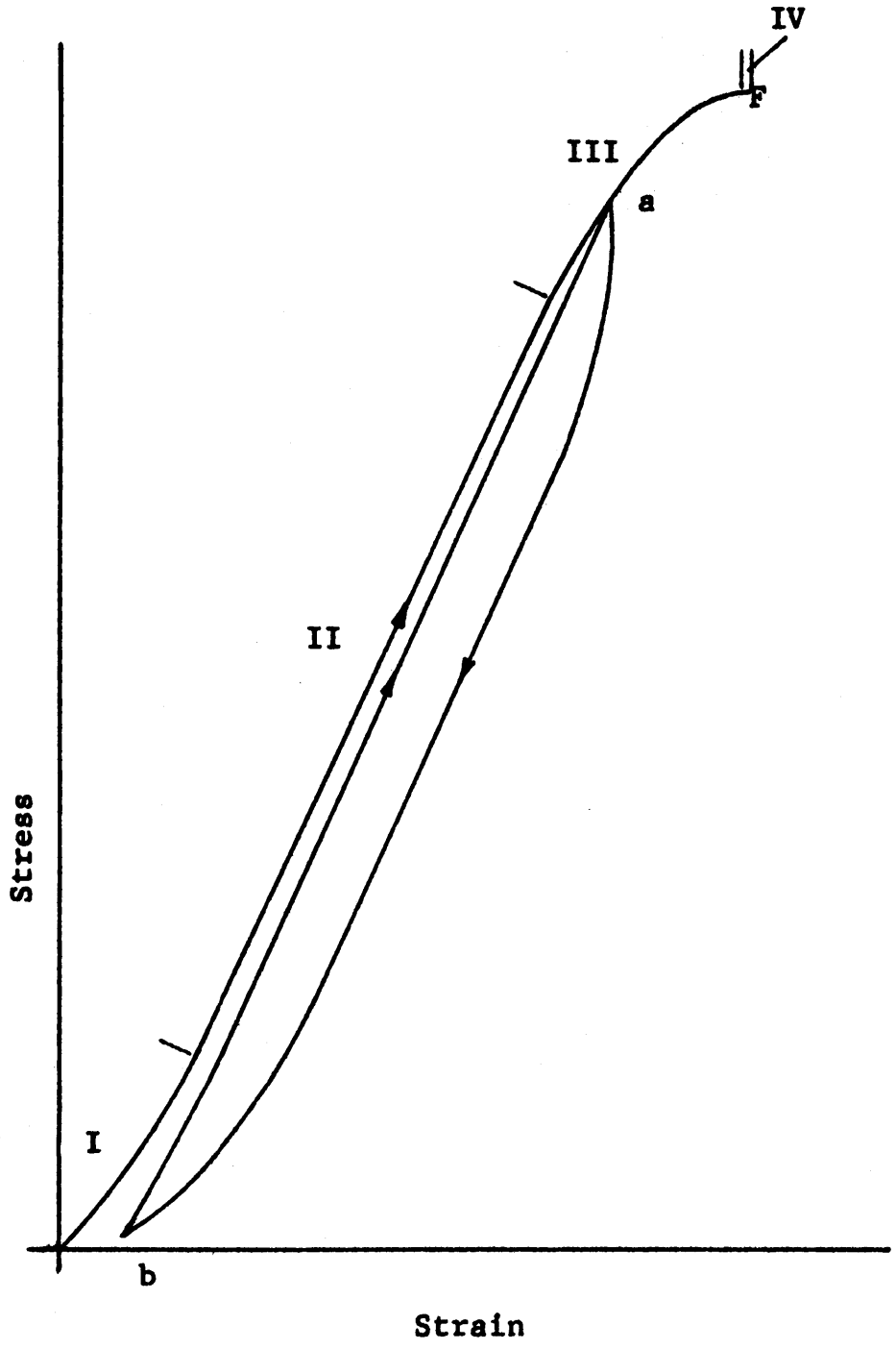

Typical Stress-Strain Curve

(Taken from Brace, 1964)

Figure 36

Another difference is that non-elastic behavior begins before the stress level of region III. In fact, for Westerly granite, departure from elastic behavior occurs at about half the compressive strength. This has been interpreted as indicating the onset of crack growth.

However, there is a possibility that the departure from elastic behavior is due to an opening of near-vertical grain boundaries. This might occur, for example, if a wedge-shaped grain was forced against a vertical grain boundary. Observation of samples loaded to just above the stress at which behavior is non-elastic did not provide conclusive evidence as to whether the first stage of fracture is an opening of near-vertical grain boundaries or the actual growth of pre-existing cracks.

However, two facts exist which qualitatively support the idea that crack growth and not the opening of vertical grain boundaries is the cause of departure from elastic behavior. First, if the wedging action of adjacent grains can open grain boundaries, there is no reason why the mechanism should be restricted to just vertical grain boundaries. If inclined grain boundaries opened the axial compressibility would have increased but it was found to remain essentially constant. Secondly, observation of material taken to region IV shows that inclined cracks do grow vertically and we have no particular reason to believe that they will not grow in

similar manner at lower stresses. It is suggested that the lack of evidence of such at the departure from elastic behavior is due to the fact that crack growth is less extensive than in material stressed to region IV.

A third difference is that less importance is attributed to grain boundaries than to pre-existing trans-granular cracks and biotite grains in initiating crack growth. Observation of the thin sections of the undeformed material, (Appendix 10), revealed the existance of many trans-granualr cracks. The fact that linear, inclined, trans-granular cracks and inclined biotite grains were incorporated into the partial fractures which extend for only a few grain diameters suggests that these elements were instrumental in initiating fracture. To be sure, grain boundaries are also incorporated into the partial fractures, but their role seems to be secondary compared to pre-existing, inclined, cracks and biotite grains.

It was found that fractures form from en échelon arrays of cracks as observed by Brace. One instance of crack growth between en échelon biotite grains was found (Figure 28). In general, the en échelon cracks were trans-granular (Figures 18 and 19). The crack growth between the inclined en échelon cracks was predominantly vertical (i.e., parallel with σ_3) and was both through and around grains.

Frequently, there were several near-vertical cracks between the inclined, en échelon flaws, (Figures 28, 32, and 33). The extensive fracturing may contribute to the powdered rock commonly associated with fracture in compression.

The existance of well-developed partial fractures parallel with the fracture surface (Figure 16) indicates that more than one fracture is developing simultaneously. However, for some reason, one grows in preference to the others to become the through-going fracture. The essentially constant shape of the partial fractures through a distance of a few grain boundaries (compare Figures 16 and 18) indicates that the width of the partial fractures is appreciable. If the partial fractures support little or no stress this appreciable width might result in a higher stress on the irreguler plane which contains the partial fracture.

To summarize, then, the microscopic picture of fracture appears as follows: At a stress difference of roughly half the strength near-vertical cracks begin to grow from pre-existing, trans-granular cracks and tabular grains which are (1) inclined to the direction of maximum compression and (2) generally en échelon. Crack growth continues as the stress is raised and the direction of growth is predominantly parallel with the direction of maximum compression. The vertical growth is both through and around the grains. Presumably, the finite width of the partial fractures tends to

restrict further crack growth to the plane containing the partial fracture. It appears that eventually some one partial fracture reaches a length and width such that the stresses on the plane containing the partial fracture are significantly higher than the applied stress and further crack growth is concentrated along this plane so that it becomes the through-going fracture.

There are many details of crack growth which require further investigation. For example, consider the problem of predicting the deformational behavior of a material from observation of a representative thin section. At present, we cannot single out a crack and predict the stress difference required to make it grow or how far and in what direction it will propagate. Such problems require a detailed knowledge of the stress conditions around cracks or flaws in elastically-anisotropic material which in turn requires knowledge the exact geometry of a crack and the coefficient of friction along the crack surfaces. In addition, one should know the tensile strength of the material at the most severely stressed point which requires knowledge of the absolute strength of minerals in any crystallographic direction and the influence of impurities on the strength of atomic bonds. The additional knowledge required to predict the path of propagation are the stress conditions around a partial fracture and the strength of grain boundaries. Concerning the latter, we do

not even know the structure of a grain boundary let alone how its strength depends on the confining pressure or the composition of the adjacent minerals.

Macroscopic

When this study was begun there was a substantial amount of evidence which indicated that the mechanism of fracture was very similar to that proposed by Griffith, i.e., that fracture occurs when the most severely stressed crack propagates. By considering grain boundaries as cracks, it was found that the uniaxial compressive strength and the maximum grain size for two crystalline limestones agreed with Griffith's predictions (Brace, 1961) and that the tensile strength of certain rocks could be predicted to within a factor of two by substituting measured quantities into Griffith's expression for tensile strength (Brace, 1964). Perhaps, the strongest support for the mechanism suggested by Griffith was the agreement of experimental data with the McClintock-Walsh fracture criterion which differed with Griffith's only in that frictional stresses on the crack surfaces were included in the analysis. The experimental results agreeed best with the McClintock-Walsh criterion which incorporated a coefficient of friction of about unity, a reasonable value in view of measured values of friction of rock surfaces.

A study of crack propagation in a compressive stress field (Brace and Bombolakis, 1963) and the change in the stress conditions when cracks are in close proximity (Bombolakis, 1963) indicated that some discrepancy between theory and actuality might exist. However, the observations that the McClintock-Walsh modification is identical with the empirical Coulomb law (Brace, 1960) and that crack growth and faulting occur in certain rocks at about the same stress difference (Brace and Bombolakis, 1963) suggested that the McClintock-Walsh modification of the Griffith theory was a valid fracture criterion.

The results of this investigation indicate that certain, rather fundamental, changes in our conception of the fracture process are necessary. One of the more important results of this study was the conclusive evidence that, in both uniaxial and confined compression tests, crack growth occurs in Westerly granite, a typical, crystalline, silicate rock, at about half the stress difference required for fracture. Crack growth at stresses much less than the compressive strength also occured in other common rock types as previously noted (page 77). Therefore, it is concluded that neither the Griffith theory nor the McClintock-Walsh modification can be expected to predict the compressive strength of common rocks.

However, the agreement between the McClintock-Walsh modification and the stress difference required to initiate crack growth (Chapter IV, Figure 26) suggests that the present modification of the Griffith theory is suitable for predicting the onset of crack growth.

The pronounced increase in volume due to crack growth has rather broad implications regarding a fracture theory. In particular, comparison of the pdV work and the total work required for fracture (Chapter IV, Table 8) suggests that an appreciable amount of the input work goes into work against the pressure medium. Orowan (1964) suggested that the strength of a material could be considered as the work required for fracture as well as the maximum stress difference the material can support. If the strength of a material is thought of as the work required for fracture, then the pdV work is obviously of importance and should be considered in developing a fracture criterion. In tension, the stress required to initiate crack growth is the fracture strength since the most critical crack becomes more severely stressed once growth occurs. Therefore, there is probably not the pronounced volume increase during tensile fracture as is observed in compression. This suggests, then, an additional fundamental difference between fracture in compression and in tension.

The compressibility tests and visual inspection of the fractured material indicated that the direction of new crack growth was essentially parallel with the direction of maximum compression, i.e., vertical. This behavior is exactly as found by Brace and Bombolakis in their study of crack growth in glass and plastic.

Examination of the polished sections (Figures 16, 17, and 32) and the surface exposure of partial faults in the deformed samples (Figure 31) indicates that some of these vertical cracks are incorporated into the fracture surface. The presence of vertical cracks along an inclined fracture results in a rough, step-like, surface. The direction of these steps is such that they resist frictional sliding in the direction imposed by the stress state which formed the fracture. Similar observations were reported by Paterson (1958). It may be that the roughness of natural faults is a result of the same mechanism. Presumably, some of these steps must be broken for frictional sliding to occur.

Brace (1960) pointed out a fundamental inconsistency in the Navier-Coulomb theory when he questioned the simultaneous existance of both the friction and cohesion terms on a given surface. Observation of the offsets in the grid of the strain gage of a partially-fractured specimen (Figure 31), indicates that motion has occurred along a fault which does not extend completely through the specimen. This

suggests that even if the Navier-Coulomb theory is modified to remove the discrepancy noted by Brace, it still could not be expected to predict the strength of a material unless it considered the relative magnitudes of the friction and cohesion terms as fracture is approached.

The stress was held essentially constant for intervals of about five minutes during some of the uniaxial compression tests. During this time the lateral strain increased at a perceptible rate, particularly in the first minute or two. It was generally impossible to detect any motion of the recording pen at the end of the five-minute interval. The increase in volume which occurred during these intervals is caused by the growth of cracks. This evidence, together with that of the experiments which show the effect of strain rate on the amount of crack growth, suggests that the growth of cracks in the Westerly granite is time-dependent.

The character of the tests during the five-minute intervals is essentially that of creep test. Therefore, the results of this study support the suggestion made by Robertson (1958) that crack growth may be an important mechanism during the creep of rock, particularly at low to moderate temperatures and confining pressures.

There are several questions, in addition to those presented earlier, which must be answered before we are able to predict the strength of rock from fundamental properties.

For example, the motion which occurs along a fault, prior to complete fracture, indicates that a theory of friction is necessary. Such a theory should extend to very rough surfaces to determine the influence of the steps along a fault in preventing motion. The appreciable pdV work which occurs during confined compression tests indicates that the relative magnitude of the three principal stresses may be more important than previously considered (Brace, 1964).

Concerning the time-dependence of crack growth, an investigation should be made of the diffusion of water vapor or other common contaminants through a rock and the effect of such contaminants on the surface energy and strength properties of minerals. In addition to a more thorough knowledge of the factors which influence the growth of cracks such a study might provide insight into the mechanism of creep of silicate rocks and the reasons for a strain-rate effect on crack growth.

ACKNOWLEDGEMENTS

The initial part of the photoelastic analysis was carried out during the summer of 1963 under the support of the theoretical Geophysics Branch of the U.S. Geological Survey. Since then, support was provided by the National Science Foundation, Project GP 1470. This support is gratefully acknowledged.

The facilities of the machine shop were available through the courtesy of Mr. Fred Gripper who provided instruction in the preparation of the rock samples and construction of several items used during the thesis.

The criticism and suggestions of Dr. E. C. Robertson and Mr. E. Hoek with regard to the photoelastic analysis were helpful. Drs. J. Handin and H. Heard assisted by discussing the experimental results. Suggestions by fellow students, in particular J. Byerlee and K. Larner are appreciated.

Special appreciation is extended to Professor W. F. Brace and Dr. J. B. Walsh. Their analysis of the experimental techniques and results, pertinent suggestions and discussion of unpublished material were of valuable assistance throughout the investigation.

I am indebted to my wife, Connie, for the typing of the manuscript. In addition, her cheerfulness and interest was a constant source of encouragement.

BIBLIOGRAPHY

Cited References

Birch, F., 1961, The velocity of compressional waves in rocks to 10 kb, Part II: Jour. Geop. Res., 66, p. 2199-2224.

Blakey, F.A., and Beresford, F.D., 1953, Tensile strains in concrete, Part I: C.S.I.R., Div. of Bldg. Res., Report C2.201, 33 pp.

Bombolakis, E.G., 1963, Photoelastic stress analysis of crack propagation within a compressive stress field: Ph.D. thesis, Massachusetts Institute of Technology.

Brace, W.F., 1960, An extension of the Griffith theory of fracture to rocks: Jour. Geop. Res., 65, p. 3477-3480.

Brace, W.F., 1961, Dependence of fracture strength of rocks on grain size: Penn. State Univ. Mineral Expt. Sta. Bull., no. 76, p. 99-103.

Brace, W.F., 1963, personal communication.

Brace, W.F. and Bombolakis, E.G., 1963, A note on brittle crack growth in compression: Jour. Geop. Res., 68, p. 3709-3713.

Brace, W.F., 1964, Brittle fracture of rocks: in State of Stress in the Earth's Crust, Ed. W.R.Judd, New York, American Elsevier Pub. Co., 110-178 pp.

Brace, W.F., 1965, Some new measurements of linear compressibility of rocks, Jour. Geop. Res., 70, no. 2.

Bridgman, P.W., 1949, Volume changes in the plastic stages of simple compression: Jour. Appl. Phys., 20, p. 1241-1251.

Christie, J.M., Heard, H.C., and LaMori, P.N., 1964, Experimental deformation of quartz single crystals at 27 to 30 kilobars confining pressure and 24°C, Am. Jour. Sci., 262, p. 26-55.

Frocht, M.M., 1941, Photoelasticity, I and II: New York, John Wiley and Sons.

Griffith, A.A., 1921, The phenomena of rupture and flow in solids: Phil. Trans. Roy. Soc. London, A., 221, p. 163-197.

Griffith, A.A., 1924, The theory of rupture: Proc. First Int. Cong. Appl. Mech., Delft, p. 55-63.

Handin, John, 1964, personal communication.

Inglis, C.E., 1913, Stresses in a plate due to the presence of cracks and sharp corners: Inst. Naval Arch. (London), 55, p. 219-230.

Jaeger, J.C., 1959, The frictional properties of joints in rocks: Geofisica pure e applicata, Milano.

Matsushima, Shogo, 1961, On the flow and fracture of igneous rocks: Jour. Phy. of the Earth, 9, p. 2-9.

McClintock, F.A., and Walsh, J.B., 1962, Friction on Griffith cracks in rocks under pressure: Proc. Natl. Congr. Appl. Mech., 4th, Berkeley, p. 1015-1021.

Obert, L., and Duvall, W., 1945, The microseismic method of predicting rock failure in underground mining, Part II - Laboratory Experiments: U.S. Bur. Mines Rpt. Inv., no. 3803.

Orowan, E., 1964, personal communication.

Paterson, M.S., 1958, Experimental deformation and faulting in Wombeyan marble: Geol. Soc. America Bull., 69, p. 465-476.

Peterson, R.E., 1953, Stress concentration design factors: New York, John Wiley and Sons, Inc., 155 pp.

Robertson, E.C., 1958, Creep of Solenhofen limestone under moderate hydrostatic pressure: Geol. Soc. America Mem., 79, p. 227-245.

Salmassy, O.K., Duckworth, W.H., and Schwope, A.D., 1955, Behavior of brittle-state materials: U.S. Air Force WADC Tech. Rpt., no. 53-50, Part I, 145 pp.

Savin, G.N., 1961, Stress concentration around holes: New York, Pergamon Press, 430 pp.

Seldengrath, T.R., and Gramberg, J., 1958, Stress-strain relations and breakage of rocks: in Mechanical properties of non-metallic brittle solids, by W.H. Walton, New York, Interscience, p. 79-102.

Timoschenko, S., and Goodier, J.N., 1951, Theory of elasticity: New York, McGraw-Hill.

Topping, J., 1957, Errors of observation and their treatment: London, Chapman and Hall, 119 pp.

Walsh, J.B., 1964, personal communication.

Walsh, J.B., 1965a, The effect of cracks on the compressibility of rock: Jour. Geop. Res., 70, no. 2.

Walsh, J.B., 1965b, The effect of cracks on the uniaxial elastic compression of rocks: Jour. Geop. Res., 70, no. 2.

Wells, A.A., and Post, D., 1958, The dynamic stress distribution surrounding a running crack - a photoelastic analysis: Proc. Soc. Exp. Stress Analysis, 16, no. 1, p. 69-92.

Supplementary References

Bredthauer, R.O., Strength characteristics of rock samples under hydrostatic pressure: Am. Soc. Mech. Engrs. Trans., 79, p. 695-708.

Bridgman, P.W., 1952, Studies in large plastic flow and fracture: New York, McGraw-Hill, 362 pp.

Clausing, D.P., 1959, Comparison of Griffith's theory and Mohr's failure criterion, Quart. Colorado School of Mines, 54, p. 285-296.

Colback, P.S.B. and Wiid, B.L., 1965, The influence of moisture content on the compressive strength of rock: South African Council for Sci. and Indust. Research Rpt., in preparation.

Griggs, D., 1942, Strength and plasticity: in Handbook of Physical Constants, Geol. Soc. America, Spec. Paper 36, p. 107-131.

Griggs, D. and Handin, J.H., Observations on fracture and a hypothesis of earthquakes: Geol. Soc. America Mem., 79, p. 347-364.

Murrell, S.A.F., 1962, The effect of high pressure on brittle fracture: Proc. of the Conference on Physics and Chemistry of High Pressure, London.

Murrell, S.A.F., 1963, A criterion for brittle fracture of rocks and concrete under triaxial stresses, and the effect of pore pressure on the criterion: Proc. 5th Symposium Rock Mechanics.

Nadai, A., Theory of flow and fracture of solids: New York, McGraw-Hill, 572 pp.

Obert, I., Windes, S.L. and Duval, W.I., 1946, Standardized tests for determining the physical properties of mine rock: U.S. Bur. Mines Rpt. Inv., no. 3891, p. 1-67.

Orowan, E., 1949, Fracture and strength of solids: Rpt. Prog. Physics, 12, p. 185-232.

Robertson, E.C., 1955, Experimental study of the strength of rocks: Geol. Soc. America Bull., 66, p. 1275-1314.

Terzaghi, K., Stress conditions for the failure of saturated concrete and rock: Am. Soc. Testing Matls. Proc., 45, P. 777-801.

Walsh, J.B. and Brace, W.F., 1964, A fracture criterion for brittle anisotropic rock, Jour. Geop. Res., 69, p. 3449-3456.

APPENDIX 1

CRITICAL ORIENTATION OF ELLIPTICAL OPENINGS IN A COMPRESSIVE STRESS FIELD

The most critical orientation of an elliptical opening in a biaxial stress field is given by (Bombolakis, 1963)

$$\cos 2\Psi = -\frac{1}{2}\left(\frac{P - Q}{P + Q} \cdot \frac{a + b}{a - b} - \frac{P + Q}{P - Q} \cdot \frac{4ab}{a^2 - b^2}\right)$$

(Equation 1)

where a and b are the semi-major and semi-minor axes, respectively,

P and Q are the principal compressive stresses, and

Ψ is the inclination of the long axis of the ellipse from the direction of Q.

For uniaxial compression, P + 0, and Equation 1 reduces to

$$\cos 2\Psi = \frac{1}{2}\left(\frac{a + b}{a - b} - \frac{4ab}{a^2 - b^2}\right)$$

$$\cos 2\Psi = \frac{1}{2}\left(\frac{\frac{a}{b} + 1}{\frac{a}{b} - 1} - \frac{4\,\frac{a}{b}}{(\frac{a}{b})^2 - 1}\right)$$

(Equation 2)

Substitution of $\frac{a}{b} = 4, 5, 6$ and 7 into Equation 2 gives $\Psi = 36.2^\circ, 35.0^\circ, 34.6^\circ$ and 34.0°, respectively.

APPENDIX 2

DESIGN OF THE STIFFENING ELEMENT

The fundamental quantity to consider in designing a "stiff" loading system is the additional amount of strain energy which is introduced into the specimen during the fracture process. A schematic diagram of a stiff loading system is shown in Figure 37 to aid an understanding of the design principles.

The spring of low spring constant, K_R, represents the rock specimen and the spring of spring constant, K_s, represents the stiffening element incorporated into a conventional loading press. The applied load is indicated by F. As the load, F, is increased to the point just before fracture, the springs deflect by the amount δ .

The strain energy in a spring of constant K subjected to a force, F, which has undergone a deflection, δ, is

$$\int_0^F \delta \, dF = \int_0^F \frac{F}{K} \, dF = \frac{F^2}{2K} = \left(\frac{K\delta^2}{2}\right)$$

(Equation 1)

Therefore, the energy in the spring which represents the rock just prior to failure is $\frac{F_R^2}{2K_R} = E_R$.

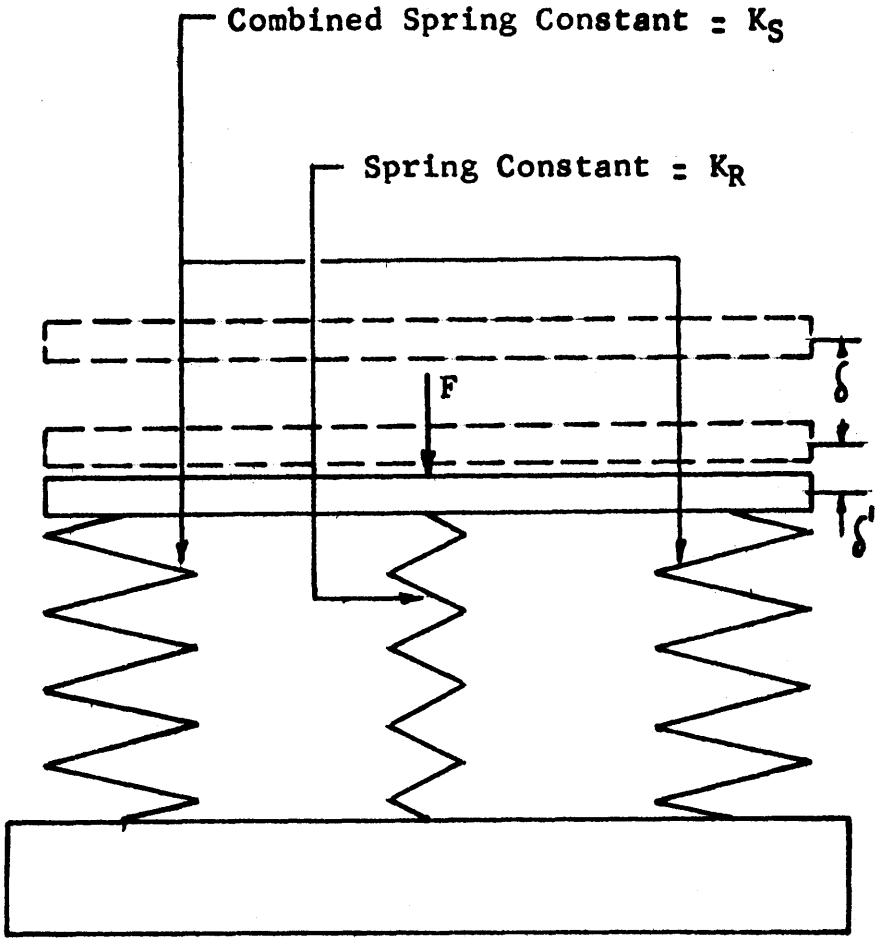

Schematic Diagram of Stiff Loading System

Figure 37

When the rock begins to fail its load-carrying ability decreases and a portion of the load, F_R, is transferred to the stiffening element which undergoes an additional displacement δ'. This deflection, δ', allowed by the stiffening element, introduces additional strain into the rock of an $\frac{K'_R \delta'^2}{2} = (\frac{K'_R}{2})(\frac{CF_R}{K_s})^2 = E'_R$, where K'_R is the spring constant of the partially broken rock and C is the percentage of the load-carrying ability lost due to the partial fracturing.

In order to terminate the fracture process the additional strain energy, E'_R should be a small percentage, n, of the strain energy in the rock just prior to failure, E_R.

Thus $E'_R = n\ E_R$. Substitution gives $(\frac{K'_R}{2})(\frac{CF_R}{K_s})^2 = n\ \frac{F_R^2}{2K_R}$ and therefore,

$$\frac{K_R K'_R}{K_s^2} = \frac{n}{C} . \qquad \text{(Equation 2)}$$

This development cannot be extended without knowledge of the stress-strain curve. However, by letting $C = 1$ and $K'_R = K_R$, one obtains

$$(\frac{K_R}{K_s})^2 = n \qquad \text{(Equation 3)}$$

which, when used for design purposes, will yield an overly-stiff loading system.

Circular Ring in Parallel with Rock Specimen

The initial modification of the hydraulic loading system consisted of placing the rock specimen within a circular ring of steel, as shown in Figure 38. The equivalent spring constants for the rock specimen and the steel ring are given by

$$K = \frac{EA}{H} \qquad \text{(Equation 4}$$

where E = Young's modulus
A = Area of cross-section normal to load
H = Height

substitution of Equation 4 into 3 gives

$$\frac{\left(\frac{E_R A_R}{H_R}\right)^2}{\left(\frac{E_S A_S}{H_S}\right)^2} = n \qquad \text{(Equation 5)}$$

It is not necessary to have the steel ring incorporated into the loading system during the elastic portion of the stress-strain curve of the rock. Therefor, the height of the rock sample exceeded that of the steel ring by a few thousanths of an inch. For design purposes, however, they may be considered equal and Equation 5 becomes

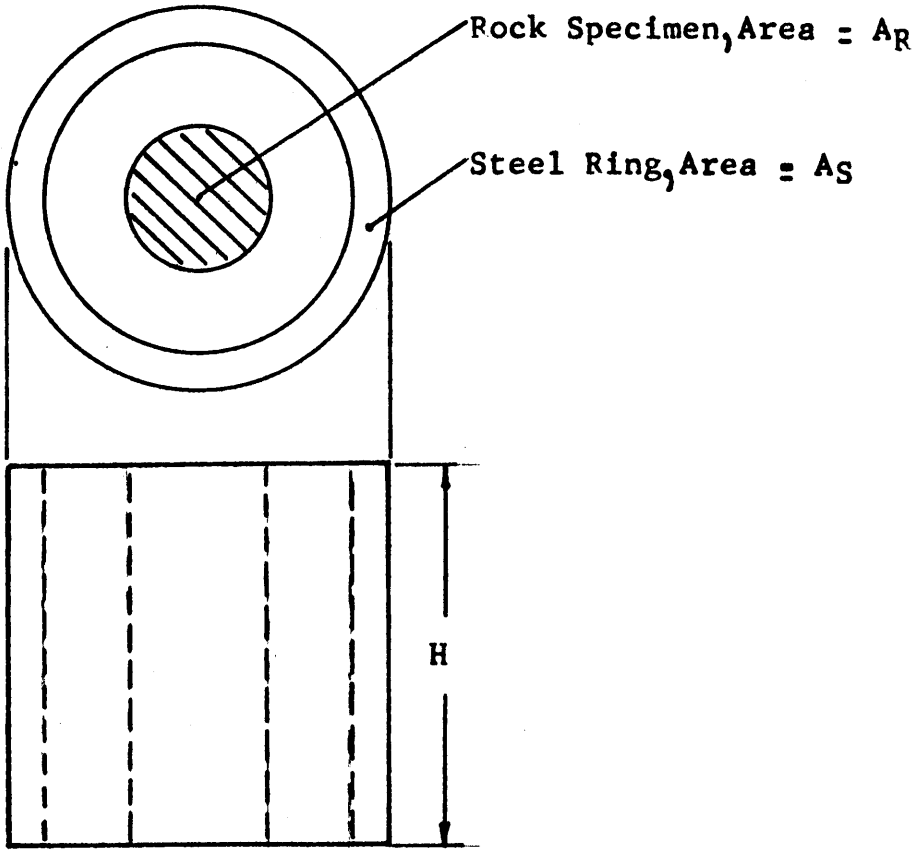

Circular Ring Used for Stiffening Element

Figure 38

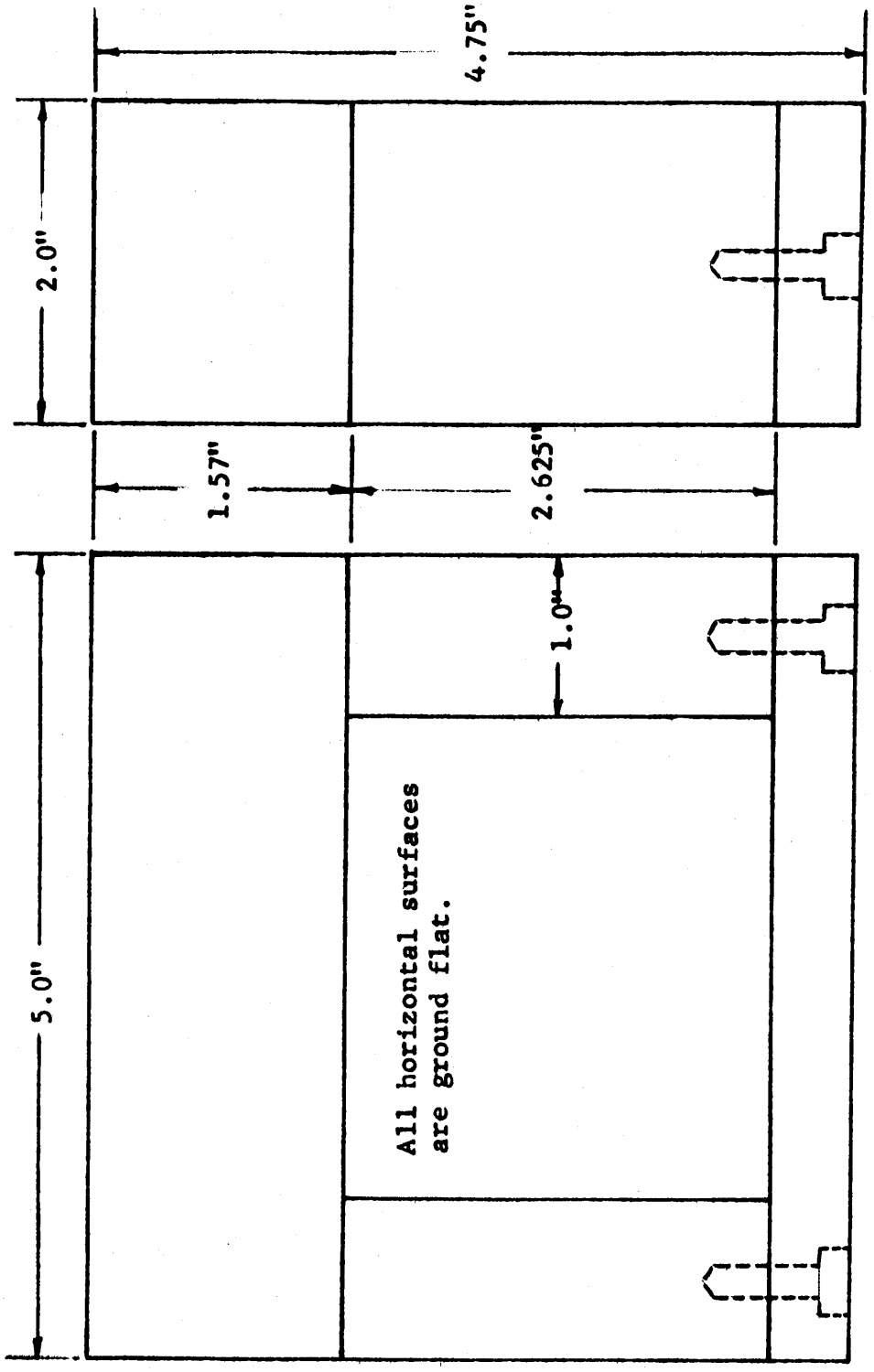

Dimensions of Stiffening Element

Figure 39

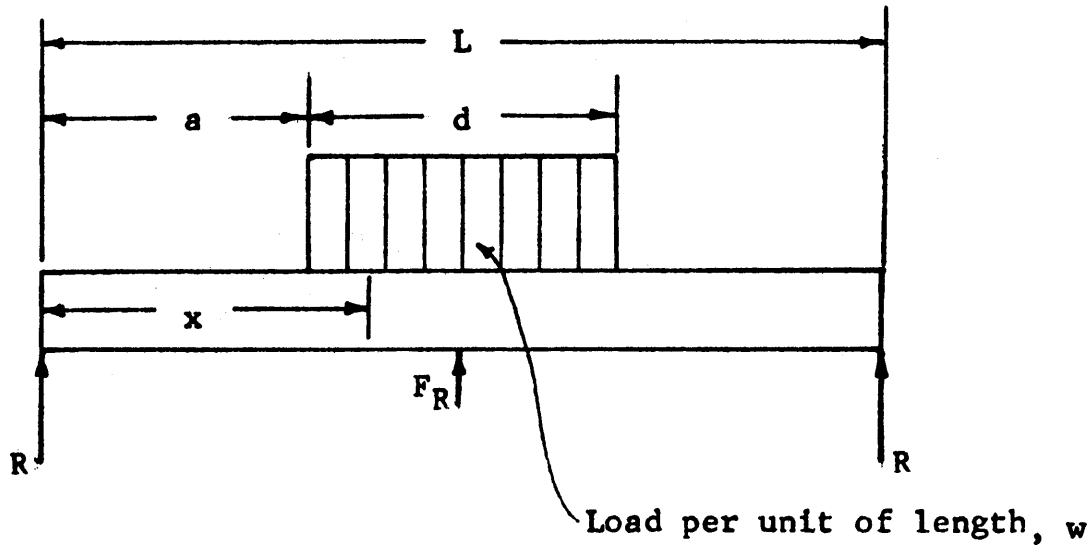

Simply Supported Beam with Uniform Load

Figure 40

$$\left(\frac{E_R}{E_S}\right)^2 \left(\frac{A_R}{A_S}\right)^2 = n \qquad \text{(Equation 6)}$$

The choice of rock type, sample size, and n determines A_S according to

$$A_S = \left(\frac{E_R}{E_S}\right)(A_R)\left(\frac{1}{\sqrt{n}}\right) \qquad \text{(Equation 7)}$$

Stiff Beam in Parallel with Rock Specimen

A more versatile modification of the loading press consisted of placing the rock sample beneath a beam as shown in Figure 39. The development of an expression for the stiffness of the element shown in Figure 39 is only an approximation for two reasons: (1) The small length to depth ratio of the beam, and (2) The relatively large width of the supports.

Three factors entered into the design of this stiffening element: (1) the necessary stiffness, (2) a convenient size, and (3) the yield strength of the steel.

The bending moment, M_x, in a simply supported beam which carries a uniform load over part of its span is given by

$$M_x = Rx - \frac{w}{2}(x - a)^2 . \qquad \text{(Equation 8)}$$

(A.I.S.C. Steel Construction Manual). A schematic diagram is presented in Figure 40 to explain the terms in Equation 8.

Let the force applied by the hydraulic ram be denoted by F. Since $w = \frac{F}{d}$, Equation 8 becomes

$$M_x = \frac{R}{x} - \frac{F}{2d}(x - a)^2 . \qquad \text{(Equation 9)}$$

The bending moment is related to Young's modulus, the moment of inertia and the curvature of the beam according to

$$EI \frac{d^2y}{dx^2} = M_x .$$

Therefore,

$$EI \frac{dy}{dx} = \int M_x dx$$

$$= R \frac{x^2}{2} - \frac{F}{2d} \left(\frac{x^3}{3} - x^2a - xa^2\right) + C_1,$$

(Equation 10)

where C_1 is a constant of integration. At $x = \frac{L}{2}$, $\frac{dy}{dx} = 0$. Therefore,

$$C_1 = \frac{F}{2d} \left(\frac{L^3}{24} - \frac{L^2a}{4} - \frac{La^2}{2}\right) - \frac{RL^2}{8} . \quad \text{(Equation 11)}$$

An additional integration gives

$$EIy = \frac{Rx^3}{6} - \frac{F}{2d} \left(\frac{x^4}{12} - \frac{x^3a}{3} - \frac{x^2a^2}{2}\right) + C_1x + C_2 .$$

(Equation 12)

At $x = 0$, $y = 0$. Therefore, $C_2 = 0$.

Substitution of C_1 into Equation 12 and rearranging gives

$$y = \left(\frac{1}{EI}\right)\left[\frac{Rx^3}{6} - \frac{F}{2d} \left(\frac{x^4}{12} - \frac{x^3a}{3} - \frac{x^2a^2}{2}\right) + x\left(\frac{F}{2d} \left(\frac{L^3}{24} - \frac{L^2a}{4} - \frac{La^2}{2}\right) - \frac{RL^2}{8}\right)\right].$$

(Equation 13)

The maximum deflection occurs at mid-span and is

$$y_{maximum} = \frac{1}{EI}\left[-\frac{RL^3}{24} + \frac{FL^2}{8d}\left(\frac{L^2}{16} - \frac{La}{3} - \frac{a^2}{2}\right)\right]$$

(Equation 14)

In addition to the deflection from bending, there is additional deflection due to the shortening of the vertical supports. The deflection resulting from this is

$$y = \frac{RH}{AE}, \qquad \text{(Equation 15)}$$

where H, A are the height and area, respectively, of the vertical supports.

The specimen exerts a force, F_R, on the beam which tends to counteract the applied force, F. Thus with $R = \frac{1}{2}(F - F_R)$ the total deflection is given by

$$y_{total} = \frac{(F - F_R)H}{2AE} + \frac{1}{EI}\left[-\frac{(F - F_R)L^3}{48} + \frac{(F-F_R)L^2}{8d}\left(\frac{L^2}{16} - \frac{La}{3} - \frac{a^2}{2}\right)\right]$$

(Equation 16)

The stiffness, K_S, of the beam is given by $\frac{F}{y_{max}}$. Since F_R is much less than F one finds that

$$\frac{1}{K_S} - = \frac{H}{2AE} + \frac{1}{8EI}\left[\frac{-L^3}{6} + \frac{L^2}{1-2a}\left(\frac{L^2}{16} - \frac{La}{3} - \frac{a^2}{2}\right)\right].$$

(Equation 17)

Substitution of Equations 4 and 17 into Equation 3 gives

$$\left(\frac{K_R}{K_S}\right)^2 = n = \left(\frac{A_R E_R}{H_R}\right)^2 \frac{H}{2AE} + \frac{1}{8EI}\left[\frac{-L^3}{6} + \frac{L^2}{1-2a}\left(\frac{L^2}{16} - \frac{La}{3} - \frac{a^2}{2}\right)\right]^2$$

(Equation 18)

Equation 18 is used to determine the moment of inertia, I, required to give the necessary stiffness once the other dimensions, rock type and n have been chosen.

In order to include the possibility of yielding of the steel a relationship must be found between the dimensions of the beam and the maximum deflection. If the yield point of steel is σ_y, then the maximum elastic strain is given by $\epsilon = \frac{\sigma_y}{E}$ (Equation 19). The maximum strain in a beam of thickness h with a radius of curvature R is

$$\epsilon = \frac{h}{2R} \qquad \text{(Equation 20)}$$

and to prevent yielding $\frac{h}{2R}$ must be less than $\frac{\sigma_y}{E}$. The relationship between the span length, thickness and maximum deflection is found with the aid of Figure 41.

From Figure 41 one sees that

$$y = R(1 - \cos\theta) \text{ and,}$$

therefore,

$$\cos\theta = \frac{R - y}{R} \quad .$$

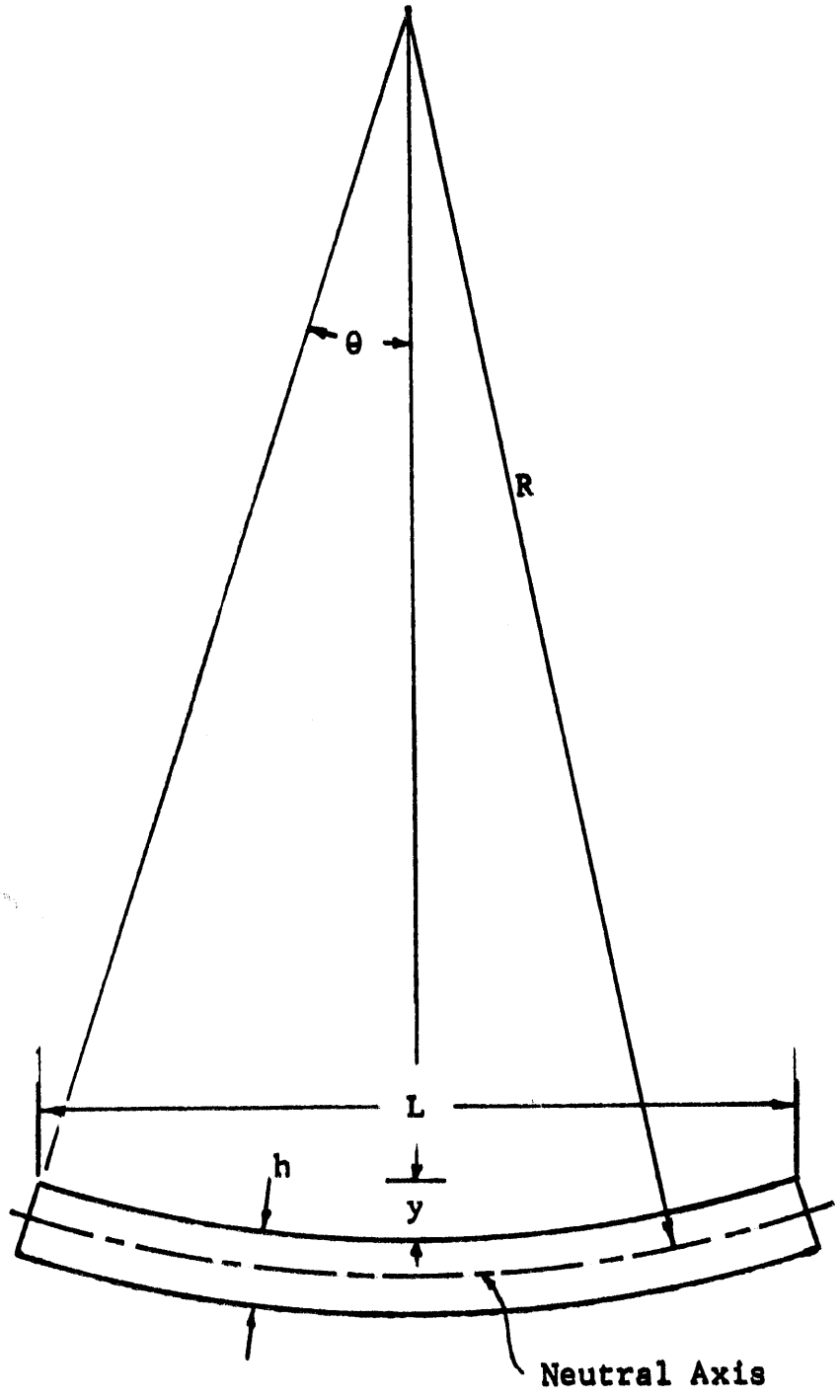

Beam in Simple Bending

Figure 41

Also, $\frac{L}{2} = R \sin \Theta$ and, therefore, $\sin \Theta = \frac{L}{2R}$. One finds with use of the identity $\sin^2\Theta + \cos^2\Theta = 1$ and some re-arranging, that

$$R = \frac{4y^2 + L^2}{8y} . \qquad \text{(Equation 21)}$$

The condition for no yielding is

$$\frac{h}{2R} < \frac{\sigma_y}{E} \qquad \text{(Equation 22)}$$

Substituting Equation 21 into Equation 22 gives

$$\frac{4hy}{4y^2 + L^2} < \frac{\sigma_y}{E} \qquad \text{(Equation 23)}$$

as the condition for no yielding.

The moment of inertia , I, was determined from Equation 18 by substitution of the appropriate values for A_R, E_R, H_R (subscripts denote rock), $\underline{a}$, E, $\underline{n}$ and arbitrary values for H, A, L. The values for H, A, and L were selected on the basis of a convenient size.

The moment of inertia, I, is given by

$$I = \frac{bh^3}{12} , \qquad \text{(Equation 24)}$$

where b = width of beam
h = thickness of beam.

A width of two inches was selected for convenience.

By solving Equation 24 for h and determining the deflection, y, required during a uniaxial compression test, the necessary yield point of the steel could be determined from Equation 23.

APPENDIX 3

LIMITATIONS OF A PRESS OF FINITE STIFFNESS

The purpose of the stiffening element in a conventional loading press is to terminate the fracture process until the load is further increased by the operator. The effectiveness of such a loading technique depends on the stiffness of the element and the complete stress-strain curve of the material being tested.

Imagine a stiffening element placed in parallel with a rock sample such as shown in Figure 7. Denoting the load on the rock sample by F_R and the load carried by the stiffening element as F_s, a load vs deflection curve would appear as shown in Figure 42.

The fracture process is controllable in the region of the load vs deflection curve denoted by B-B'. However, at point B' (corresponding to A on the F_T curve, C on the F_s curve) the stiff modification becomes unstable and the deflection d occurs instantaneously, resulting in complete fracture of the specimen.

The instability occurs when $\frac{dF_T}{d\delta} = 0$. Since $F_T = F_R + F_s$, the press is unstable when $\frac{dF_R}{d\delta} = -\frac{dF_s}{d\delta}$, i.e., when the slopes

of the two curves F_R and F_S are equal but of opposite sign. The fracture process is controllable as long as $\frac{dF_S}{d\delta} > \left|\frac{dF_R}{d\delta}\right|$. Any press is limited in that it allows control of the fracture process only up to the point at which the load-deflection curve of the rock begins to decrease at a rate faster than the rate of increase of the load-deflection curve of the stiffening element.

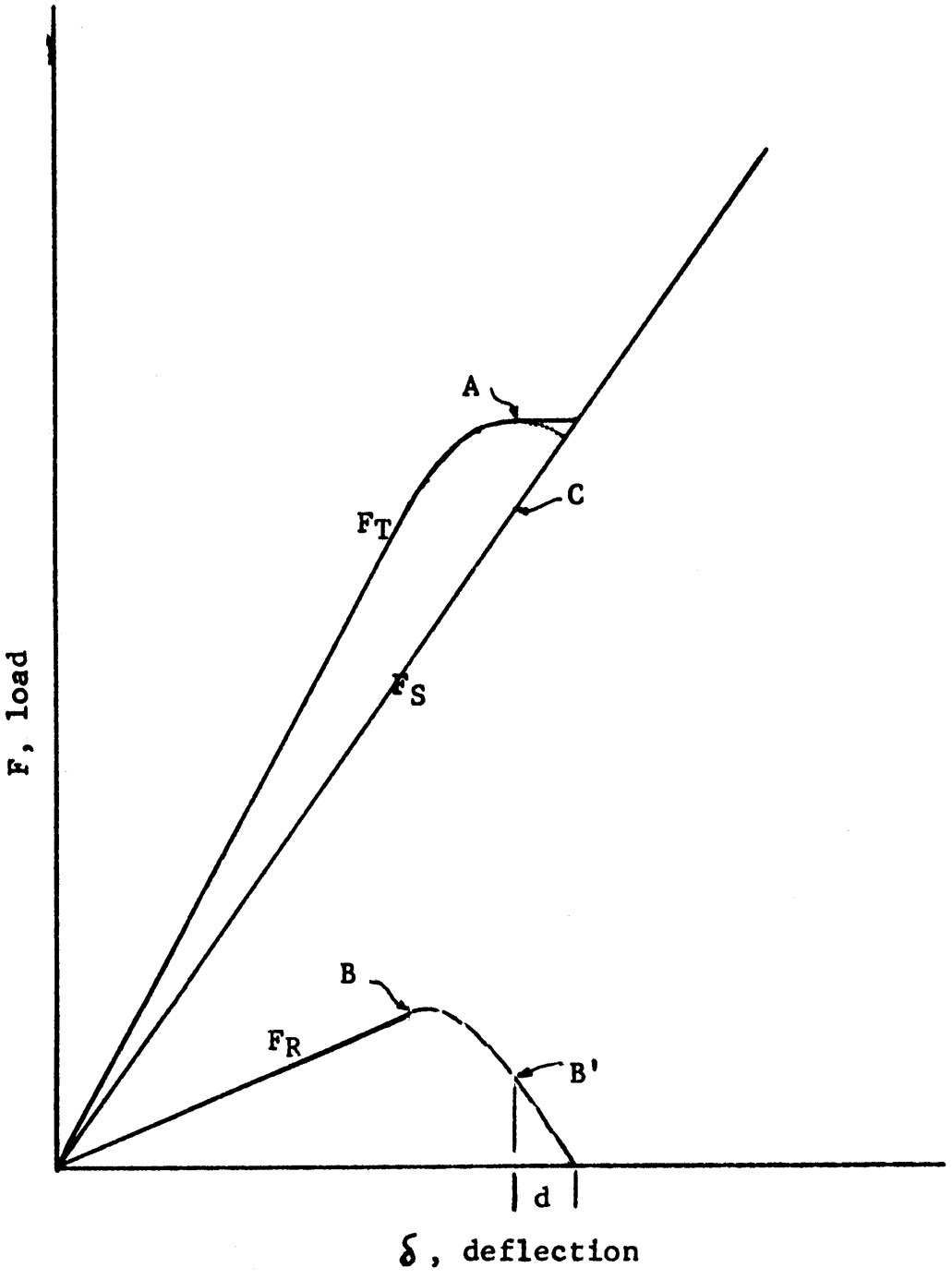

Load vs. Deflection Curve of
Rock Specimen and Stiffening Element

Figure 42

APPENDIX 4

PREPARATION OF SAMPLES

The dimensions of the sample are shown in Figure 43. Figure 44 is a photograph of the sample. Cores with a diameter slightly greater than 0.625" were placed in a cylindrical grinder and the entire surface was ground to the finished diameter of the heads. The diamond wheel (Crystalon, by Norton Company) was then shaped to produce the radius of the fillet and the throat region was shaped.

The core, which at this point consisted of three to four samples joined end to end, was cut on a diamond saw into lengths of about 2.050". The ends were then ground parallel on a surface grinder to the final length.

Damage to the sample during preparation was minimized by means of coolants and restricting cuts to less than 0.005". In general, the final sample had a smooth finish and all edges were undamaged.

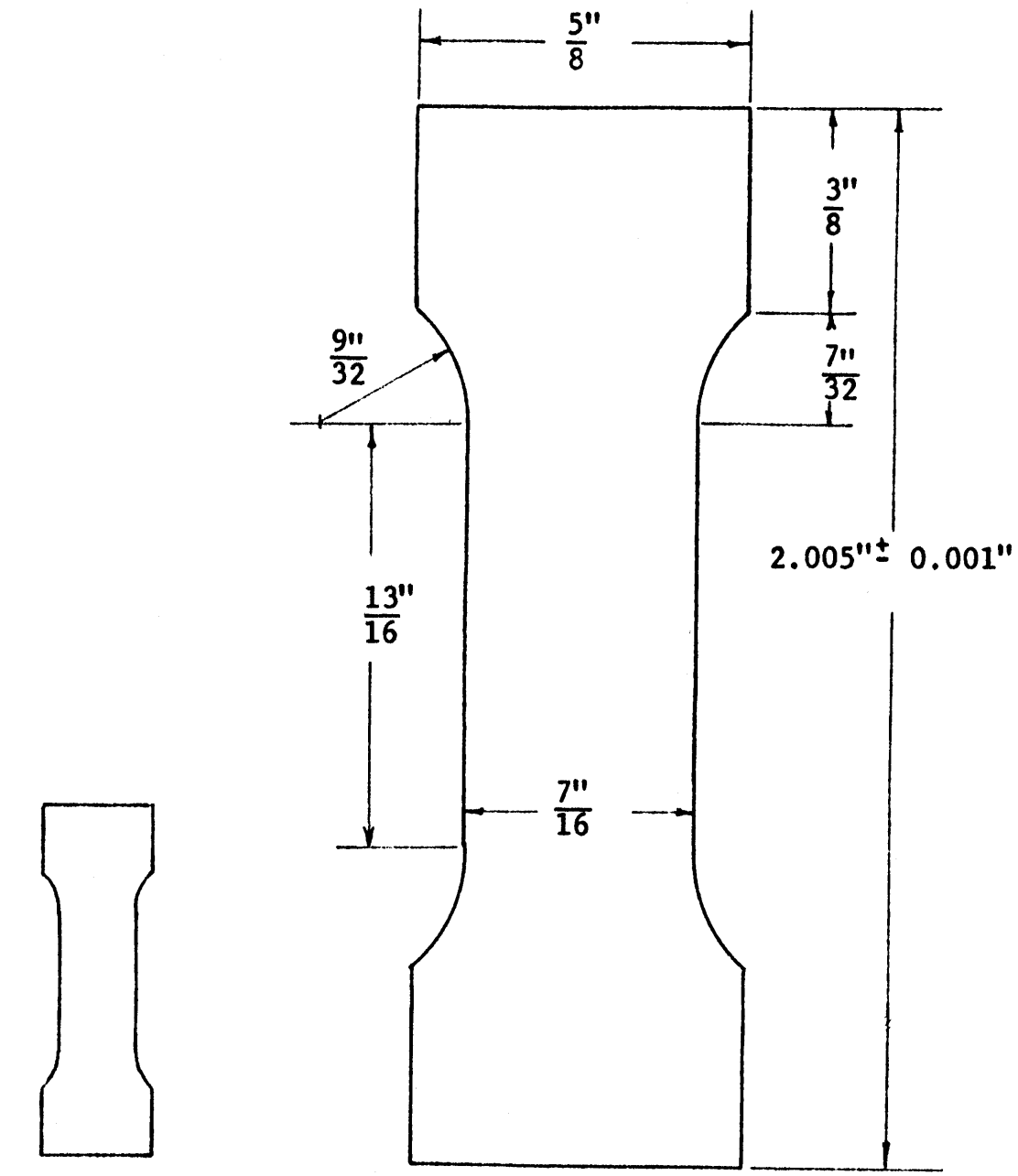

Dimensions of Rock Specimen

Figure 43

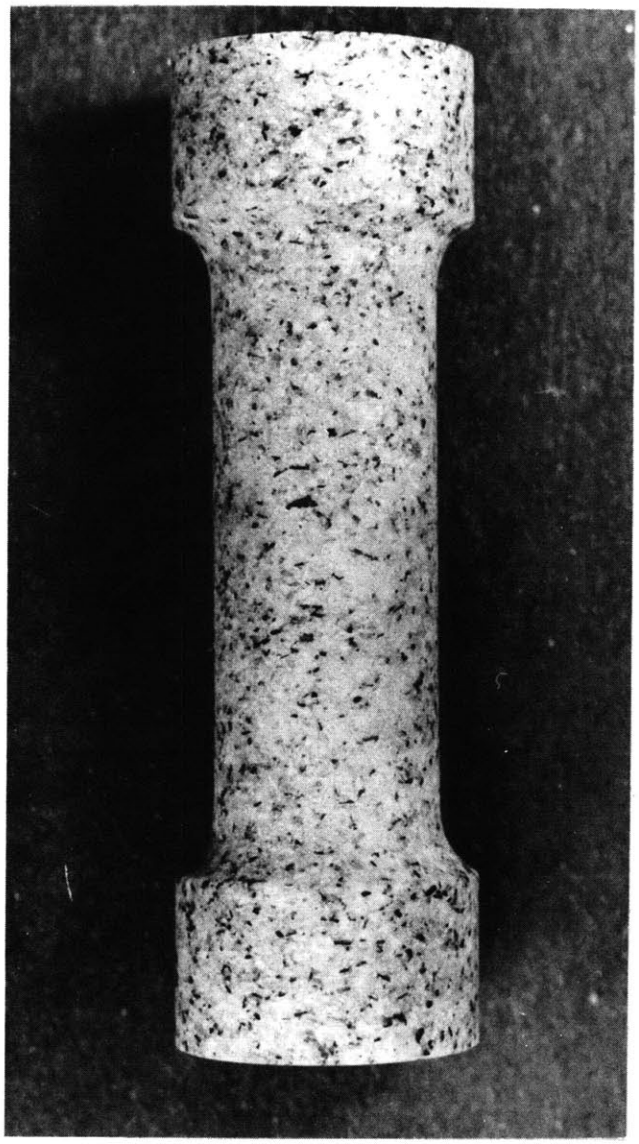

Rock Specimen

Figure 44

APPENDIX 5

DESIGN AND CALIBRATION OF THE LOAD CELL

Design

As shown in Figure 7, a load cell was placed in series with the rock sample to obtain the stress supported by the specimen.

The load cell is a straight cylinder of hardened (Rockwell 55c) drill steel to which are affixed four strain gages (BLH FAC-12-50), as shown in Figure 46.

Gages 1 and 3 measure longitudinal strain and gages 2 and 4 measure lateral strain. For recording purposes, the four gages are incorporated into the four arms of a Wheatstone bridge, as shown in Figure 46.

The output of this Wheatstone bridge is given by

$$\Delta G = \frac{E}{4}\left[\frac{\Delta R_1 - \Delta R_2 + \Delta R_3 - \Delta R_4}{R_o}\right] \quad \text{(Equation 1)}$$

where ΔG = output voltage
E = input voltage
R_o = initial resistance of strain gage
ΔR_i = change in resistance of i^{th} gage.

Wheatstone Bridge

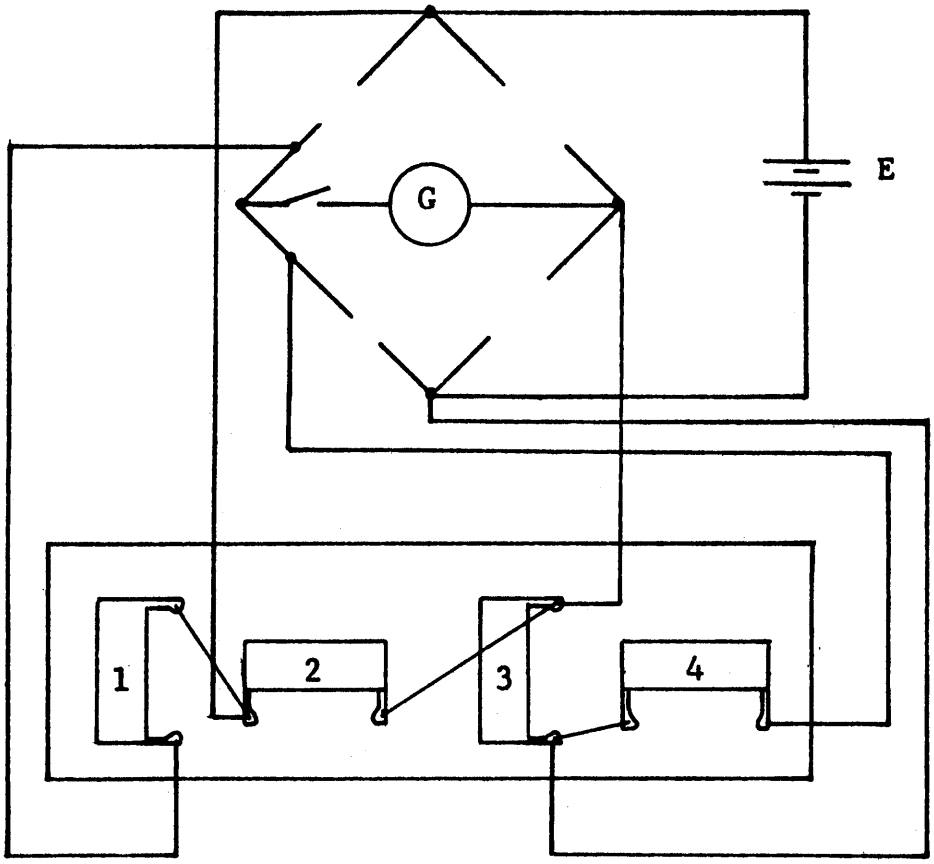

360° View of Load Cell

Load Cell and Strain Gage Circuit

Figure 46

The resistance of a strain gage increases with an increase in length. Therefore, when the load cell is compressed, the resistance of gages 1 and 3 decreases and the resistance of gages 2 and 4 increases. Gages 2 and 4 are in adjacent arms of the bridge with respect to gages 1 and 3, so that the changes in resistance of all the gages due to strain are additive whereas changes in resistance due to temperature are self-canceling.

With $\Delta R_1 = \Delta R_3$ and $\Delta R_2 = \Delta R_4$, Equation 1 becomes

$$\Delta G = \frac{E}{2} \left(\frac{\Delta R_1 + \Delta R_2}{R_o} \right) . \qquad \text{(Equation 2)}$$

The change in resistance of a strain gage is given by

$$\frac{\Delta R}{R_o} = (G.F.)(\epsilon), \qquad \text{(Equation 3)}$$

where G.F. = gage factor
ϵ = linear strain

The output of the Wheatstone bridge can be determined by calculating the strain which the load cell will experience, determining the change in resistance of the four gages with Equation 3, and substituting into Equation 2.

For example, the maximum load experienced by the load cell during a uniaxial compression test on Solenhofen limestone would be about 6000 pounds. The area of the load

cell is 0.306 in^2 and Young's modulus is 30×10^6 psi. Therefore,

$$\epsilon_{longitudinal} = \left(\frac{6000}{0.306}\right)\left(\frac{1}{30 \times 10^6}\right) = -653 \times 10^{-6}$$

$$\epsilon_{lateral} = (-\nu)(\epsilon_{long.}) = (0.28)(-653 \times 10^{-6}) = 183 \times 10^{-6}$$

where ν = Poisson's ratio of steel.

Substituting these values into Equation 3, one finds that

$$\frac{\Delta R_1}{R_o} = \frac{\Delta R_3}{R_o} = (G.F.)(-653 \times 10^{-6}) = (2.1)(-653 \times 10^{-6})$$

$$= -1372 \times 10^{-6}$$

$$\frac{R_2}{R_o} = \frac{R_4}{R_o} = (2.1)(183 \times 10^{-6}) = 384 \times 10^{-6}$$

The magnitude of the input voltage, E, in Equation 2, is limited to avoid heating of the strain gages. For the particular gages used $R_o = 500$ and the safe value of E was determined to be 10 volts.

Therefore, according to Equation 2, the output of the Wheatstone bridge is

$$\Delta G = \frac{10}{2}(1372 + 384) \times 10^{-6} = 8780 \times 10^{-6} = 8.7 \text{ millivolts.}$$

The most sensitive scale on the recording apparatus (Moseley Autograph Model 136) is 5 millivolts for full scale deflection. Therefore, the load cell, as designed, is sensitive enough to give sufficient record.

Calibration

For recording purposes, it is desirable to know the stiffness of the load cell in terms of pounds per change in resistance of the Wheatstone bridge. An approximate value for the stiffness can be computed as follows: Denoting the strain gages by subscripts,

$$\left(\frac{\Delta R}{R_o}\right)_{1,3} = \left(\frac{F}{AE}\right)(G.F.)$$

$$\left(\frac{\Delta R}{R_o}\right)_{2,4} = (\nu)\left(\frac{F}{AE}\right)(G.F.),$$

where F = pounds force applied to the load cell. Therefore,

$$\sum \frac{\Delta R}{R_o} = 2\left(\frac{F}{AE}\right)(G.F.)(1 + \nu)$$

and

$$\frac{F}{R} = \frac{AE}{2(R_o)(G.F.)(1 + \nu)} \cdot \qquad \text{(Equation 4)}$$

Substitution of the appropriate values into Equation 4 gives

$$\frac{F}{R} = \frac{(0.306\ \text{in}^2)(30 \times 10^6\ \frac{\#}{\text{in}^2})}{(2)(500\Omega)\ (2.1)\ (1.28)} = 3420\ \frac{\#}{\Omega}$$

This value differed from the measured value by only 2.5 per cent.

The load cell is calibrated by placing it in series with a load cell of known stiffness. The stiffness of the load cell was found to be $3340\frac{\#}{\Omega} \pm 30\ \frac{\#}{\Omega}$. The range of values was less than 1 per cent from the median value.

APPENDIX 6

RECORDING INSTRUMENTATION

A three-channel recorder (Moseley Model 136) was used to obtain a graphic tracing of the DC output from the strain gages and load cell during the compression tests and the strain gages and manganin coil during the compressibility tests. The recorder was calibrated prior to a test to plot the data on a convenient scale, e.g. 500 strain units per inch. This was done by calculating from the strain gage equation,

$$\Delta R = (R_o)(\epsilon)(G.F.),$$

where ΔR = change in resistance due to a strain,
R_o = initial resistance of the strain gage
G.F.= gage factor of the strain gage,

the change in resistance associated with a certain strain. The gain on the recorder was then adjusted so that such a change in resistance would extend over a desired interval of the graph.

A null detector (Leeds and Northrup, D-C Model 9834) was used in conjunction with a guarded Wheatstone bridge (Leeds and Northrup, Model 4735) to determine the magnitude of the confining pressure during the confined compression

test. The resistance of the manganin coil increased with increasing confining pressure and the change in resistance was balanced with the Wheatstone bridge. The null detector was used to determine when balance was obtained.

APPENDIX 7

CALCULATION OF $\frac{\Delta V}{V}$ FROM TWO STRAIN GAGES

The volumetric strain experienced by anisotropic material may be determined according to

$$\frac{\Delta V}{V} = \epsilon_1 + \epsilon_2 + \epsilon_3 \quad , \qquad \text{(Equation 1)}$$

where ϵ_1, ϵ_2, and ϵ_3 are the principal linear strains.

In this study the volumetric strain was determined by summing the linear strains according to

$$\frac{\Delta V}{V} = \epsilon_{\shortparallel} + 2\,\epsilon_{\perp} \qquad \text{(Equation 2)}$$

where $\epsilon_{\shortparallel}$ and $\epsilon_{\perp}$ are the strains measured by the axial and lateral strain gages, respectively.

Use of Equation 2 assumes that

$$\epsilon_{\perp} = \frac{\epsilon_2 + \epsilon_3}{2} \quad . \qquad \text{(Equation 3)}$$

If the lateral strain gage extends over half the circumference of the sample and if the originally circular

cross-section of the specimen becomes elliptical then Equation 2 gives the true volumetric strain experienced by the sample. This is shown in the following analysis.

Imagine that the originally circular cross-section of radius r_o deforms into an ellipse of and major and minor axes, $\underline{a}$ and $\underline{b}$, respectively. If ϵ_2 and ϵ_3 are the principal strains in the plane of the cross-section then

$$a = r_o (1 + \epsilon_2)$$

$$b = r_o (1 + \epsilon_3) \qquad \text{(Equation 4)}$$

The orginal length, l_o, of a strain gage which extends over half the circumference of the sample is

$$l_o = \pi r_o \qquad \text{(Equation 5)}$$

The final length, $\underline{l}$, is to a small approximation, (C.R.C. Standard Mathematical Tables),

$$l = \left(\frac{a^2 + b^2}{2}\right)^{\frac{1}{2}} . \qquad \text{(Equation 6)}$$

The strain experienced by the strain gage is

$$\epsilon_1 = \frac{l - l_o}{l_o} \qquad \text{(Equation 7)}$$

Substitution of Equations 4, 5, and 6 into Equation 7 gives

$$\epsilon_1 = \frac{\pi\left(\frac{r_o^2(1+\epsilon_2)^2 + r_o^2(1+\epsilon_3)^2}{2}\right)^{\frac{1}{2}} - \pi r_o}{\pi r_o}$$

$$= (1 + \epsilon_2 + \epsilon_3 + \epsilon_2^2 + \epsilon_3^2)^{\frac{1}{2}} - 1 .$$

(Equation 8)

The strains are of the order of 10^{-3}. Therefore, to a small approximation,

$$\epsilon_1 = (1 + (\epsilon_2 + \epsilon_3))^{\frac{1}{2}} - 1 . \quad \text{(Equation 9)}$$

Using the binomial expansion:

$$(1 + x)^n = 1 + nx + \text{higher powers of } x$$

one finds, from Equation 9 that

$$\epsilon_1 = \frac{\epsilon_2 + \epsilon_3}{2} ,$$

to within an error of the order of ϵ^2.

Therefore, for the conditions specified, Equation 2 gives the true volumetric strain. It is recognized that an indeterminant error exists if the strain gage extends over other than half the circumference and if the cross-section deforms to a shape other than elliptical. However,

except at just before fracture, it is expected that, (1) the strains vary uniformly around the sample, and (2) the difference between the principal strains is small. Therefore, small departures from the original assumptions should not significantly affect the validity of Equation 2.

APPENDIX 8

ERROR ANALYSIS

Recording System

The changes in resistance of the strain gages, load cell, and manganin coil were either displayed on the three-channel recorder or measured directly with a Wheatstone bridge.

The three-channel recorder (Moseley, Model 136) has a reported accuracy better than 0.20 per cent. Therefore the maximum error in measuring changes in resistance is 0.20 per cent.

Linear Strain Measurement

The error of the strain measurements is less than two per cent. Bending in samples with a length to diameter ratio slightly greater than the samples used in this study caused errors in the strain measurements of about one per cent (Brace, 1964). The initial resistance and the gage factor of the strain gages are given to within 0.16 and 0.50 per cent, respectively. Therefore, the maximum error (Topping, 1955) in the strain measurements is

$$\frac{\delta \epsilon}{\epsilon} = 0.01 + \frac{\delta(\Delta R)}{\Delta R} + \frac{\delta(G.F.)}{G.F.} + \frac{\delta R_o}{R_o}$$

$$= 0.01 + 0.002 + 0.005 + 0.0016 = 0.0186,$$

or less than two per cent. Maximum sensitivity is from 5 to 60 x 10^{-6}, depending on the scale of the trace obtained from the recorder.

Stress Measurements

The load cell used for the uniaxial tests was calibrated against a known load cell and has an accuracy of better than two per cent. The diameter, d, of the throat region of the sample was measured to within 0.0005". The maximum error of the uniaxial compressive stress is

$$\frac{\delta \sigma_3}{\sigma_3} = \frac{\delta F}{F} + 2\,\frac{\delta d}{d} = 0.02 + \text{nil},$$

or about two per cent. Sensitivity was about 50 pounds.

The load cell used for the confined compression tests was calibrated by a Moorehouse proving ring and has an accuracy better than one per cent. Sensitivity was about 50 pounds. The sensitivity of the pressure measurements was about 20 bars (about 300 psi). For pressures greater than 1 kb this represents an error of less than

two per cent. Therefore, the maximum error of the stress difference, $(\sigma_3 - \sigma_1)$, in confined compression tests is

$$\frac{\delta(\sigma_3 - \sigma_1)}{(\sigma_3 - \sigma_1)} = \frac{\delta F}{F} + \frac{\delta \sigma_1}{\sigma_1} = 0.01 + 0.02 ,$$

or about three per cent.

Volumetric Strain Calculation

The maximum error in the calculated values of volumetric strain is

$$\frac{\delta(\frac{\Delta V}{V})}{\frac{\Delta V}{V}} = \frac{\delta \epsilon_{\shortparallel}}{\epsilon_{\shortparallel}} + 2 \frac{\delta \epsilon_{\perp}}{\epsilon_{\perp}} = 0.02 + 2(0.02) ,$$

or about six per cent

Stress At Onset of Crack Growth

The range of values of the uniaxial compressive stress at which crack growth began is about ten per cent of the average value. This is taken to be the maximum error in determining the stress at the onset of crack growth in uniaxial and confined compression tests.

The points on the McClintock-Walsh plot (Figure 26, Chapter IV) have a maximum error of 20 per cent for the ordinate and 13 per cent for the abscissa.

Work Required for Fracture and pdV Work

The areas were measured with planimeter to within 0.10 in^2 which represents an error of about two per cent. The error in the work equivalent per unit area is

$$\frac{\delta(\Delta W)}{\Delta W} = \frac{\delta(\Delta \sigma_3)}{\Delta \sigma_3} + \frac{\delta(\Delta \epsilon_{11})}{\Delta \epsilon_{11}}$$

$$+ 0.03 + 0.02,$$

or about five per cent. Therefore the maximum error in determining the work required for fracture was approximately seven per cent.

The maximum error in determining the work done against the confining pressure is

$$\frac{\delta(pdV)}{pdV} = \frac{\delta(\frac{\Delta V}{V})}{\frac{\Delta V}{V}} + \frac{\delta \sigma_1}{\sigma_1} = 0.06 + 0.03,$$

or about nine per cent.

APPENDIX 9

USE OF COMPRESSIBILITY TESTS IN DETERMINING THE POROSITY DUE TO CRACKS

Walsh (1965a) made a theoretical study of the effect of cracks on the compressibility of rocks. He considered rock to be an elastic isotropic material containing randomly oriented narrow cracks. With this model he derived an expression for the effective compressibility, β_{eff} in terms of the compressibility β of the solid material and the rate of change of porosity, n , with external pressure p:

$$\frac{1}{V_o}\frac{dV_o}{dp} = \beta + \frac{1}{V_o}\frac{dV_c}{dp} \qquad \text{(Equation 1)}$$

This can be rearranged to give

$$\beta_{eff} = \frac{\beta V_o pdp + pdV_c}{V_o pdp} \qquad \text{(Equation 2)}$$

He then divides the body into regimes each of which contains one cracks. The effective compressibility of each regime is

$$\beta_{eff} = \frac{\beta v_o pdp + pdv_c}{v_o pdp} \qquad \text{(Equation 3)}$$

The compressibility of a regime after the crack has closed is the same as for the uncracked material. Thus the stiffness of the rock gradually increases as the cracks close under increased confining pressure. For rocks where the entire porosity is caused by cracks which close completely under pressure, the compressibility decreases to the value of the uncracked material.

Walsh's analysis provides a convenient method of determining the porosity of rocks whose porosity is due entirely to narrow cracks. Figure 47 is a conventional plot obtained during a compressibility test on a jacketed sample of rock which contains cracks. As the pressure is increased, the rock becomes noticeably stiffer. Above a certain pressure all the cracks are closed and the curve becomes essentially linear. This linear portion represents the compressibility of the uncracked material.

The volumetric strain at any pressure is due to the compressibility of the solid material and the closing of cracks. The amount of volumetric strain due to the compressibility of the uncracked material at a pressure, p, can be found by extending a line back from the curve at

pressure p which has a slope equal to the compressibility of the uncracked material. The difference between the total volumetric strain at a pressure p and the intercept of this line is the volumetric strain due to the compressibility of the uncracked material. The volumetric strain due to the closing of cracks up to the pressure p, i.e., the decrease in porosity, is given by the intercept of this line and is represented by n_c in Figure 47.

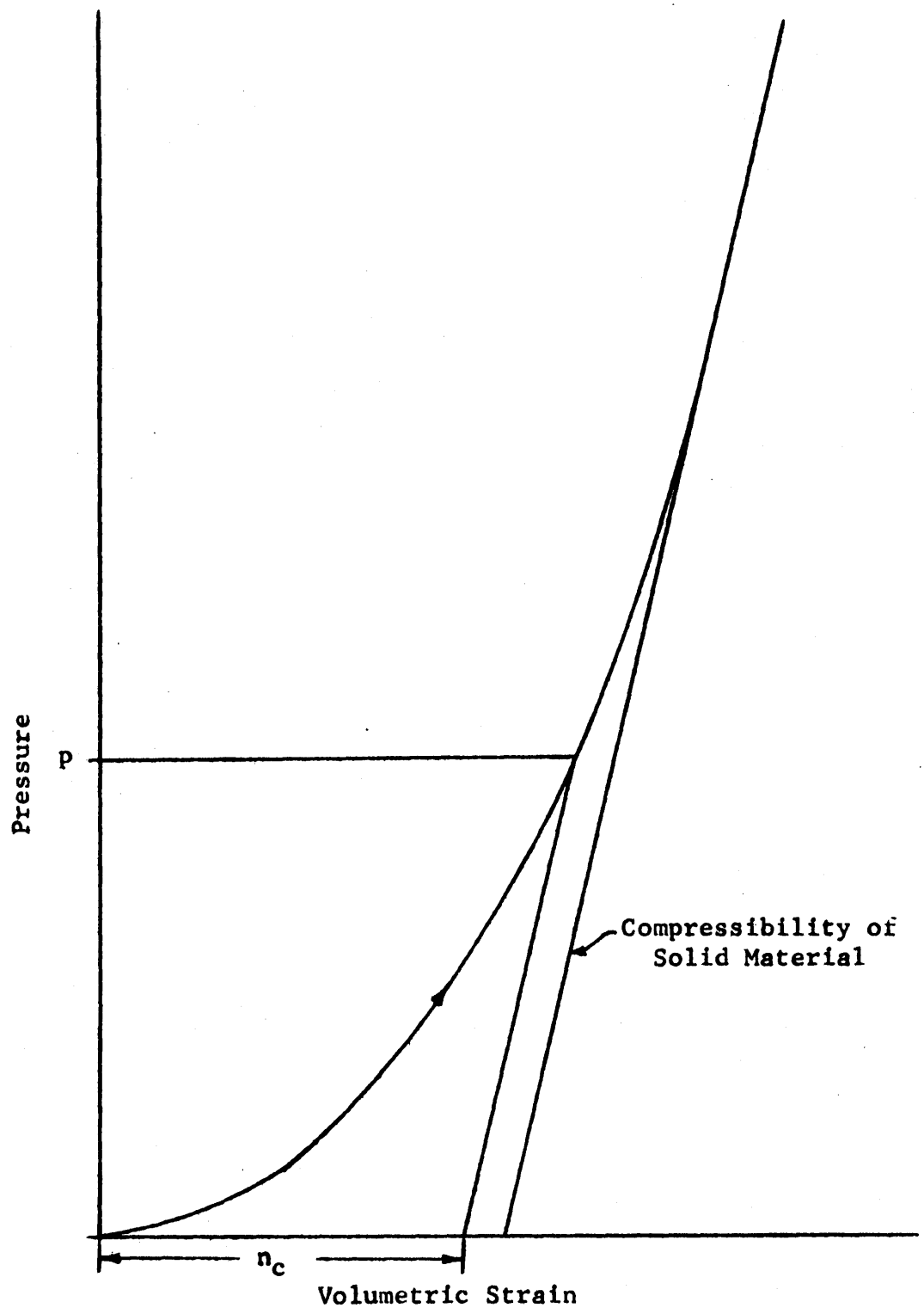

Compressibility of Rock Containing Narrow Cracks

Figure 47

APPENDIX 10

PREFERRED DIRECTION OF CRACKS AND INITIAL LINEAR COMPRESSIBILITY OF WESTERLY GRANITE

The preferred orientation of the cracks in Westerly granite was determined by traversing thin sections and recording the orientation of each crack. About 500 cracks in each of two perpendicular sections were mapped. The preferred orientation in each thin section was found by plotting a histogram of the number of cracks in each 10 degree interval. The histograms are shown in Figure 48. The three-dimensional orientation of the preferred direction of cracks was found with the aid of a stereographic projection. The preferred orientation in the thin sections were treated as apparent dips.

The relationship between the preferred direction of cracks and the directions in which the linear compressibility were measured by Brace (1965) is shown in Figure 49. Brace found that the maximum value of the initial compressibility was measured in the C direction which, as shown in Figure 49, is the direction most nearly normal to the preferred orientation.

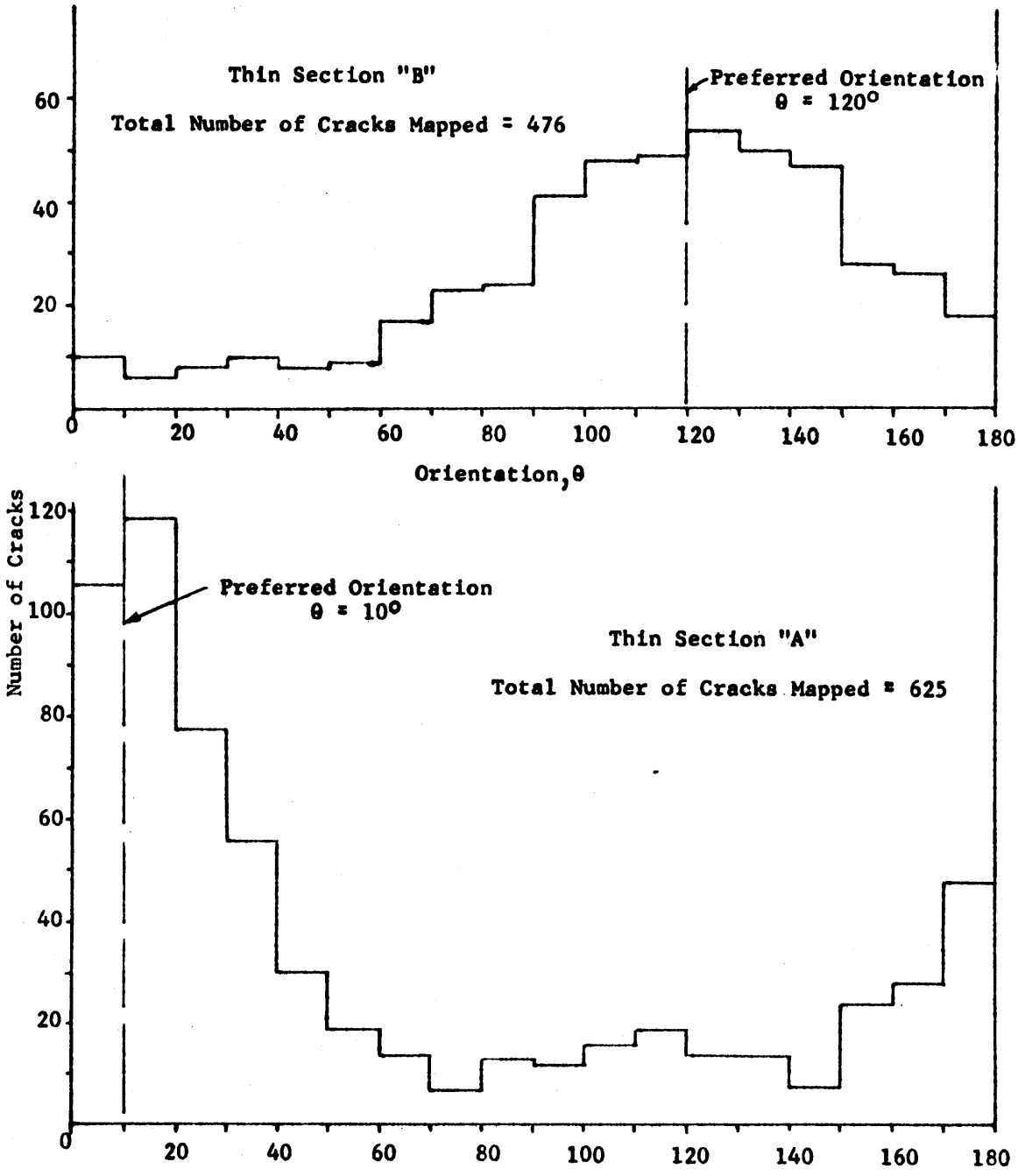

Histograms Used in Determining Preferred Direction of Cracks

Figure 48

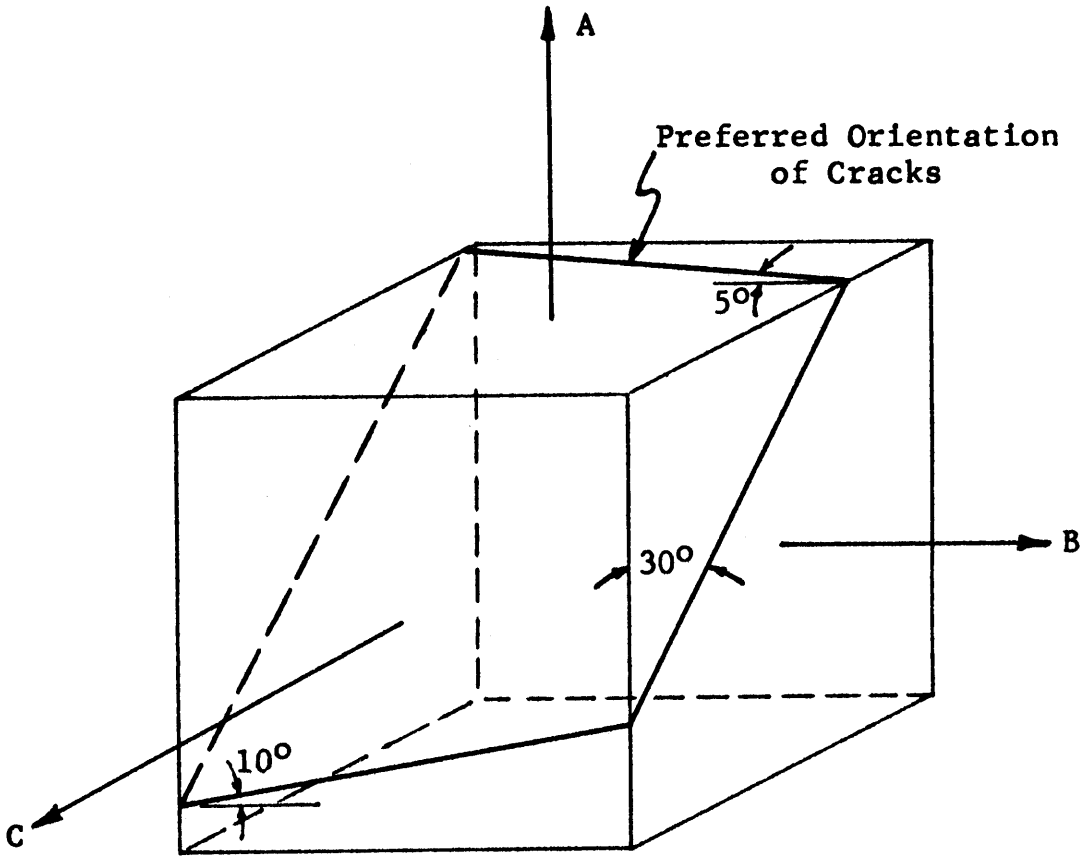

Preferred Direction of Cracks and Directions

in Which the Linear Compressibility was Measured

Figure 49

APPENDIX 11

JACKETING OF SAMPLES

For the compressibility tests, the samples were jacketed in silicon rubber (General Electric, RTV 102). This material is easy to apply, dries within 48 hours at room temperature, has a low modulus (about 50 psi), and transmits a hydrostatic stress. The jacketed sample is shown in Figure 50.

The samples used in the confined compression tests required a different jacket to allow the rams to come in uniform contact with the ends of the sample. The vertical surfaces of the head region was jacketed with 0.002" copper sheet which was crimped around the fillet. Copper caps were spun from 0.005" thick sheet and placed over the ends of the sample. In direct contact with the ends of the sample is 0.002" thick stainless steel to prevent possible intrusion of the copper cap. The throat and part of the head were then covered with silicon rubber. The copper jacketing is shown in Figure 51.

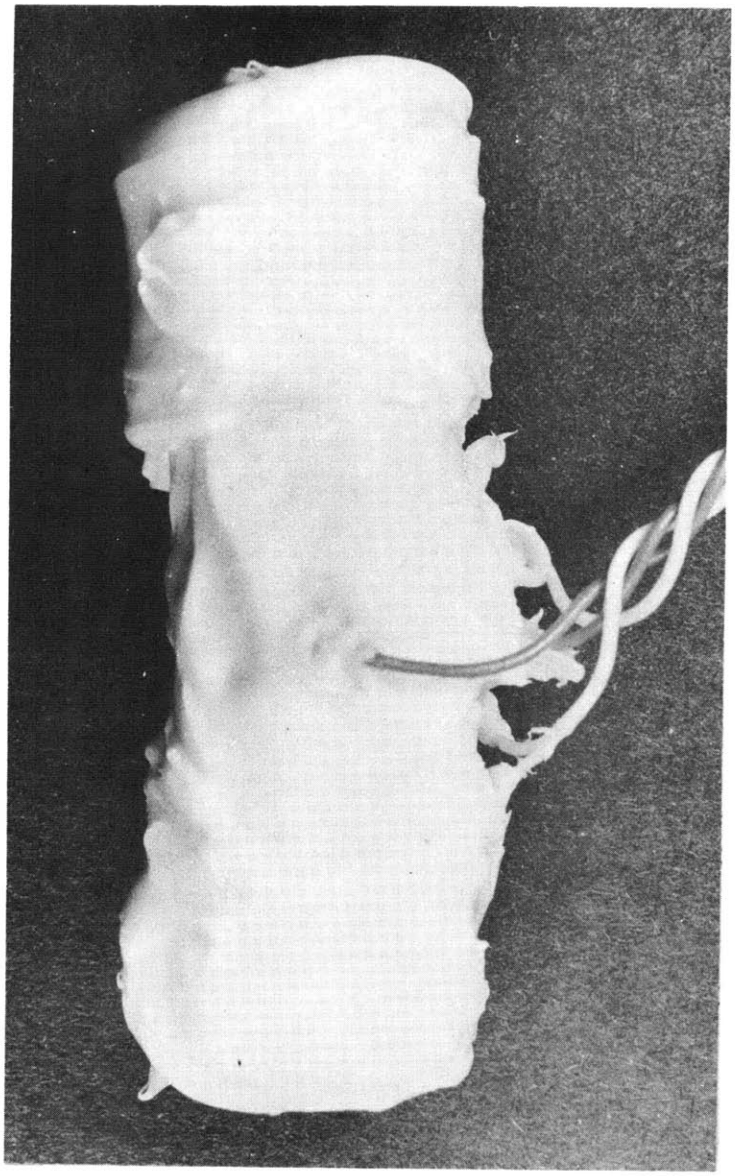

Compressibility Sample

Figure 50

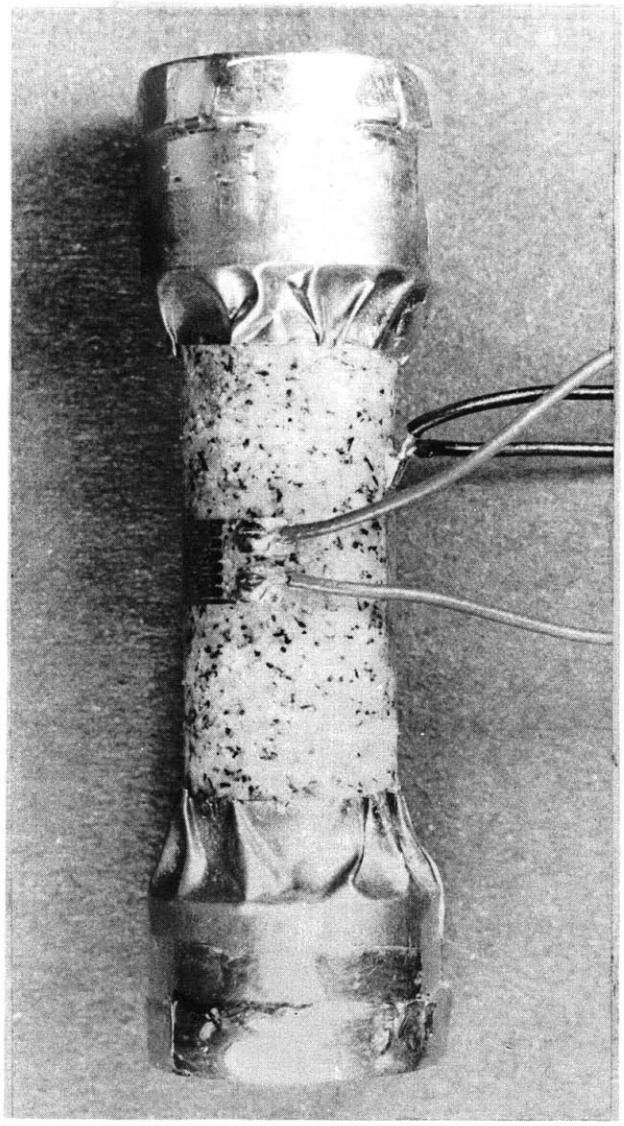

Copper Jacketing

Figure 51

APPENDIX 12

THE McCLINTOCK-WALSH MODIFICATION OF THE GRIFFITH THEORY

According to the McClintock-Walsh modification of the Griffith theory, the condition for the growth of cracks after they have closed is

$$(\sigma_3 + \sigma_1 - 2\sigma_c) + (\sigma_1 - \sigma_3)(1 + \mu^2)^{\frac{1}{2}} = 4K(1 - \frac{\sigma_c}{K})^{\frac{1}{2}}$$

(Equation 1)

where μ = coefficient of friction of the crack walls
K = tensile strength
σ_c = normal stress required to close a crack
σ_3 = maximum compressive stress
σ_1 = minimum compressive stress.

Considering σ_c to be negligible, Equation 1 becomes

$$(\sigma_3 + \sigma_1) + (\sigma_1 - \sigma_3)(1 + \mu^2)^{\frac{1}{2}} = 4K .$$

(Equation 2)

When $\sigma_1 = 0$, the uniaxial compressive strength, σ_3^o, is given by

$$\sigma_3^o = \frac{4K}{(\mu - (1 + \mu^2)^{\frac{1}{2}}} .$$ (Equation 3)

Solving Equation 3 for 4K and substituting into Equation 1, one finds that, in terms of the uniaxial compressive strength, the fracture condition becomes

$$\frac{\sigma_3 - \sigma_1}{\sigma_3^o} = 1 + \frac{\sigma_1}{\sigma_3^o}\left[\frac{2}{\left(\frac{1+\mu^2}{\mu^2}\right)^{\frac{1}{2}} - 1}\right] .$$

(Equation 4)

The dependence of their fracture criterion on the coefficient of friction, μ, may be determined by solving $\left[\frac{2}{\left(\frac{1+\mu^2}{\mu^2}\right)^{\frac{1}{2}} - 1}\right]$ for various values of μ and plotting Equation 4.

The values of $\left[\frac{2}{\left(\frac{1+\mu^2}{\mu^2}\right)^{\frac{1}{2}} - 1}\right]$ for μ between 0.1 and 1.0 are presented below.

μ	$\left[\frac{2}{\left(\frac{1+\mu^2}{\mu^2}\right)^{\frac{1}{2}} - 1}\right]$
0.1	0.22
0.2	0.50
0.3	0.81
0.4	1.12
0.5	1.61
0.6	2.13
0.7	2.74
0.8	3.34
0.9	3.95
1.0	4.83

McClintock and Walsh plotted their fracture criterion with $\frac{\sigma_3 - \sigma_1}{\sigma_3^o}$ as the ordinate and $\frac{\sigma_1}{\sigma_3^o}$ as the abscissa.

If cracks grow at stresses much less than the fracture strength, the McClintock-Walsh modification cannot be expected to predict the fracture strength of a material. It could be anticipated, however, that their analysis would lead to a criterion which predicts the stress difference required to initiate crack growth.

The extension of the modified Griffith theory appears as shown in Figure 52. Several curves are drawn to indicate the dependence of the criterion on the coefficient of friction. The ordinate is $\frac{(\sigma_3 - \sigma_1)'}{\sigma_3'}$ and the abscissa is $\frac{\sigma_1}{\sigma_3'}$. The primes denote the stress difference at the onset of crack growth.

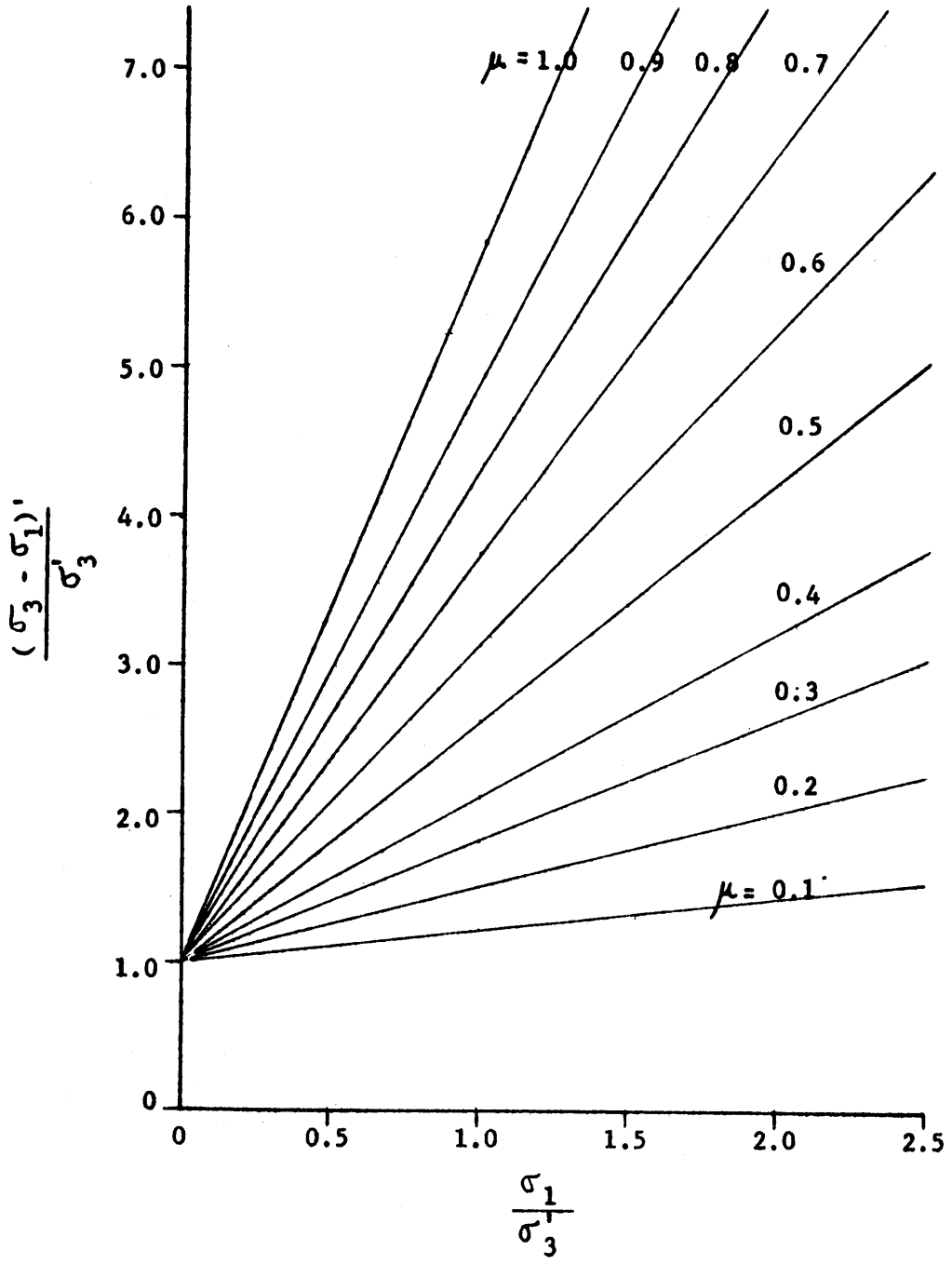

Stress Difference to Initiate Crack Growth vs Confining Pressure

Figure 52

APPENDIX 13

DETERMINATION OF $(\sigma_3 - \sigma_1)$ IN CONFINED COMPRESSION TESTS

The position of the rock specimen during confined compression tests is shown, schematically, in Figure 53.

The total force, F, which is measured by the load cell, is balanced by the pressure medium, the axial load on the sample, and friction at the O-rings according to

$$F = f + \sigma_1(A_R - A_T) + \sigma_3 A_T , \qquad \text{(Equation 1)}$$

where f = frictional force at the O-rings
A_R = cross-sectional area of the ram
A_T = cross-sectional area of the reduced section of the specimen
σ_1 = confining pressure
σ_3 = axial stress in the reduced section of the sample.

The variation of the frictional force with confining pressure was determined as described in Appendix 14. The frictional force is negligible below a confining pressure of 1 kb. Above this value, the frictional force was 1.7 per cent of $\sigma_1 A_R$. Equation 1 may be rearranged to give

$$(\sigma_3 - \sigma_1) = \frac{F - f}{A_T} - \sigma_1 \left(\frac{A_R}{A_T}\right) .$$

(Equation 2)

For this study $\frac{A_R}{A_T} = \frac{0.785 \text{ in}^2}{0.169 \text{ in}^2} = 4.65$. Therefore, in terms of pounds per square inch

$$(\sigma_3 - \sigma_1) = 5.92 \ (F - f) \text{ in}^{-2} - 4.65 \sigma_1 \ .$$

In terms of kilobars

$$(\sigma_3 - \sigma_1) = 4.08 \times 10^{-4} \ (F - f) \text{ in}^{-2} - 4.65 \sigma_1 \ .$$

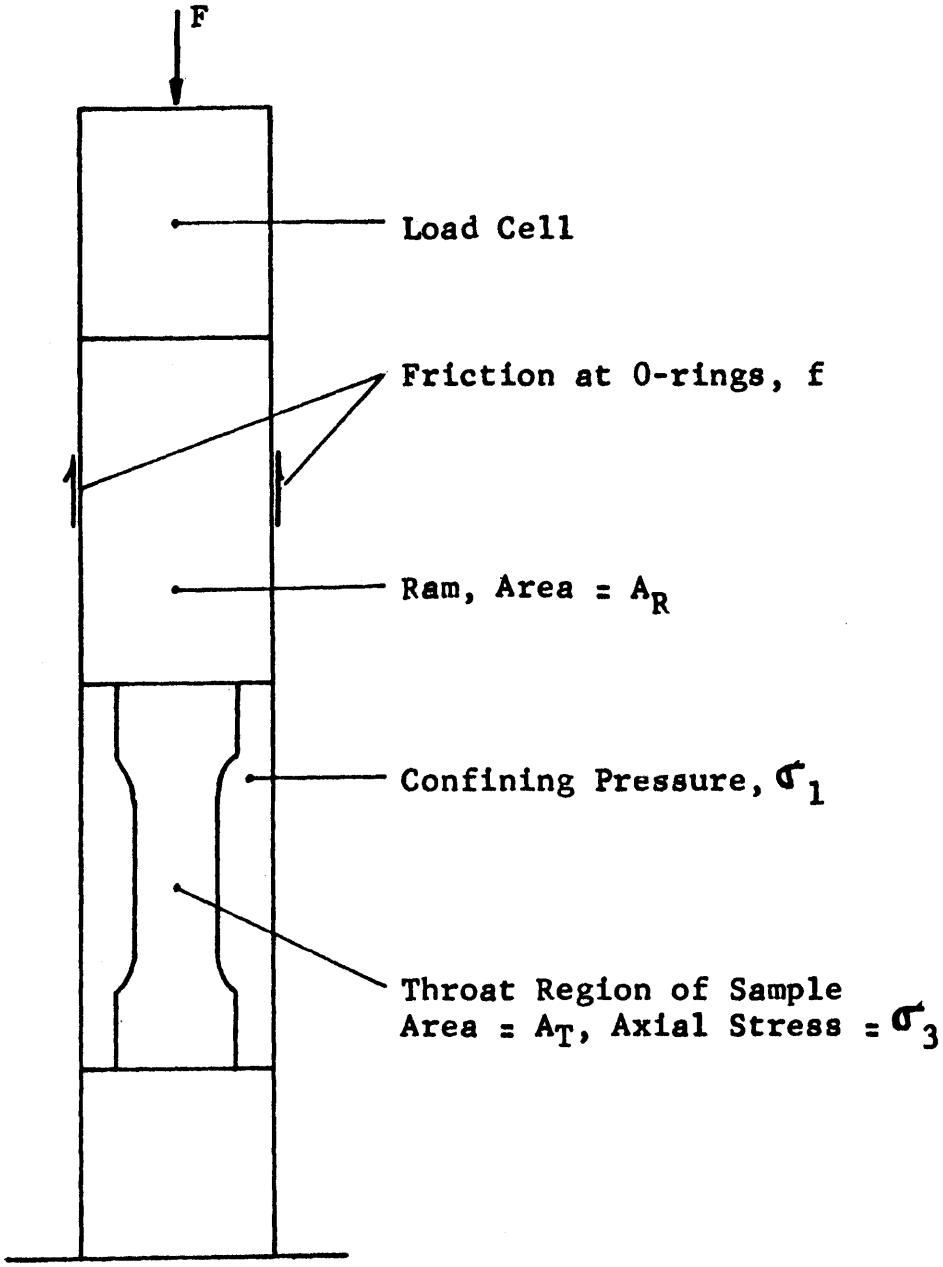

Diagram for Determining ($\sigma_3 - \sigma_1$)

Figure 53

APPENDIX 14

FRICTION AT O-RINGS DURING CONFINED COMPRESSION TESTS

Friction at the O-ring tends to resist the motion of the ram during the confined compression tests (Figure 53, Appendix 13). This frictional force must be considered when computing the stress difference in the rock specimen.

The magnitude of this frictional force was determined by filling the vessel with oil and increasing the pressure by advancing the ram. Pressure in the chamber was plotted against the load on the ram (Figure 54). The ascending and descending curves differ by twice the frictional force.

Below 1 kb the frictional force was negligible. From 1 to 2 kb the frictional force was 1.7 per cent of the force applied by the pressure:

$$f = (0.017)(\sigma_1)(A_R) \ .$$

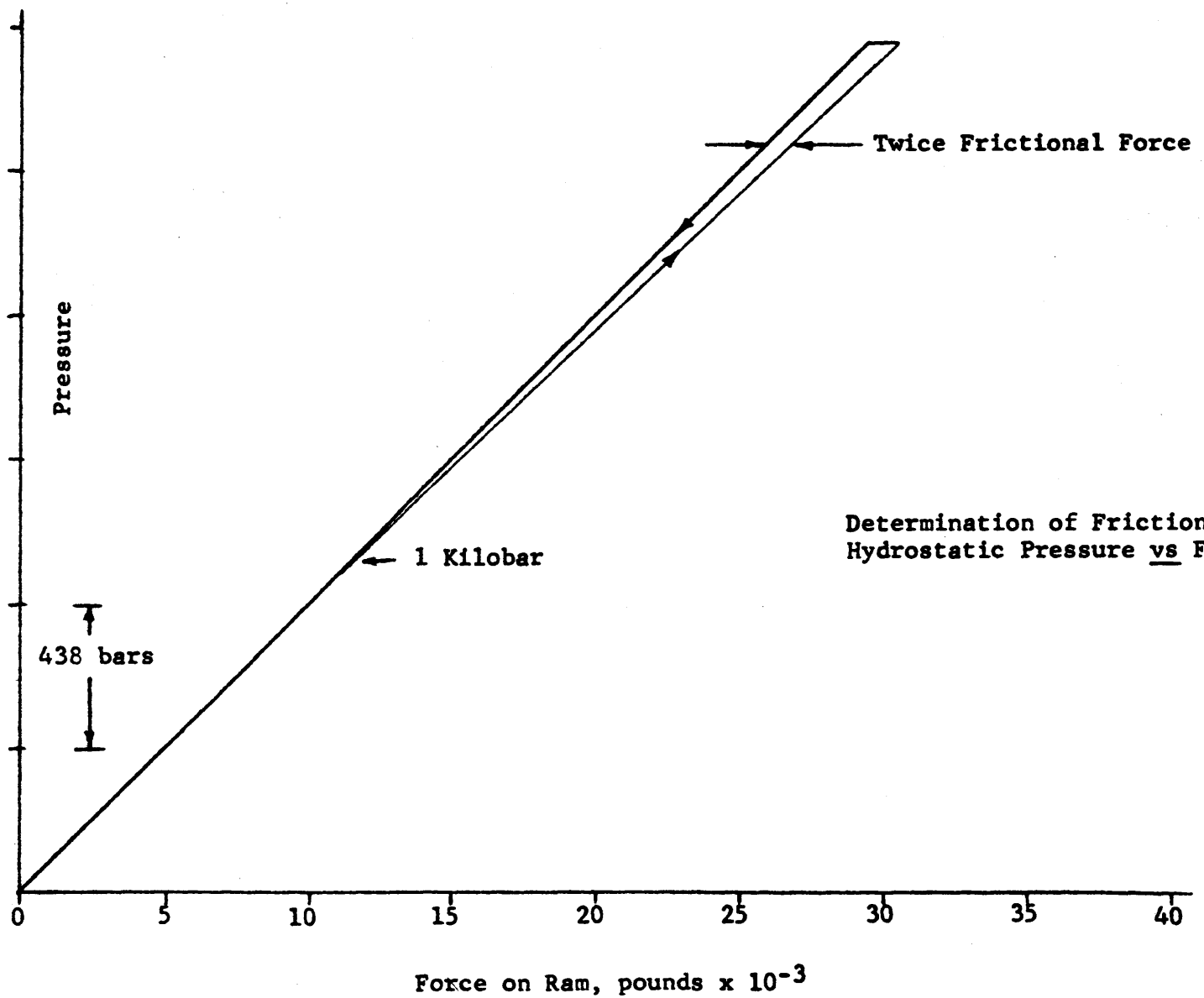

Figure 54

Determination of Friction at O-Rings
Hydrostatic Pressure vs Force on Ram

APPENDIX 15

ANALYSIS OF ELASTIC STABILITY OF SAMPLE

One must consider the possibility of failure by elastic instability when choosing a sample shape for compressive tests. If the dimensions and Young's modulus, E, of a sample are such that it is, stability-wise, a "long column", it will fail by elastic instability. In the event that this happens, the maximum load (and therefore the maximum stress) depends only on the length to diameter ratio and E and is independent of the strength of the material. "Short columns", on the other hand, fail when the compressive strength has been reached.

The dimensions of the samples used in this study are shown in Figure 43, Appendix 4. The loading conditions imposed on the sample prevent both lateral displacements and change in slope of the ends of the sample. This loading condition corresponds to a Euler column with fixed ends and the load, P, at which such a column becomes elastically unstable is (Timoschenko and Gere, 1961)

$$P = \frac{4\pi^2 EI}{L^2},$$

where E = Young's modulus
I = moment of inertia
L = length of sample

For the samples used in this study $E = 8.3 \times 10^6$ psi and $L = 2$ in. Since the buckling will occur in the plane of minimum flexural rigidity the moment of inertia, I, is computed for the throat section of the sample where the diameter is 0.463 in.:

$$I = \frac{\pi d^4}{64} = (\frac{\pi}{64})(0.049 \text{ in}^4) = 2.19 \times 10^{-3} \text{ in}^4$$

Therefore, the compressive load, P, required to cause the sample to fail by elastic instability is

$$P = \frac{(4\pi^2)(8.3 \times 10^6 \text{ psi})(2.19 \times 10^{-3} \text{ in}^4)}{4 \text{ in}^2} = 1.79 \times 10^5 \text{ lbs.}$$

This value of P would correspond to a compressive stress, σ_3, of

$$\sigma_3 = \frac{179{,}000\#}{0.169 \text{ in}^2} = 1.06 \times 10^6 \text{ psi} .$$

The uniaxial compressive strength is approximately 3.4×10^4 psi. Therefore the load at which the sample would become elastically unstable is approximately 31 times greater than the load required to reach the compressive strength of the material.

Even though the compressive strength increases significantly with confining pressure, the fracture load is still considerably less than the load required for elastic instability.

BIOGRAPHY OF THE AUTHOR

Name: Bartlett W. Paulding, Jr.

Born: December, 1936, in Attleboro, Massachusetts

Education:

Secondary Schools in Attleboro and Norton, Massachusetts

Sept. 1954 to June 1956:	University of Massachusetts
Sept. 1956 to May 1959:	Colorado School of Mines
Sept. 1959 to present:	Massachusetts Institute of Technology

Received the degree of Geological Engineer from the Colorado School of Mines in May, 1959.

Professional Experience:

In addition to research and teaching assistantships at M.I.T., the author's experience indludes the following:

June - Sept., 1962: Research geophysicist with the California Research Corporation. Measured velocity of sound in sintered glass.

June - Sept., 1961: Exploration geophysicist with the Standard Oil Company of California. Conducted a water borne gravity survey.

Feb. - May, 1961: Scientific assistant with the Woods Hole Oceanographic Institution. Provided general shipboard assistance.

June - Sept., 1960: Field geologist with the Quebec Department of Mines. Assisted in reconnaissance mapping near Hudson Bay.

August - Sept., 1957: Field assistant with the Bureau of Land Management. Investigated mining claims in connection with Public Law 167.

June - Sept., 1956: Field assistant with the Geophysics Division of the U.S. Geological Survey. Assisted with the duties associated with seismic exploration.

Additional experience includes: field engineer with an earthmoving concern, construction laborer and geological consulting for several engineering firms in the Boston area.

In June, 1962, it was the author's good fortune to marry Constance C. Robbins.

The author is joining the Solid Mechanics Division of the Illinois Institute of Technology Research Institute.